# USC–SIPI REPORT #309

**Cumulants and SubspaceTechnique for Array Processing**

**by**

**Egemen Gonen**

**May 1997**

Signal and Image Processing Institute
**UNIVERSITY OF SOUTHERN CALIFORNIA**
Department of Electrical Engineering-Systems
3740 McClintock Avenue, Room 400
Los Angeles, CA 90089-2564 U.S.A.

# Acknowledgements

I am indepted to my advisor, Professor Jerry M. Mendel who has guided and supported my doctoral research at USC. I gratefully acknowledge his continuous encouragement throughout my studies. Our fruitful discussions and exchange of ideas have been the key ingredients in the development of the work in this thesis. His wisdom and professional attitude will always be great examples for me.

I am deeply grateful to my mother and father for providing the best possible education, support and inspiration. Very special thanks go to my mother who has been my first teacher. Thanks to my brothers Edip and Eren, and to my sister Emel. Eren deserves a special thanks since he has been a very good assistant during my amateur radio experiments.

Many thanks to all the teachers who have inspired me. I am grateful especially to Professors Yalcin Tanik, Altunkan Hizal, Tuncay Birand, Nilgun Gunalp, Yildiz Arikan and Ruyal Ergul of Middle East Technical University for providing me with an excellent undergraduate education, and a strong background on communications, microwave and antenna theory.

I would like to thank Professors William C. Lindsey, Andreas Polydoros and Vijay Kumar who have been instructors of some of the best communication courses I have taken at USC.

I would like to thank Professors Robert Scholtz, Crysostomos L. Nikias and William A. Harris for their participation in my dissertation comittee.

This work was supported by Center for Research on Applied Signal Processing at the University of Southern California. Thanks to Micheal O'Brian, Dr. Douglas Nelson and others for their support.

I am indepted to the Ministry of Education of Turkey for offering me the government scholarship for masters education in the United States.

I would like to thank all of my friends at USC, especially Dr. Mithat C. Dogan and Dr. Levent Aydin for many useful technical discussions.

Finally, thanks are due to the staff of Signal and Image Processing Institute (SIPI), especially to Linda Varilla, Mercedes Morente, Regina Morton, Allan Weber and Dawn Ernst.

# Contents

# List of Tables

# List of Figures

# Chapter 1

# Introduction to Array Signal Processing and Higher-Order Statistics

The goal of array signal processing is to extract certain parameters or waveforms of signal sources of interest from the spatial and temporal information obtained by sampling the signal field via an array of sensors that are placed at different locations in the signal environment. Some of the source parameters which are of interest are directions of arrival (DOAs), time delay differences, ranges, velocities, and polarizations.

Typical application areas of array signal processing are communications, radar, sonar, medical imaging, radio astronomy and exploration seismology.

In communications, using antenna arrays offers selectivity and spatial diversity which are useful for combating multiuser interference, fading and multipath propagation. To combat multiuser interference, arrays can be employed to steer the receiver antenna response in the direction of one group of users at a time while rejecting the interference from other users. Using multiple antennas offers spatial diversity which can be used to mitigate the effect of fading; signals received by antennas which are spatially separated can be combined as they may fade independently. As shown in this thesis, multipaths can be combined using an array of antennas. Arrays are also used for blind separation of communication signals by

exploiting certain features of the signals.

In radar, a transmitting antenna radiates electromagnetic waves to probe the surrounding field, and a receiving antenna array listens for the echoes from targets in the field. The received echoes are processed to estimate parameters such as DOAs, ranges and velocities of the targets.

Sonar is similar to radar in principle. The receiving array consists of pressure sensitive transducers called *hydrophones*, and may be towed under water. The received echoes are used for estimating the target parameters. Radar and sonar can operate in passive, listening as well as active mode.

In medical imaging, cross-sectional images of objects are obtained by processing the array data collected from either transmission or reflection of a signal scanning the object.

In radio astronomy, antenna arrays are employed to record radio emissions from celestial objects. These emissions carry various information about the structure of the celestial objects.

In exploration seismology, an acoustic signal is sent to the interior of the earth and the reflected signal received at the surface by an array of sensors known as *geophones* is recorded. This signal is used for imaging of an interior region.

The conventional approach to solving array processing problems is to use the first- and second-order statistics of the measurements. In this thesis, the emphasis is on the advantages of using higher-order statistics (cumulants) in addition to first- and second order statistics of the signals for array signal processing.

In the next section, the physics of the array signal processing problem is introduced. Higher-order statistics are reviewed in Section 1.2. Then, an overview of the thesis is presented in Section 1.3.

## 1.1 Physics of Array Signal Processing

The problems of interest in array signal processing are estimation of parameters and recovery of the signal sources given the measurement samples. For this purpose, an array of sensors is used to collect measurements in the field of disturbance

created by the signal sources. The type of disturbance may be either electromagnetic or acoustic, depending on the application. Then, the collected measurements are processed suitably to yield the desired signals and their parameters.

Signal emitters are in general point sources which produce traveling waves whose amplitudes at a point in space are inversely proportional to the distance to the respective sources. Therefore, the amplitude and phase of a traveling wave at any two points lying on the surface of a sphere are equal; hence, the set of all points lying on a sphere centered at the location of the source is called a *wavefront.* If the distance of the source to the sensor array is so large that the sphericity of the wavefront can be neglected, and the wavefront can be assumed a *plane wave.* This assumption is called the *far-field assumption.*

Before starting any formulation, we first introduce the notation which will be used throughout the thesis. Lower-case boldface letters represent vectors; upper-case boldface letters represent matrices; and, lower and upper-case letters represent scalars. The symbol "*" is used for conjugation operation, and the superscript "$.^H$" is used to denote complex conjugate transpose.

Consider the scenario in Figure 1.1. In this scenario, the antenna array is a two dimensional one having $M$ elements. There are $P$ far-field sources $\{s_1(t), \cdots, s_P(t)\}$. Suppose that the directions of arrival of the signals are $\{\theta_1, \cdots, \theta_P\}$. In narrowband communication applications, source signal is typically a sinusoidal carrier modulated by a message signal, as

$$\bar{s}(t) = a(t)\cos(j2\pi f_c t + \phi(t)) \tag{1.1}$$

in which $f_c$ is the *carrier frequency,* and the *message signal* $m(t) \triangleq a(t)\exp(j\phi(t))$ which has a bandwidth much less than the carrier frequency (i.e., the message signal is slowly-varying as compared to the carrier signal).

In the array processing literature, it is conventional to use the *analytic signal* representations. Using this convention

$$\bar{s}(t) = \mathrm{Re}\{s(t)\} \tag{1.2}$$

where $s(t) = a(t)\exp(\phi(t))\exp(j2\pi f_c t)$ is the analytical signal.

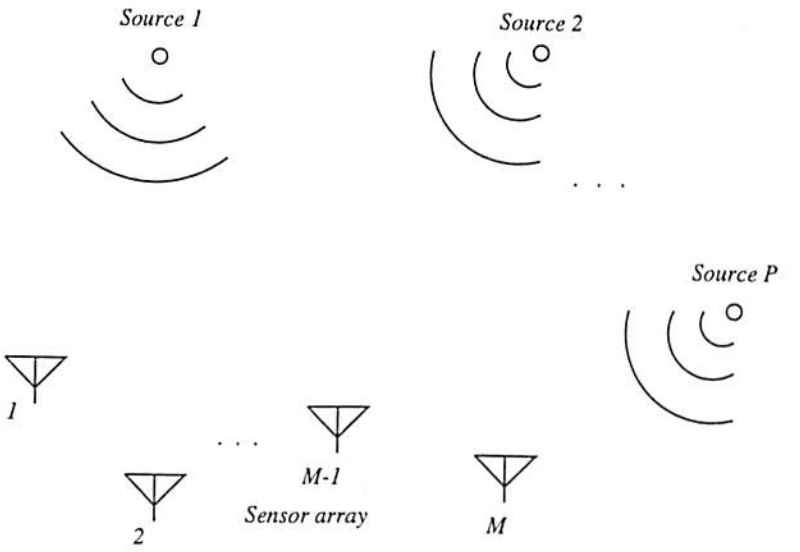


Figure 1.1: An $M$ element antenna array and $P$ sources

From the plane wave assumption, it follows that received signals by different sensors due to a single source are scaled and delayed replicas of that source. Let the response of the $m$th antenna to a signal from direction $\theta$ be $g_m(\theta)$. Then, the (analytical) signal received by the $m$th antenna is a superposition of the contributions from each source

$$r_m(t) = \sum_{p=1}^{P} g_m(\theta_p) s_p(t - \tau_m(\theta_p)) + n_m(t) \tag{1.3}$$

where $\tau_m(\theta_p)$ is the time delay of the $p$th signal at the $m$th sensor, and is given by $\tau_m(\theta_p) = \vec{\alpha_p} \vec{d_m}$ in which $\vec{\alpha_p}$ is called the *slowness vector* of the $p$th signal, with $|\vec{\alpha_p}| = 1/c$ where $c$ is the speed of propagation of the signal. The term $n_m(t)$ in (1.3) represents the sensor noise which accounts for any phenomenon that can not be modeled by our assumptions.

Another common assumption in array signal processing is narrowband operation. According to this assumption, the message part of the signal does not change significantly during the time it takes for a wavefront to travel through the aperture of the array. Consequently, $a_p(t - \tau_m(\theta_p)) \approx a_p(t)$ and $\phi_p(t - \tau_m(\theta_p)) \approx \phi_p(t)$

for $p = 1, \cdots, P$ and $m = 1, \cdots, M$, and, therefore

$$s_p(t-\tau_m(\theta_p)) \approx a_p(t)\exp(\phi_p(t))\exp(j2\pi f_c(t-\tau_m(\theta_p))) \approx s_p(t)\exp(-j2\pi f_c\tau_m(\theta_p)) \tag{1.4}$$

From (1.3) and (1.4), it follows that

$$r_m(t) = \sum_{p=1}^{P} g_m(\theta_p)\exp(-j2\pi f_c\tau_m(\theta_p)s_p(t) + n_m(t) \quad m = 1, \cdots, M \tag{1.5}$$

Introducing $M$-vector $\mathbf{r}(t) \triangleq [r1(t), r_2(t), \cdots, r_M(t)]^T$, $\mathbf{a}(\theta) \triangleq [g_1(\theta)e^{-j2\pi f_c\tau_1(\theta)}$, $\cdots$, $g_M(\theta)e^{-j2\pi f_c\tau_M(\theta)}]^T$, $\mathbf{s}(t) \triangleq [s_1(t), \cdots, s_P(t)]^T$, and $\mathbf{n}(t) = [n_1(t), \cdots, n_M(t)]^T$, we obtain the fundamental array processing *measurement equation*

$$\mathbf{r}(t) = \sum_{p=1}^{P} \mathbf{a}(\theta_p)s_p(t) + \mathbf{n}(t) = \mathbf{A}\mathbf{s}(t) + \mathbf{n}(t) \tag{1.6}$$

where $\mathbf{A} \triangleq [\mathbf{a}(\theta_1), \cdots, \mathbf{a}(\theta_P)]$. The $M$-vector $\mathbf{a}(\theta)$ and the $M \times P$ matrix $\mathbf{A}$ are generally referred to as the *steering vector* and the *steering matrix*, respectively.

Steering vector of an array represents the response of the array to an incoming signal, and it depends on various parameters such as direction of arrival, polarization, range and frequency of the signals . We refer to the set of steering vectors by scanning the whole range of source parameters as the *array manifold.*

An important assumption in array processing is the *non ambiguity* condition which requires any set of $P$ $(P < M)$ steering vectors be linearly independent. Under this assumption, $\mathbf{A}$ has rank $P$.

The additive noise is generally assumed to be a complex and circularly symmetric stationary Gaussian random process with statistically independent components which have identical variance, and

$$E\{\mathbf{n}(t)\} = \mathbf{0}, \quad E\{\mathbf{n}(t)\mathbf{n}^H(t)\} = \sigma\mathbf{I} \tag{1.7}$$

The source signals are modeled as either deterministic or non-Gaussian random processes; however, for analysis purposes such as deriving Cramer-Rao bounds, it is common to assume the sources as independent Gaussian random processes.

## 1.2 A Review of Higher-Order Statistics

In this section, we first present a definiton of higher-order statistics. Then, the properties of higher-order statistics are reviewed. This section is intended to be a brief introduction to the area. The interested reader is referred to the tutorial papers [47, 51] and to the books [64, 50, 3] for a detailed treatment of the topic.

### 1.2.1 Definition of Cumulants

The joint cumulants of order $r = k_1 + k_2 + \cdots + k_n$ of a given set of real random variables $\{x_1, x_2, \cdots, x_n\}$ are defined [51] as

$$c_{k_1,k_2,\cdots,k_n} \triangleq (-j)^r \left. \frac{\partial^r \ln \Phi(w_1, \ldots, w_n)}{\partial \omega^{k_1} \ldots \partial \omega^{k_n}} \right|_{w_1=,\ldots,=w_n=0} \tag{1.8}$$

where

$$\Phi(w_1, \ldots, w_n) = E\{\exp j(w_1 x_1 + \cdots + w_n x_n)\} \tag{1.9}$$

is the joint characteristics function of $\{x_1, x_2, \cdots, x_n\}$. The joint moments of the same set of real variables are defined as

$$m_{k_1,k_2,\cdots,k_n} \triangleq (-j)^r \left. \frac{\partial^r \Phi(w_1, \ldots, w_n)}{\partial \omega^{k_1} \ldots \partial \omega^{k_n}} \right|_{w_1=,\ldots,=w_n=0} \tag{1.10}$$

The joint cumulants can therefore be expressed in terms of the joint moments of the same random variables. Formulas for calculation of cumulants from moments and vice versa are is provided in [47]. Here we present the calculation of second-, third- and fourth-order cumulants in terms of moments as these are the only statistics used in the thesis. For zero-mean real random variables, the second-, third- and fourth-order cumulants are calculated from the moments as follows

$$\begin{aligned} cum\,(x_1, x_2) &= E\{x_1 x_2\} \\ cum\,(x_1, x_2, x_3) &= E\{x_1 x_2 x_3\} \\ cum\,(x_1, x_2, x_3, x_4) &= E\{x_1 x_2 x_3 x_4\} - E\{x_1 x_2\} E\{x_3 x_4\} \\ &\quad -\{x_1 x_3\} E\{x_2 x_4\} \end{aligned}$$

$$-\{x_1x_4\}E\{x_2x_3\} \tag{1.11}$$

When the random variables have non-zero means, one replaces $x_i$ by $x_i - E\{x_i\}$ in the above formulas.

For complex random variables the above formulas are modified as

$$\begin{aligned} cum\,(x_1, x_2^*) &= E\{x_1x_2^*\} \\ cum\,(x_1, x_2, x_3^*) &= E\{x_1x_2x_3^*\} \\ cum\,(x_1, x_2, x_3^*, x_4^*) &= E\{x_1x_2x_3^*x_4^*\} - E\{x_1x_2\}E\{x_3^*x_4^*\} \\ &\quad -\{x_1x_3^*\}E\{x_2x_4^*\} \\ &\quad -\{x_1x_4^*\}E\{x_2x_3^*\} \end{aligned} \tag{1.12}$$

Depending on the application, the arguments of a cumulant can be arranged in different ways. In array signal processing for example, one is often interested in the *spatial* information collected by a set of sensors. For this type of applications, therefore, signals sampled simultaneously from the array sensors are used as the arguments of various cumulants. On the other hand, in the system identification context, *temporal* information contained in successive samples of the system output reveal important parameters of the system. In this case, the $k$th order cumulant of a stationary random process, $x(t)$ is defined as

$$C_{k,x}(\tau_1, \ldots, \tau_{k-1}) = cum\,(x(t), x(t+\tau_1), \ldots, x(t+\tau_{k-1}). \tag{1.13}$$

Higher-order spectra are simple extensions of power spectrum. The $k$th order polyspectrum of a random process $x(t)$ is defined as the Fourier transform of its cumulant, and is formulated as follows:

$$S_{k,x}(\omega_1, \ldots, \omega_{k-1}) = \sum_{\tau_1,\ldots,\tau_{k-1}=-\infty}^{\infty} C_{k,x}(\tau_1, \ldots, \tau_{k-1}) \exp\left(-j\sum_{i=1}^{k}\omega_i\tau_i\right). \tag{1.14}$$

In practice, cumulants can be estimated by approximating expectations by

sample averages, e.g.,

$$\widehat{C}_{3,x}(\tau_1, \tau_2) = \frac{1}{N} \sum_{n=1}^{N} x(t_n)x(t_n + \tau_1)x(t_n + \tau_2) \tag{1.15}$$

where $x(t_n)$ is the sample recorded at time point $t_n$, and $N$ is the number of records.

### 1.2.2 Properties of Cumulants

Following are some properties of cumulants [47], which will be used frequently in the thesis:

**[CP1]** If $c_i$, $i = 1, \ldots, k$ are constants, and $x_i$, $i = 1, \ldots, k$ are random variables, then

$$cum\,(c_1 x_1, \ldots, c_k x_k) = \left( \prod_{i=1}^{k} c_k \right) cum\,(x_1, \ldots, x_k) \tag{1.16}$$

**[CP2]** Any permutation of the arguments of a cumulant gives the same cumulant.

**[CP3]** Cumulants are additive in their arguments, i.e.,

$$cum\,(x_1 + y_1, x_2, \ldots, x_k) = cum\,(x_1, x_2, \ldots, x_k) + cum\,(y_1, x_2, \ldots, x_k) \tag{1.17}$$

**[CP4]** Addition of constants to the arguments of a cumulant does not change the value of the cumulant, i.e.,

$$cum\,(c + x_1, x_2, \ldots, x_k) = cum\,(x_1, x_2, \ldots, x_k) \tag{1.18}$$

**[CP5]** If the random variables $\{x_i\}_{i=1}^{k}$ are independent of the random variables $\{y_i\}_{i=1}^{k}$, then

$$cum\,(x_1 + y_1, x_2 + y_2, \ldots, x_k + y_k) = cum\,(x_1, x_2, \ldots, x_k) + cum\,(y_1, y_2, \ldots, y_k) \tag{1.19}$$

**[CP6]** If a subset of the random variables $\{x_i\}_{i=1}^{k}$ are independent of the rest, then

$$cum\,(x_1, x_2, \ldots, x_k) = 0 \tag{1.20}$$

### 1.2.3 Applications of Cumulants

Cumulants are advantageous to use over second-order statistics for certain type of problems. For example, cumulants preserve the phase information, and therefore they are useful for identification of MA, AR and ARMA non-minimum phase systems. On the other hand, autocorrelation is unable to convey complete phase information about non-minimum phase models, and fails to completely characterize non-Gaussian processes. As another example, higher than second order statistics of Gaussian signals are zero; hence, this property can be used as an indication of deviation from Gaussianity. Using higher than second-order statistics offers also immunity to additive Gaussian noise for non-Gaussian signals with non-zero cumulant. Note that third-order cumulants of symmetrically distributed signals (such as uniform, binary symmetric or Bernoulli-Gaussian) are zero; therefore, fourth-order statistics can be used for these types of signals. As shown in [16], the "balanced" way of calculating a fourth-order cumulant can be used to increase the number of signals that can be detected by a given array. Other applications of cumulants include those in the areas of communications, time series analysis, geophysics, sonar, radar, oceanography, and speech processing.

The drawback to the use of higher-order statistics is that they require longer data lengths than do correlation-based methods.

## 1.3 Overview

In Chapter 2, a comprehensive survey of existing subspace-based (or, high resolution) approaches to the problem of direction finding with passive antenna arrays is presented. Both second- and higher-order statistics-based approaches are included. Except for the method of Estimation of Signal Parameters via Rotational Invariance Techniques (ESPRIT) [65] and its derivatives, all of these methods require that the array response is either known analytically as a function of arrival angle, or is obtained through the calibration of the array. Array calibration is a very undesirable process, since it requires measurement and storage of the array response for every possible combination of the source parameters. Moreover, calibration has to be redone frequently; because, the array response may change with

time due to environmental disturbances. In this respect, ESPRIT has a fundamental advantage over the other subspace-based methods. Another advantage of ESPRIT is its computational simplicity. However, ESPRIT is applicable only to arrays which are "translationally invariant", i.e., arrays which consist of a subarray and its *identical copy* displaced in space. The geometry of the subarray may be arbitrary as long as its copy exists; only the measurements, and the displacement between the identical arrays are required. However, there is a major drawback to implementing ESPRIT arrays in practice: the main subarray and its copy must be exactly identical; and, any mismatch in the hardware results in performance degradation. In the cumulant-based processing framework, the method of virtual ESPRIT [17] (VESPA) has removed the restriction of having to have an identical copy of the subarray, while retaining the computational advantages of ESPRIT; instead of two identical subarrays, only a subarray having two sensors that have identical response is required. The rest of the array may have arbitrary response and geometry. VESPA is based on the fundamental observation that given an array of sensors, the directional information which would be obtained from the cross correlation between certain sensors in the array and nonexisting sensors at certain virtual locations in space can be obtained from suitably defined cumulants that use the actual sensor measurements. Both ESPRIT and VESPA are based on the concept of rotationally invariant subspaces, which is also the basis for the algorithms developed in this thesis.

In Chapter 3, a subspace-based direction finding method for coherent signal environments using cumulants is developed. The coherent (or, completely correlated) signals case often arises when multipath propagation or smart jammers are present. In this case, most of the subspace-based approaches described in Chapter 2, including ESPRIT and VESPA, fail; because, some of the signal eigenvectors diverge into the noise subspace when some of the received signals are coherent. The only approach which survives in coherent signal case is the Weighted Subspace Fitting (WSF) method; however, WSF has implementational problems, such as the need for accurate calibration of the array and complete knowledge of the derivative of the steering vectors with respect to the arrival angle, and a complicated multidimensional search is required. The spatial smoothing method

was proposed as a solution to the coherency problem for second-order statistics-based methods; however, spatial smoothing is limited to uniform linear arrays, and it reduces the number of resolvable signals. It is shown in Chapter 3 that, using fourth-order cumulants, direction finding is possible in the case of coherent signals, with a larger class of arrays than just uniform linear arrays. A uniform linear subarray is still needed; but, the rest of the array may have arbitrary and unknown response, and does not require calibration. The solution is based on the same idea of VESPA. The number of resolvable signals may exceed the number of sensors with our method. On the other hand, given the same type of an array, the number of resolvable signals can not exceed the number of signals with second-order statistics-based subspace methods even if there is no coherence.

In Chapter 4, we address the *blind* beamforming problem for coherent signal environments assuming no knowledge about the array structure or response. Beamforming is the process of combining the sensor outputs of an array with suitable weight vectors such that desired signals are recovered subject to an optimality criterion. When there are coherent signals, the optimum MVDR beamformer using spatial array covariance matrix tends to cancel the desired signal and it fails to perform optimally. A cumulant-based blind beamforming method is developed in Chapter 4. The method is based on the fact that for a blind beamformer the presence of coherent multipaths does not make any difference. In other words, the case of coherent multipath signals is identical to that of statistically independent signals with no multipath; because, as shown in Section 4.1, each coherent multipath from a given source causes only a reparameterization of the steering vector of that source. Therefore, the developed method is applicable to independent sources as well. Since the steering vectors are estimated from the data, in some sense, the our beamformer is tuned to the data, thereby avoiding sensitivity problems associated with mismatch in the assumed steering vectors, which occurs in the case of covariance-based processing.

In Chapter 5, direction finding in beamspace is addressed. In beamspace processing the array data is first projected into several beamspaces of lower equal dimension than the number of elements in the array; then, each beamspace data is processed to obtain DOAs and source signals in the same way as if it were

received from a pseudoarray of lower dimension. A beamspace transformation results in a reduced parameter space, which brings a cubic decrease in computational complexity for subspace-based methods, because, an eigendecomposition requires computations on the order of $M^3$ for $M$ sensors. Besides, beamspace transformation has been shown to offer numerous benefits such as enhanced resolution, improved performance in colored noise, and reduced sensitivity to sensor perturbations. ESPRIT can not be performed in beamspace unless the beamspace transformation has the same invariance as the array shift invariance. However, this requirement restricts the usefulness of desired beamformers, which is a limitation of covariance-based processing. Using the fact that fourth-order cumulants have more than two arguments, we develop a beamspace VESPA which works with arbitrary and unknown arrays provided there is an identical response sensor pair in the array. Based on the beamspace approach, we also develop an iterative VESPA. The motivation behind the iterative VESPA is to overcome the problem that occurs with estimating the array cumulants in VESPA when the source signals have highly separated cumulants and powers. In this case, it is impossible to localize all of the sources correctly with VESPA because of the undesirable cross terms present in the sample statistics of the weakest source due to the dominant sources. The iterative VESPA handles the cross terms by eliminating one source (which is the strongest one) at each step of the iteration. A real data experiment which supports our conclusions is presented.

In Chapter 6, a subspace-based joint estimation method for polarization parameters and directions of arrival is developed. Polarized signals and antennas are useful for several reasons. Diversity in signal polarization can be used to improve the receiver performance. Multiple signals arriving from close directions can be resolved on the basis of their polarizations. If the receiver antenna is matched with that of the incoming wave, the induced power in the receiver is maximized. Otherwise, there is a polarization mismatch, which may cause a very low signal power in the receiver; this lets two signals having orthogonal polarizations share the same frequency without interfering with each other. It is shown in Chapter 6 that, using fourth-order cumulants, both directions of arrival and polarization parameters of at most $M-1$ cochannel signals can be estimated using any $M$

element array by adding a subarray consisting of three short dipole antennas displaced in space and configured in a certain fashion. This way the constraint on the array configuration is minimized.

Conclusions and directions for future research are presented in Chapter 7.

# Chapter 2

# Subspace-Based Direction Finding Methods

Estimating direction of arrivals (DOAs) of multiple narrowband signals from measurements collected by an array of sensors has been a very active research problem for the last two decades. Typical applications of this problem are radar, communication, and underwater acoustics. One of the first techniques used for direction finding was beamforming which has a resolution limited by the array aperture. Spectral estimation techniques were also applied to the problem. However, these techniques fail to resolve closely spaced arrival angles for low signal-to-noise ratios. Another approach is the maximum-likelihood (ML) solution. This approach has been well documented in the literature. In the stochastic ML method [67], the signals are assumed to be Gaussian whereas they are regarded arbitrary and deterministic in the deterministic ML method [84]. The sensor noise is modeled as Gaussian in both methods, which is a reasonable assumption due to the central limit theorem. The stochastic ML estimates of the DOAs achieve the Cramer-Rao bound (CRB). On the other hand this does not hold for deterministic ML estimates [76]. The common problem with the ML methods in general is the necessity of solving a nonlinear multidimensional optimization problem which has a high computational cost and for which there is no guarantee of global convergence.

*Subspace-based* approaches have attracted much attention, after the work of [67], due to their computational simplicity as compared to the ML approach,

and their possibility of overcoming the Rayleigh bound on the resolution power of classical direction finding methods. Subspace-based methods are also referred to as *super-resolution* methods. Subspace-based direction finding methods are summarized in this section.

## 2.1 Formulation of the Problem

Consider the signal scenario described in Chapter 1 where an array of $M$ antenna elements is receiving a set of plane waves emitted by $P$ ($P < M$) narrowband sources in the far field of the array. The received $M$-vector $\mathbf{r}(t)$ at time $t$ is

$$\mathbf{r}(t) = \mathbf{A}\mathbf{s}(t) + \mathbf{n}(t) \tag{2.1}$$

where $\mathbf{s}(t) = [s_1(t), \cdots, s_P(t)]^T$ is the $P$-vector of sources; $\mathbf{A} = [\mathbf{a}(\theta_1), \cdots, \mathbf{a}(\theta_P)]$ is the $M \times P$ steering matrix in which $\mathbf{a}(\theta_i)$, the $i$th steering vector, is the response of the array to the $i$th source arriving from $\theta_i$; and, $\mathbf{n}(t) = [n_1(t), \cdots, n_M(t)]^T$ is a complex and circularly symmetric Gaussian noise process.

We assume: (1) The source signals are stationary random processes that may be statistically independent of each other, partially correlated, or completely correlated (i.e., coherent); the distributions are unknown; (2) The array may have an arbitrary shape and response; and, (3) The Gaussian noise process is statistically independent of the sources, zero-mean, and it may be either spatially white or colored. These assumptions will be relaxed, as required by specific methods, as we proceed.

The direction finding problem is to estimate the bearings [i.e., directions of arrival (DOA)] $\{\theta_i\}_{i=1}^P$ of the sources from the snapshots $\mathbf{r}(t)$, $t = 1, \cdots, N$.

In applications, the Rayleigh criterion sets a bound on the resolution power of classical direction finding methods. In the next sections we summarize some of the so-called super-resolution direction finding methods which may overcome the Rayleigh bound. We divide these methods into two classes, those that use second-order and those that use second- and higher-order statistics.

## 2.2 Second-Order Statistics-Based Methods

The second-order methods use the sample estimate of the array spatial covariance matrix

$$\mathbf{R} = E\{\mathbf{r}(t)\mathbf{r}(t)^H\} = \mathbf{A}\mathbf{R}_s\mathbf{A}^H + \mathbf{R}_n \tag{2.2}$$

where $\mathbf{R}_s = E\{\mathbf{s}(t)\mathbf{s}(t)^H\}$ is the $P \times P$ signal covariance matrix and $\mathbf{R}_n = E\{\mathbf{n}(t)\mathbf{n}(t)^H\}$ is the $M \times M$ noise covariance matrix. For the time being, let us assume that the noise is spatially white, i.e., $\mathbf{R}_n = \sigma^2\mathbf{I}$. If the noise is colored and its covariance matrix is known or can be estimated, the measurements can be "whitened" by multiplying the measurements from the left by the matrix $\mathbf{\Lambda}^{-1/2}\mathbf{E}_n^H$ obtained by the orthogonal eigendecomposition $\mathbf{R}_n = \mathbf{E}_n\mathbf{\Lambda}\mathbf{E}_n^H$.

The array spatial covariance matrix is estimated as follows:

$$\hat{\mathbf{R}} = \frac{1}{N}\sum_{t=1}^{N}\mathbf{r}(t)\mathbf{r}(t)^H. \tag{2.3}$$

Some spectral estimation approaches to the direction finding problem are based on optimization. Consider the *minimum variance* algorithm, for example. The received signal is processed by a beamforming vector $\mathbf{w}_o$ which is designed such that the output power is minimized subject to the constraint that a signal from a desired direction is passed to the output with unit gain. Solving this optimization problem, we obtain the array output power as a function of the arrival angle $\theta$ as

$$P_{mv}(\theta) = \frac{1}{\mathbf{a}^H(\theta)\mathbf{R}^{-1}\mathbf{a}(\theta)} \tag{2.4}$$

The arrival angles are obtained by scanning the range $[-90^o, 90^o]$ of $\theta$ and locating the peaks of $P_{mv}(\theta)$. At low signal-to-noise ratios, the conventional methods, like minimum variance fail to resolve closely spaced arrival angles. The resolution of conventional methods are limited by signal-to-noise ratio even if exact $\mathbf{R}$ is used, whereas in subspace methods, there is no resolution limit; hence, the latter are also referred to as *super-resolution* methods. The limit comes from the sample estimate of $\mathbf{R}$.

The super-resolution methods exploit the eigendecomposition of the estimated

array covariance matrix $\hat{\mathbf{R}}$. To see the implications of the eigendecomposition of $\hat{\mathbf{R}}$, let us first state the properties of $\mathbf{R}$:

1. If the source signals are independent or partially correlated, $rank(\mathbf{R}_s) = P$. If there are coherent sources, $rank(\mathbf{R}_s) < P$. In the methods explained in Sections 2.2.1 and 2.2.2, except for the WSF method (see Section 2.2.1.a), it will be assumed that there are no coherent sources. The case of coherent signals case is considered partially in Section 2.2.3; and, a detailed treatment of this case is presented in Chapter 3 .

2. If the columns of $\mathbf{A}$ are independent, which is generally true when the source bearings are different, then $\mathbf{A}$ is of full-rank $P$.

3. Properties 1 and 2 imply $rank(\mathbf{A}\mathbf{R}_s\mathbf{A}^H) = P$; therefore, $\mathbf{A}\mathbf{R}_s\mathbf{A}^H$ must have $P$ nonzero eigenvalues and $M - P$ zero eigenvalues. Let the eigendecomposition of $\mathbf{A}\mathbf{R}_s\mathbf{A}^H$ be

$$\mathbf{A}\mathbf{R}_s\mathbf{A}^H = \sum_{i=1}^{M} \alpha_i \mathbf{e}_i \mathbf{e}_i^H; \tag{2.5}$$

then $\alpha_1 \geq \alpha_2 \geq \cdots \geq \alpha_P \geq \alpha_{P+1} = \cdots = \alpha_M = 0$ are the rank-ordered eigenvalues, and $\{\mathbf{e}_i\}_{i=1}^{M}$ are the corresponding eigenvectors.

4. Because $\mathbf{R}_n = \sigma^2\mathbf{I}$, the eigenvectors of $\mathbf{R}$ are the same as those of $\mathbf{A}\mathbf{R}_s\mathbf{A}^H$, and its eigenvalues are

$$\lambda_i = \begin{cases} \alpha_i + \sigma^2, & \text{if } 1 \leq i \leq P, \\ \sigma^2, & \text{if } P+1 \leq i \leq M. \end{cases} \tag{2.6}$$

The eigenvectors can be partitioned into two sets: $\mathbf{E}_s \triangleq [\mathbf{e}_1, \cdots, \mathbf{e}_P]$ forms the *signal subspace*, whereas $\mathbf{E}_n \triangleq [\mathbf{e}_{P+1}, \cdots, \mathbf{e}_M]$ forms the *noise subspace*. These subspaces are orthogonal. The signal eigenvalues $\mathbf{\Lambda}_s \triangleq diag\{\lambda_1, \cdots, \lambda_P\}$, and the noise eigenvalues $\mathbf{\Lambda}_n \triangleq diag\{\lambda_{P+1}, \cdots, \lambda_M\}$.

5. The eigenvectors corresponding to zero eigenvalues satisfy

$$\mathbf{A}\mathbf{R}_s\mathbf{A}^H\mathbf{e}_i = \mathbf{0}, \quad i = P+1, \cdots, M \tag{2.7}$$

and, hence

$$\mathbf{A}^H\mathbf{e}_i = \mathbf{0}, \quad i = P+1, \cdots, M, \tag{2.8}$$

because $\mathbf{A}$ and $\mathbf{R}_s$ are full rank. Equation (2.8) means that *steering vectors are orthogonal to noise subspace eigenvectors.* It further implies that, because of the orthogonality of signal and noise subspaces, *spans of signal eigenvectors and steering vectors are equal.* Consequently there exists a nonsingular $P \times P$ matrix $\mathbf{T}$ such that

$$\mathbf{E}_s = \mathbf{AT}. \tag{2.9}$$

Alternatively, the signal and noise subspaces can also be obtained by performing a singular value decomposition directly on the received data without having to calculate the array covariance matrix. Li and Vaccaro [45] state that the properties of the bearing estimates do not depend on which method is used; however, singular value decomposition must then deal with a data matrix that increases in size as the new snapshots are received. In the sequel, we assume that the array covariance matrix is estimated from the data and an eigendecomposition is performed on the estimated covariance matrix.

The eigenvalue decomposition of the spatial array covariance matrix, and the eigenvector partitionment into signal and noise subspaces, leads to a number of subspace-based direction finding methods. The signal subspace contains information about where the signals are whereas the noise subspace informs us where they are not. Using either subspace results in better resolution performance than conventional methods. In practice, the performance of the subspace-based methods is limited fundamentally by the accuracy of separating the two subspaces when the measurements are noisy [46]. These methods can be broadly classified into signal subspace and noise subspace methods. A summary of direction-finding methods based on both approaches follows next.

### 2.2.1 Signal Subspace Methods

In these methods, only the signal subspace information is retained. Their rationale is that by discarding the noise subspace we effectively enhance the SNR, because the contribution of the noise power to the covariance matrix is eliminated. Signal subspace methods are divided into search-based and algebraic methods, which are explained next.

### 2.2.1.a Search-based methods

In search-based methods, it is assumed that the response of the array to a single source, *the array manifold* $\{\mathbf{a}(\theta)|\forall\theta\}$, is either known analytically as a function of arrival angle, or is obtained through the calibration of the array. For example, for an M-element uniform linear array, the array response to a signal from angle $\theta$ (measured with respect to the normal of the array) is analytically known and is given by

$$\mathbf{a}(\theta) = \left[1, e^{-j2\pi\frac{d}{\lambda}\sin(\theta)}, \cdots, e^{-j2\pi(M-1)\frac{d}{\lambda}\sin(\theta)}\right]^T \tag{2.10}$$

where $d$ is the separation between the elements, and $\lambda$ is the wavelength. Calibration of an array is performed by employing a high-power transmitter in the far-field of the array, and recording the array response $\mathbf{a}(\theta)$ for each possible value of the transmitter direction $\theta$. In general, array calibration is very costly and time-consuming, and it needs to be redone frequently since the array response may change due to physical distrubances.

In search-based methods to follow (except for the subspace fitting methods), which are spatial versions of widely-known power spectral density estimators, the estimated array covariance matrix is approximated by its signal subspace eigenvectors, or its *principal components*, as

$$\hat{\mathbf{R}} \approx \sum_{i=1}^{P} \lambda_i \mathbf{e}_i \mathbf{e}_i^H, \tag{2.11}$$

Then the arrival angles are estimated by locating the peaks of a function, $S(\theta)$ $(-90^o \leq \theta \leq 90^o)$ which depends on the particular method. Some of these methods and the associated function $S(\theta)$ are summarized in the following [35, 46, 50]:

**Correlogram method:**

In this method,

$$S(\theta) = \mathbf{a}(\theta)^H \hat{\mathbf{R}} \mathbf{a}(\theta) \tag{2.12}$$

The resolution obtained from the Correlogram method is lower than that obtained from the MV and AR methods.

**Minimum Variance (MV) [5] method:**

$$S(\theta) = \frac{1}{\mathbf{a}(\theta)^H \hat{\mathbf{R}}^{-1} \mathbf{a}(\theta)} \tag{2.13}$$

The MV method is known to have a higher resolution than the correlogram method, but lower resolution and variance than the AR method.

**Autoregressive (AR) method:**

In this method,

$$S(\theta) = \frac{1}{|\mathbf{u}^T \hat{\mathbf{R}}^{-1} \mathbf{a}(\theta)|^2} \tag{2.14}$$

where $\mathbf{u} = [1, 0, \cdots, 0]^T$. This method is known to have a better resolution than the previous ones.

**Subspace Fitting (SSF) and Weighted Subspace Fitting (WSF) Methods:**

In Section 2.2 we saw that the spans of signal eigenvectors and steering vectors are equal; therefore, bearings can be solved from the best least-squares fit of the two spanning sets when the array is calibrated [82]. In the Subspace Fitting Method the following criterion is used

$$[\hat{\theta}, \hat{\mathbf{T}}] = argmin \ \ ||\mathbf{E}_s \mathbf{W}^{1/2} - \mathbf{A}(\theta)\mathbf{T}||^2, \tag{2.15}$$

where $||.||$ denotes the Frobenius norm, $\mathbf{W}$ is a positive definite weighting matrix, $\mathbf{E}_s$ and $T$ are defined by (2.9), and the notation for the steering matrix is changed to show its dependence on the bearing vector $\theta$. Criterion (2.15), can be minimized directly with respect to $\mathbf{T}$, and the result for $\mathbf{T}$ can then be substituted back into (2.15), so that

$$\hat{\theta} = argmin \ \ Tr\{(\mathbf{I} - \mathbf{A}(\theta)\mathbf{A}(\theta)^{\#})\mathbf{E}_s \mathbf{W} \mathbf{E}_s^H\} \tag{2.16}$$

where $\mathbf{A}^{\#} = (\mathbf{A}^H \mathbf{A})^{-1} \mathbf{A}^H$.

Viberg and Ottersten [81] have shown that a class of direction finding algorithms can be approximated by this subspace fitting formulation for appropriate choices of the weighting matrix $\mathbf{W}$. For example, for the deterministic ML method $\mathbf{W} = \mathbf{\Lambda}_s - \sigma^2 \mathbf{I}$, which is implemented using the empirical values of the signal eigenvalues, $\mathbf{\Lambda}_s$, and the noise eigenvalue $\sigma^2$. TLS-ESPRIT, which is explained in

the next subsection, can also be formulated in a similar but more involved way. Viberg and Ottersten have also derived an optimal Weighted Subspace Fitting (WSF) Method, which yields the smallest estimation error variance among the class of subspace fitting methods. In WSF

$$\mathbf{W} = (\mathbf{\Lambda}_s - \sigma^2\mathbf{I})^2\mathbf{\Lambda}_s^{-1} \tag{2.17}$$

The WSF method works regardless of the source covariance (including coherence) and has been shown to have the same asymptotic properties as the stochastic ML method; hence, it is asymptotically efficient for Gaussian signals (i.e., it achieves the stochastic CRB). Its behavior in the finite sample case may be different from the asymptotic case [81]. Viberg and Ottersten have also shown that the asymptotic properties of the WSF estimates are identical for both cases of Gaussian and non-Gaussian sources. They have also developed a consistent detection method for arbitrary signal correlation, and an algorithm for minimizing the WSF criterion. They do point out several practical implementation problems of their method, such as the need for accurate calibrations of the array manifold and knowledge of the derivative of the steering vectors w.r.t $\theta$. For nonlinear and nonuniform arrays, multidimensional search methods are required for SSF, hence it is computationally expensive.

#### 2.2.1.b Algebraic methods

Algebraic methods do not require a search procedure and yield DOA estimates directly.

**ESPRIT (Estimation of Signal Parameters via Rotational Invariance Techniques) [55, 65] :**

The ESPRIT Algorithm has a fundamental advantage over the other methods being that calibration of the array is not required. However, ESPRIT is applicable only to arrays which are "translationally invariant", i.e., arrays which consist of a subarray and its *identical copy* displaced in space with a known distance. The responses of the sensors do not have to be known and the geometry of the subarray may be arbitrary, only the measurements, and the displacement between

the identical arrays are required. The computational complexity of ESPRIT is less than that of the search-based methods.

Let $\mathbf{r}^1(t)$ and $\mathbf{r}^2(t)$ be the measurements from these arrays. Due to the displacement of the arrays the following holds:

$$\begin{aligned} \mathbf{r}^1(t) &= \mathbf{A}\mathbf{s}(t) + \mathbf{n}_1(t) \\ \mathbf{r}^2(t) &= \mathbf{A}\mathbf{\Phi}\mathbf{s}(t) + \mathbf{n}_2(t) \end{aligned} \tag{2.18}$$

where $\mathbf{\Phi} = diag\{e^{-j2\pi\frac{d}{\lambda}\sin\theta_1}, \cdots, e^{-j2\pi\frac{d}{\lambda}\sin\theta_P}\}$ in which $d$ is the separation between the identical arrays, and the angles $\{\theta_i\}_{i=1}^P$ are measured with respect to the normal to the displacement vector between the identical arrays.

Note that the auto covariance of $\mathbf{r}^1(t)$, $\mathbf{R}^{11}$, and the cross covariance between $\mathbf{r}^1(t)$ and $\mathbf{r}^2(t)$, $\mathbf{R}^{21}$, are given by

$$\mathbf{R}^{11} = \mathbf{A}\mathbf{D}\mathbf{A}^H + \mathbf{R}_{n_1} \tag{2.19}$$

and

$$\mathbf{R}^{21} = \mathbf{A}\mathbf{\Phi}\mathbf{D}\mathbf{A}^H + \mathbf{R}_{n_2 n_1} \tag{2.20}$$

where $\mathbf{D}$ is the covariance matrix of the sources, and $\mathbf{R}_{n_1}$ and $\mathbf{R}_{n_2 n_1}$ are the autocovariance of $\mathbf{n}_1$ and cross-covariance of $\mathbf{n}_1$ and $\mathbf{n}_2$, respectively.

The ESPRIT algorithm solves for $\mathbf{\Phi}$, which then gives the bearing estimates. Although the subspace separation concept is not used in ESPRIT, its LS and TLS versions are based on a signal subspace formulation. The LS and TLS versions are more complicated, but are more accurate than the original ESPRIT, and are summarized in the next subsection. Here we summarize the original ESPRIT:
(1) Estimate the autocovariance of $\mathbf{r}^1(t)$ and cross covariance between $\mathbf{r}^1(t)$ and $\mathbf{r}^2(t)$, as

$$\mathbf{R}^{11} = \frac{1}{N}\sum_{t=1}^{N}\mathbf{r}^1(t)\mathbf{r}^1(t)^H \tag{2.21}$$

$$\mathbf{R}^{21} = \frac{1}{N}\sum_{t=1}^{N}\mathbf{r}^2(t)\mathbf{r}^1(t)^H. \tag{2.22}$$

(2) Calculate

$$\hat{\mathbf{R}}^{11} = \mathbf{R}^{11} - \mathbf{R}_{n_1} \tag{2.23}$$

$$\hat{\mathbf{R}}^{21} = \mathbf{R}^{21} - \mathbf{R}_{n_2 n_1} \tag{2.24}$$

where $\mathbf{R}_{n_1}$ and $\mathbf{R}_{n_2 n_1}$ are either known or estimated.

(3) Find the singular values $\lambda_i$ of the matrix pencil

$$\hat{\mathbf{R}}^{11} - \lambda_i \hat{\mathbf{R}}^{21}, \quad i = 1, \cdots, P \tag{2.25}$$

(4) The bearings, $\theta_i$ $(i = 1, \cdots, P)$, are readily obtained by solving the equation

$$\lambda_i = e^{j2\pi \frac{d}{\lambda} \sin\theta_i}. \tag{2.26}$$

for $\theta_i$.

**LS and TLS ESPRIT [65]:**

(1) Follow Steps 1 and 2 of ESPRIT.

(2) Stack $\hat{\mathbf{R}}^{11}$ and $\hat{\mathbf{R}}^{21}$ into a $2M \times M$ matrix $\mathbf{R}$, as follows:

$$\mathbf{R} \triangleq \begin{bmatrix} \hat{\mathbf{R}}^{11} \\ \hat{\mathbf{R}}^{21} \end{bmatrix} \tag{2.27}$$

and, perform an SVD of $\mathbf{R}$, keeping the first $2M \times P$ submatrix of the left singular vectors of $\mathbf{R}$. Let this submatrix be $\mathbf{E}_s$.

(3) Partition $\mathbf{E}_s$ into two $M \times P$ matrices $\mathbf{E}_{s1}$ and $\mathbf{E}_{s2}$ such that $\mathbf{E}_s = \begin{bmatrix} \mathbf{E}_{s1} \\ \mathbf{E}_{s2} \end{bmatrix}$.

(4) For LS-ESPRIT, calculate the eigendecomposition of $(\mathbf{E}_{s1}^H \mathbf{E}_{s1})^{-1} \mathbf{E}_{s1}^H \mathbf{E}_{s2}$. The eigenvalue matrix gives $\mathbf{\Phi} = diag\{e^{-j2\pi \frac{d}{\lambda} \sin\theta_1}, \cdots, e^{-j2\pi \frac{d}{\lambda} \sin\theta_P}\}$ from which the arrival angles are readily obtained. For TLS-ESPRIT, proceed as follows:

(5) Perform an SVD of the $M \times 2P$ matrix $[\mathbf{E}_{s1}, \mathbf{E}_{s2}]$, and stack the last $P$ right singular vectors of $[\mathbf{E}_{s1}, \mathbf{E}_{s2}]$ into a $2P \times P$ matrix denoted $\mathbf{F}$.

(6) Partition $\mathbf{F}$ as $\mathbf{F} \triangleq \begin{bmatrix} \mathbf{F}_x \\ \mathbf{F}_y \end{bmatrix}$ where $\mathbf{F}_x$ and $\mathbf{F}_y$ are $P \times P$ .

(7) Perform the eigendecomposition of $-\mathbf{F}_x \mathbf{F}_y^{-1}$. The eigenvalue matrix gives

$\Phi = diag\{e^{-j2\pi\frac{d}{\lambda}\sin\theta_1}, \cdots, e^{-j2\pi\frac{d}{\lambda}\sin\theta_P}\}$ from which the arrival angles are readily obtained.

Different versions of ESPRIT have different statistical properties. The Toeplitz Approximation Method (TAM) [38], in which the array measurement model is represented as a state-variable model, although different in implementation from LS-ESPRIT, is equivalent to LS-ESPRIT; hence, it has the same error variance as LS-ESPRIT.

A performance analysis of LS-ESPRIT for finite amount of data and the high SNR case is presented by [45], and an expression is derived for the variance of the DOA estimates with respect to perturbations in the assumed model due to various factors such as finite sampling effects, calibration errors, and noise modeling inaccuracies. Asymptotic variances of the DOA estimates obtained from LS-ESPRIT and TLS-ESPRIT are derived in [60] and [53], respectively. Rao and Hari [60] note that the LS and TLS versions of ESPRIT have the same asymptotic accuracies; however, TLS-ESPRIT converges faster than LS-ESPRIT and may be better for low SNR and short data lengths. In [53], the CRB is derived for the DOA estimation error in the ESPRIT problem, and the TLS-ESPRIT algorithm is shown, by numerical examples, to attain the CRB for the special case of a uniform linear array and Gaussian sources. They also remark that the performance of TLS-ESPRIT deviates from the CRB for highly correlated sources.

The asymptotic performance of a generalized class of ESPRIT algorithms, referred to as *subspace rotation (SR) methods* is compared to the MUSIC algorithm in [74]; they show that the variance of SR methods (including LS-ESPRIT) can not be less than that of MUSIC; hence, the SR methods are less efficient than the MUSIC algorithm especially for large arrays and large samples. They also propose an optimally weighted SR method which can achieve the same performance as MUSIC.

**Generalized Eigenvalues Utilizing Signal Subspace Eigenvectors (GEESE):**
(1) Follow Steps 1-3 of TLS ESPRIT.

(2) Find the singular values $\lambda_i$ of the pencil

$$\mathbf{E}_{s1} - \lambda_i \mathbf{E}_{s2}, \quad i = 1, \cdots, P \tag{2.28}$$

(3) The bearings, $\theta_i$ $(i = 1, \cdots, P)$, are readily obtained from

$$\lambda_i = e^{j2\pi \frac{d}{\lambda} \sin\theta_i}. \tag{2.29}$$

The GEESE method [56] is claimed to be better than ESPRIT.

### 2.2.2 Noise Subspace Methods

These methods, in which only the noise subspace information is retained, are based on the property that the steering vectors are orthogonal to any linear combination of the noise subspace eigenvectors. Noise subspace methods are also divided into search-based and algebraic methods, which are explained next.

#### 2.2.2.a Search-based methods

In search-based methods, the array manifold is assumed to be known, and the arrival angles are estimated by locating the peaks of the function

$$S(\theta) = \frac{1}{\mathbf{a}(\theta)^H \mathbf{N} \mathbf{a}(\theta)} \tag{2.30}$$

where $\mathbf{N}$ is a matrix formed using the noise space eigenvectors.

**Pisarenko method:**

In this method,

$$\mathbf{N} = \mathbf{e}_M \mathbf{e}_M{}^H \tag{2.31}$$

where $\mathbf{e}_M$ is the eigenvector corresponding to the minimum eigenvalue of $\mathbf{R}$. If the minimum eigenvalue is repeated, any unit-norm vector which is a linear combination of the eigenvectors corresponding to the minimum eigenvalue can be used as $\mathbf{e}_M$. The basis of this method is that when the search angle $\theta$ corresponds to an actual arrival angle, the denominator of (2.30), $|\mathbf{a}(\theta)^H \mathbf{e}_M|^2$, becomes small due to orthogonality of steering vectors and noise subspace eigenvectors; hence, $S(\theta)$

will peak at an arrival angle.

**MUSIC (Multiple Signal Classification) [67] method:**

In this method,

$$\mathrm{N} = \sum_{i=P+1}^{M} \mathbf{e}_i \mathbf{e}_i^H \tag{2.32}$$

The idea is similar to that of the Pisarenko method; the inner product $|\mathbf{a}(\theta)^H \sum_{i=P+1}^{M} \mathbf{e}_i|^2$ is small when $\theta$ is an actual arrival angle. The MUSIC spectrum is equivalent to the MV method using the exact covariance matrix when SNR is infinite, and therefore performs better than the MV method.

Asymptotic properties of MUSIC are well established [75, 76, 74, 73, 24, 57, 78, 87, 79], e.g., MUSIC is known to have the same asymptotic variance as the deterministic ML method for uncorrelated sources. Expressions for the variance of the bearing estimates were derived for finite number of samples, by Li and Vaccaro [45] for high SNR case, and by Stoica and Nehorai [75] without restriction to high SNR. Xu and Buckley [86] present a bias analysis of the MUSIC bearing estimates for a wide range of SNR values. It is shown by Xu and Buckley that although, asymptotically, bias is insignificant compared to standard deviation, it is an important factor limiting the performance for resolving closely spaced sources when they are correlated.

In order to overcome the problems due to finite sample effects and source correlation, a multidimensional (MD) version of MUSIC has been proposed [67, 65, 4]; however, this approach involves a computationally involved search, as in the ML method. MD MUSIC can be interpreted as a norm minimization problem, as shown in [21]; using this interpretation, strong consistency of MD MUSIC has been demonstrated. An optimally weighted version of MD MUSIC, which outperforms the deterministic ML method, has also been proposed in [82].

**Eigenvector (EV) method:**

In this method,

$$\mathrm{N} = \sum_{i=P+1}^{M} \frac{1}{\lambda_i} \mathbf{e}_i \mathbf{e}_i^H \tag{2.33}$$

The only difference between the EV method and MUSIC is the use of inverse eigenvalue [the $\lambda_i$ are the noise subspace eigenvalues of $\mathbf{R}$ (see (2.6))] weighting in

EV and unity weighting in MUSIC, which causes EV to yield fewer spurious peaks than MUSIC [35]. The EV Method is also claimed to shape the noise spectrum better than MUSIC.

**Method of Direction Estimation (MODE):**

MODE is equivalent to WSF when there are no coherent sources. Viberg and Ottersten [82] claim that, for coherent sources, only WSF is asymptotically efficient. A minimum norm interpretation and proof of strong consistency of MODE for ergodic and stationary signals, has also been reported [21]. The norm measure used in that work involves the source covariance matrix. By contrasting this norm with the Frobenius norm that is used in MD MUSIC, Ephraim *et al* [21] relate MODE and MD MUSIC.

**Minimum-Norm [37] method:**

In this method, the matrix $\mathbf{N}$ is obtained as follows [33]:

(1) Form

$$\mathbf{E}_n = [\mathbf{e}_{P+1}, \cdots, \mathbf{e}_M], \tag{2.34}$$

(2) Partition $\mathbf{E}_n$,

$$\mathbf{E}_n = \begin{bmatrix} \mathbf{c}^T \\ \mathbf{C} \end{bmatrix}, \tag{2.35}$$

to establish $\mathbf{c}$ and $\mathbf{C}$.

(3) Compute

$$\mathbf{d} = \begin{bmatrix} 1 \\ (\mathbf{c}^H\mathbf{c})^{-1}\mathbf{C}^*\mathbf{c} \end{bmatrix}, \tag{2.36}$$

and, finally,

$$\mathbf{N} = \mathbf{d}\mathbf{d}^H. \tag{2.37}$$

For two closely spaced, equal power signals, the Minimum Norm method has been shown to have a lower SNR threshold (i.e., the minimum SNR required to separate the two sources) than MUSIC [36]. Li and Vaccaro [45] derive and compare the mean-squared errors of the DOA estimates from Minimum Norm and MUSIC

algorithms due to finite sample effects, calibration errors, and, noise modeling errors for the case of finite samples and high SNR. They show that mean-squared errors for DOA estimates produced by the MUSIC algorithm are always lower than the corresponding mean-squared errors for the Minimum Norm algorithm.

#### 2.2.2.b Algebraic methods

When the array is uniform linear, so that $\mathbf{a}(\theta)$ is given by (2.10), the search in (2.30) for the peaks can be replaced by a root-finding procedure which yields the arrival angles. So doing, results in better resolution than the search-based alternative, because the root-finding procedure can give distinct roots corresponding to each source whereas the search function may not have distinct maxima for closely spaced sources. In addition, the computational complexity of algebraic methods is lower than that of the search-based ones. The algebraic version of MUSIC is given next; for algebraic versions of Pisarenko, EV and Minimum-Norm, the matrix $\mathbf{N}$ in (2.38) is replaced by (2.31), (2.33) and (2.37), respectively.

**Root-MUSIC:**

In root-MUSIC, the array is required to be uniform linear, and the search procedure in MUSIC is converted into the following root-finding approach:

(1) Form the $M \times M$ matrix

$$\mathbf{N} = \sum_{i=P+1}^{M} \mathbf{e}_i \mathbf{e}_i^H, \tag{2.38}$$

(2) Form a polynomial $p(z)$ of degree $2M-1$ which has for its $i$th coefficient $c_i = tr_i[\mathbf{N}]$, where $tr_i$ denotes the trace of the $i$th diagonal, and $i = -(M-1), \cdots, 0, \cdots, M-1$. Note that $tr_0$ denotes the main diagonal, $tr_1$ denotes the first super-diagonal, and $tr_{-1}$denotes the first sub-diagonal.

(3) The roots of $p(z)$ exhibit inverse symmetry with respect to the unit circle in the $z$-plane. Express $p(z)$ as the product of two polynomials $p(z) = h(z)h^*(z^{-1})$,

(4) Find the roots $z_i$ $(i = 1, \cdots, M)$ of $h(z)$. The angles of the roots that are very close to (or, ideally on) the unit circle yield the direction of arrival estimates, as $\theta_i = \sin^{-1}(\frac{\lambda}{2\pi d} \angle z_i)$, where $i = 1, \cdots, P$.

The root-MUSIC algorithm has been shown to have better resolution power

than MUSIC [61]; however, as mentioned previously, root-MUSIC is restricted to uniform linear arrays. Steps (2)-(4) make use of this knowledge. Li and Vaccaro [45] show that algebraic versions of the MUSIC and Minimum Norm algorithms have the same mean-squared errors as their search-based versions for finite samples and high SNR case. The advantages of root-MUSIC over search-based MUSIC is increased resolution of closely spaced sources and reduced computations.

### 2.2.3 Spatial Smoothing

When there are coherent signals, $rank(\mathbf{R}_s)$, and consequently $rank(\mathbf{R})$ is less than $P$, and hence the above described subspace methods fail. If the array is uniform linear, then by applying the spatial smoothing method [22, 71], described below, a new rank-$P$ matrix is obtained which can be used in place of $\mathbf{R}$ in any of the subspace methods described earlier.

Spatial smoothing starts by dividing the $M$-vector $\mathbf{r}(t)$ of the ULA into $K = M - S + 1$ overlapping subvectors of size $S$, $\mathbf{r}^f_{S,k}$ $(k = 1, \cdots, K)$, with elements $\{r_k, \cdots, r_{k+S-1}\}$, and $\mathbf{r}^b_{S,k}$ $(k = 1, \cdots, K)$, with elements $\{r^*_{M-k+1}, \cdots, r^*_{M-S-k+2}\}$. Then, a forward and backward spatially smoothed matrix $\mathbf{R}^{fb}$ is calculated as

$$\mathbf{R}^{fb} = \frac{1}{KN} \sum_{t=1}^{N} \sum_{k=1}^{K} (\mathbf{r}^f_{S,k}(t) {\mathbf{r}^f_{S,k}}^H(t) + \mathbf{r}^b_{S,k}(t) {\mathbf{r}^b_{S,k}}^H(t)) \tag{2.39}$$

The rank of $\mathbf{R}^{fb}$ is $P$ if there are at most $2M/3$ coherent sources. $S$ must be selected such that $P_c + 1 \leq S \leq M - P_c/2 + 1$ in which $P_c$ is the number of coherent sources. Then, any subspace-based method can be applied to $\mathbf{R}^{fb}$ to determine the directions of arrival. It is also possible to do spatial smoothing based only on $\mathbf{r}^f_{S,k}$ or $\mathbf{r}^b_{S,k}$, but in this case at most $M/2$ coherent sources can be handled.

### 2.2.4 Discussion

The application of all the subspace-based methods requires exact knowledge of the number of signals, in order to separate the signal and noise subspaces. The number

of signals can be estimated from the data using either the Akaike Information Criterion (AIC) [83] or Minimum Descriptive Length (MDL) [84] methods. The effect of underestimating the number of sources is analysed in [59], whereas the case of overestimating the number of signals can be treated as a special case of the analysis in [76].

The second-order methods described above have the following disadvantages: (1) Except for ESPRIT, all of the above methods require calibration of the array which means that the response of the array for every possible combination of the source parameters should be measured and stored; or, analytical knowledge of the array response is required. However, at any time, the antenna response can be different from when it was last calibrated due to environmental effects such as weather conditions for radar, or water waves for sonar. Even if the analytical response of the array elements are known, it may be impossible to know or track the precise locations of the elements in some applications (e.g., towed array). Consequently, these methods are sensitive to errors and perturbations in the array response. In addition, physically identical sensors may not respond identically in practice due to lack of synchronization or imbalances in the associated electronic circuitry. (2) In deriving the above methods it was assumed that the noise covariance structure is known; however, it is often unrealistic to assume that the noise statistics are known due to several reasons. In practice, the noise is not isolated; it is often observed along with the signals. Moreover, as stated in [78], there are noise phonemena effects which can not be modeled accurately, e.g., channel crosstalk, reverberation, near-field, wide-band and distributed sources. (3) None of the methods in Sections 2.2.1 and 2.2.2, except for the WSF method, work when there are coherent (completely correlated) sources. Only if the array is uniform linear, the spatial smoothing method in Section 2.2.3 can be used. On the other hand, higher-order statistics of the received signals can be exploited to develop direction finding methods which have less restrictive requirements.

## 2.3 Higher-Order Statistics-Based Methods

The higher-order statistical direction finding methods use the spatial cumulant matrices of the array. They require that the source signals be non-Gaussian so that their higher- than second order statistics convey extra information. Most communication signals are symmetrically distributed and hence their third-order cumulants vanish; therefore, even-order cumulants are used, and, usually fourth-order cumulants are employed. The fourth-order cumulant of the source signals must be nonzero in order to use these methods. One important feature of cumulant-based methods is that they can suppress Gaussian noise regardless of its coloring. Consequently, the requirement of having to estimate the noise covariance, as in second-order statistical processing methods, is avoided in cumulant-based methods. It is also possible to suppress non-Gaussian noise, [18], and, when properly applied, cumulants extend the aperture of an array [17, 69] which means that more sources than sensors can be detected. On the other hand, sample estimates of higher-order statistics require longer data lengths than covariances; hence, computational complexity is increased. As in the second-order statistics-based methods, the number of sources is estimated from the data before applying any higher-order statistics-based direction finding method.

The fourth-order moments of the signal $\mathbf{s}(t)$ are

$$E\{s_i s_j^* s_k s_l^*\} \quad 1 \leq i,j,k,l \leq P \tag{2.40}$$

and the fourth-order cumulants are defined as

$$\begin{aligned} c_{4,s}(i,j,k,l) \triangleq cum(s_i, s_j^*, s_k, s_l^*) &= E\{s_i s_j^* s_k s_l^*\} - E\{s_i s_j^*\}E\{s_k s_l^*\} \\ &\quad -E\{s_i s_l^*\}E\{s_k s_j^*\} - E\{s_i s_j\}E\{s_k^* s_l^*\} \end{aligned} \tag{2.41}$$

where $1 \leq i,j,k,l \leq P$. Note that two arguments in the above fourth-order moments and cumulants are conjugated and the other two are unconjugated. For circularly symmetric signals, which is often the case in communication applications, the last term in (2.42) is zero.

In practice, sample estimates of the cumulants are used in place of the theoretical cumulants, and these sample estimates are obtained from the received signal vector $\mathbf{r}(t)$ $(t = 1, \cdots, N)$ as follows:

$$\begin{aligned} \hat{c}_{4,r}(i,j,k,l) &= \frac{1}{N}\sum_{t=1}^{N} r_i(t) r_j^*(t) r_k(t) r_l^*(t) \\ &- \frac{1}{N^2}\sum_{t=1}^{N} r_i(t) r_j^*(t) \sum_{t=1}^{N} r_k(t) r_l^*(t) - \frac{1}{N^2}\sum_{t=1}^{N} r_i(t) r_l^*(t) \sum_{t=1}^{N} r_k(t) r_j^*(t) \end{aligned} \tag{2.42}$$

where $1 \leq i, j, k, l \leq M$. Note that the last term in (2.42) is zero, and therefore, it is omitted.

Higher-order statistical subspace methods use fourth-order spatial cumulant matrices of the array output, which can be obtained in a number of ways by suitably selecting the arguments $i, j, k, l$ of $c_{4,r}(i, j, k, l)$. Existing methods for the selection of the cumulant matrix, and their associated processing schemes are summarized next.

**Pan-Nikias [54] and Cardoso-Moulines [6] method:**
In this method, the array needs to be calibrated, or its response must be known in analytical form. The source signals are assumed to be independent or partially correlated [i.e, there are no coherent signals]. The method is as follows:
(1) An estimate of an $M \times M$ fourth-order cumulant matrix $\mathbf{C}$ is obtained from the data. The following two selections for $\mathbf{C}$ are possible [6]:

$$c_{ij} = c_{4,r}(i, j, j, j) \quad 1 \leq i, j \leq M \tag{2.43}$$

or

$$c_{ij} = \sum_{m=1}^{M} c_{4,r}(i, j, m, m) \quad 1 \leq i, j \leq M \tag{2.44}$$

Using cumulant properties [47], and (2.1), and $a_{ij}$ for the $ij$th element of $\mathbf{A}$, it is easy to verify that (2.43) becomes

$$c_{ij} = \sum_{p=1}^{P} a_{ip} \sum_{q,r,s=1}^{P} a_{jq}^* a_{jr} a_{js}^* c_{4,s}(p, q, r, s), \tag{2.45}$$

which, in matrix format, is

$$\mathbf{C} = \mathbf{AB} \tag{2.46}$$

where $\mathbf{A}$ is the steering matrix and $\mathbf{B}$ is a $P \times M$ matrix with elements

$$b_{ij} = \sum_{q,r,s=1}^{P} a_{jq}{}^{*} a_{jr} a_{js}{}^{*} c_{4,s}(i,q,r,s). \tag{2.47}$$

Similarly, (2.44) becomes

$$c_{ij} = \sum_{p,q=1}^{P} a_{ip} \left( \sum_{r,s=1}^{P} \sum_{m=1}^{M} a_{mr} a_{ms}{}^{*} c_{4,s}(p,q,r,s) \right) a_{jq}{}^{*} \; 1 \leq i,j \leq M \tag{2.48}$$

which, in matrix form can be expressed as

$$\mathbf{C} = \mathbf{ADA}^{H} \tag{2.49}$$

where $\mathbf{D}$ is a $P \times P$ matrix with elements

$$d_{ij} = \sum_{r,s=1}^{P} \sum_{m=1}^{M} a_{mr} a_{ms}{}^{*} c_{4,s}(i,j,r,s). \tag{2.50}$$

Note that additive Gaussian noise is suppressed in (2.46) and (2.49), because higher than second-order statistics of a Gaussian process are zero.

(2) The $P$ left singular vectors of the cumulant matrix in (2.46) corresponding to nonzero singular values, or the $P$ eigenvectors of the cumulant matrix in (2.49) corresponding to nonzero eigenvalues form the signal subspace. The orthogonal complement of the signal subspace gives the noise subspace. Any of the Section 2.2 covariance-based search and algebraic DF methods (except for the EV method and ESPRIT) can now be applied (in exactly the same way as described in Section 2.2) either by replacing the signal and noise subspace eigenvectors and eigenvalues of the array covariance matrix by the corresponding subspace eigenvectors and eigenvalues of (2.49), or by the corresponding subspace singular vectors and singular values of (2.46). A cumulant-based analog of the EV method does not exist, because the eigenvalues and singular values of (2.49) and (2.46) corresponding to the noise subspace are theoretically zero. The cumulant-based

analog of ESPRIT is explained later.

The same assumptions and restrictions for the covariance-based methods apply to their analogs in the cumulant domain. The advantage of using the cumulant-based analogs of these methods is that there is no need to know or estimate the noise-covariance matrix.

The asymptotic covariance of the DOA estimates obtained by MUSIC based on the above fourth-order cumulant matrices are derived in [6] for the case of Gaussian measurement noise with arbitrary spatial covariance, and are compared to the asymptotic covariance of the DOA estimates from the covariance-based MUSIC algorithm. Cardoso and Moulines [6] show that covariance- and fourth-order cumulant-based MUSIC have similar performance for the high SNR case, and that, as SNR decreases below a certain SNR threshold, the variances of the fourth-order cumulant-based MUSIC DOA estimates increase with the fourth power of the reciprocal of the SNR, whereas the variances of covariance-based MUSIC DOA estimates increase with the square of the reciprocal of the SNR. They also observe that for high SNR and uncorrelated sources, the covariance-based MUSIC DOA estimates are uncorrelated, and the asymptotic variance of any particular source depends only on the power of that source (i.e., it is independent of the powers of the other sources). They observe, on the other hand, that DOA estimates from cumulant-based MUSIC, for the same case, are correlated, and the variance of the DOA estimate of a weak source increases in the presence of strong sources. This observation limits the use of cumulant-based MUSIC when the sources have a high dynamic range, even for the case of high SNR. Cardoso and Moulines state that this problem may be alleviated when the source of interest has a large fourth-order cumulant.

**Porat and Friedlander [58] method:**

In this method, the array also needs to be calibrated, or its response is required in analytical form. The model used in this method divides the sources into groups that are partially correlated (but, not coherent) within each group, but are statistically independent across the groups, i.e.,

$$\mathbf{r}(t) = \sum_{g=1}^{G} \mathbf{A}_g \mathbf{s}_g + \mathbf{n}(t) \tag{2.51}$$

where $G$ is the number of groups each having $p_g$ sources ($\sum_{g=1}^{G} p_g = P$). In this model, the $p_g$ sources in the $g$th group are partially correlated, and they are received from different directions. The method is as follows:
(1) Estimate the fourth-order cumulant matrix, $\mathbf{C}_r$, of $\mathbf{r}(t) \otimes \mathbf{r}(t)^*$ where $\otimes$ denotes the Kronecker product. It can be verified that

$$\mathbf{C}_r = \sum_{g=1}^{G} (\mathbf{A}_g \otimes \mathbf{A}^*{}_g) \mathbf{C}_{s_g} (\mathbf{A}_g \otimes \mathbf{A}^*{}_g)^H \tag{2.52}$$

where $\mathbf{C}_{s_g}$ is the fourth-order cumulant matrix of $\mathbf{s}_g$. The rank of $\mathbf{C}_r$ is $\sum_{g=1}^{G} {p_g}^2$, and since $\mathbf{C}_r$ is $M^2 \times M^2$, it has $M^2 - \sum_{g=1}^{G} {p_g}^2$ zero eigenvalues which correspond to the noise subspace. The other eigenvalues corrrespond to the signal subspace.
(2) Compute the SVD of $\mathbf{C}_r$ and identify the signal and noise subspace singular vectors. Now, second-order subspace-based search methods can be applied, using the signal or noise subspaces, by replacing the array response vector $\mathbf{a}(\theta)$ by $\mathbf{a}(\theta) \otimes \mathbf{a}^*(\theta)$.

The eigendecomposition in this method has computational complexity $O(M^6)$ due to the Kronecker product, whereas the second-order statistical-based methods (e.g., MUSIC) have complexity $O(M^3)$.

**Chiang and Nikias [11] method:**

This method uses the ESPRIT algorithm and requires an array with its entire identical copy displaced in space by distance $d$; however, no calibration of the array is required. The signals $\mathbf{r}^1(t)$ and $\mathbf{r}^2(t)$ received by these arrays are given by (2.18).
(1) Two $M \times M$ matrices $\mathbf{C}^1$ and $\mathbf{C}^2$ are generated as follows:

$$c^1{}_{ij} = cum({r^1}_i, {r^1}_j{}^*, {r^1}_k, {r^1}_k{}^*) \quad 1 \leq i, j, k \leq M \tag{2.53}$$

and

$$c^2{}_{ij} = cum({r^2}_i, {r^1}_j{}^*, {r^1}_k, {r^1}_k{}^*) \quad 1 \leq i, j, k \leq M. \tag{2.54}$$

It can be shown that

$$c^1{}_{ij} = \sum_{p,s=1}^{P} a_{ip} \left( \sum_{q,r=1}^{P} a_{kq} a_{kr}{}^* c_{4,s}(p,q,r,s) \right) a_{js} \tag{2.55}$$

and

$$c^2{}_{ij} = \sum_{p,s=1}^{P} a_{ip} \exp^{-j2\pi \frac{d}{\lambda} \sin(\theta_p)} \left( \sum_{q,r=1}^{P} a_{kq} a_{kr}{}^* c_{4,s}(p,q,r,s) \right) a_{js} \tag{2.56}$$

These relations can be expressed, in matrix form, as

$$\mathbf{C}^1 = \mathbf{A}\mathbf{E}\mathbf{A}^H \tag{2.57}$$

and

$$\mathbf{C}^2 = \mathbf{A}\mathbf{\Phi}\mathbf{E}\mathbf{A}^H \tag{2.58}$$

where $\mathbf{\Phi} = diag\{e^{-j2\pi \frac{d}{\lambda} \sin\theta_1}, \cdots, e^{-j2\pi \frac{d}{\lambda} \sin\theta_P}\}$ in which $d$ is the separation between the identical arrays, and $\mathbf{E}$ is a $P \times P$ matrix with $e_{ij} = \sum_{q,r=1}^{P} a_{kq} a_{kr}{}^* c_{4,s}(i,q,r,j)$. (2) Note that these equations are in the same form as (2.19) and (2.20) for covariance-based ESPRIT [the noise cumulants do not appear in (2.57) and (2.58) because the fourth-order cumulants of Gaussian noises are zero]; therefore, any version of ESPRIT or GEESE can be used to solve for $\mathbf{\Phi}$ by replacing $\mathbf{R}^{11}$ and $\mathbf{R}^{21}$ by $\mathbf{C}^1$ and $\mathbf{C}^2$, respectively.

**Virtual Cross Correlation Computer ($VC^3$) [17]:**

In $VC^3$, the source signals are assumed to be statistically independent. The idea of $VC^3$ can be demonstrated as follows: Suppose we have 3 identical sensors as in Fig. 4.1, where $r_1(t)$, $r_2(t)$ and $r_3(t)$ are measurements, and, $\vec{d_1}$, $\vec{d_2}$ and $\vec{d_3}$ ($\vec{d_3} = \vec{d_1} + \vec{d_2}$) are the vectors joining these sensors. Let the response of each sensor to a signal from $\theta$ be $a(\theta)$. A *virtual* sensor is one at which no measurement is actually made. Suppose that we wish to compute the correlation between the

virtual sensor $v_1(t)$ and $r_2(t)$, which (using the plane wave assumption) is

$$E\{r_2^*(t)v_1(t)\} = \sum_{p=1}^{P} |a(\theta_p)|^2 {\sigma_p}^2 e^{-j\vec{k_p}.\vec{d_3}} \tag{2.59}$$

Consider the following cumulant

$$\begin{aligned} cum(r_2^*(t), r_1(t), r_2^*(t), r_3(t)) &= \sum_{p=1}^{P} |a(\theta_p)|^4 \gamma_p e^{-j\vec{k_p}.\vec{d_1}} e^{-j\vec{k_p}.\vec{d_2}} & (2.60) \\ &= \sum_{p=1}^{P} |a(\theta_p)|^4 \gamma_p e^{-j\vec{k_p}.\vec{d_3}} & (2.61) \end{aligned}$$

which shows that the cumulant in (2.61) carries the same angular information as the cross correlation in (2.59), but for sources having different powers.

The fact that we are interested only in the directional information carried by correlations between the sensors lets us therefore interpret a cross correlation as a vector (e.g., $\vec{d_3}$), and a fourth-order cumulant as the addition of two vectors (e.g., $\vec{d_1} + \vec{d_2}$). This interpretation leads to the idea of decomposing the computation of a cross correlation into that of computing a cumulant. Doing this means that the directional information that would be obtained from the cross correlation between nonexisting sensors (or between an actual sensor and a nonexisting sensor) at certain virtual locations in the space can be obtained from a suitably defined cumulant that uses the real sensor measurements.

One advantage of virtual cross correlation computation is that it is possible to obtain a larger aperture than would be obtained by using only second-order statistics. This means that more sources than sensors can be detected using cumulants. For example, given an $M$ element uniform linear array, $VC^3$ lets its aperture be extended from $M$ to $2M-1$ sensors, so that $2M-2$ targets can be detected (rather than $M-1$) just by using the array covariance matrix obtained by $VC^3$ in any of the subspace-based search methods explained earlier. This use of $VC^3$ requires the array to be calibrated.

Another advantage of $VC^3$ is a fault tolerance capability. If sensors at certain locations in a given array fail to operate properly, these sensors can be replaced using $VC^3$.

**Virtual ESPRIT (VESPA) [17]:**

For VESPA, the array only needs two identical sensors; the rest of the array may have arbitrary and unknown geometry and response. The sources are assumed to be statistically independent. VESPA uses the ESPRIT solution applied to cumulant matrices. By choosing a suitable pair of cumulants in VESPA, the need for a copy of the entire array, as required in ESPRIT, is totally eliminated. VESPA preserves the computational advantage of ESPRIT over search-based algorithms. An example array configuration is given in Figure 4.2.

Without loss of generality, let the signals received by the identical sensor pair be $r_1$ and $r_2$. They are separated by $d$. The sensors $r_1$ and $r_2$ are collectively referred to as the *guiding sensor pair*. Let the bearings $\{\theta_1, \cdots, \theta_P\}$ be measured with respect to the normal to the line joining the identical sensors. We present VESPA in a slightly different manner than is done in [17]. The VESPA algorithm is:

(1) Two $M \times M$ matrices, $\mathbf{C}^1$ and $\mathbf{C}^2$, are generated as follows:

$$c^1{}_{ij} = cum(r_1, r_1{}^*, r_i, r_j{}^*) \quad 1 \leq i, j \leq M. \tag{2.62}$$

and

$$c^2{}_{ij} = cum(r_2, r_1{}^*, r_i, r_j{}^*) \quad 1 \leq i, j \leq M. \tag{2.63}$$

It is shown in Appendix A that

$$c^1{}_{ij} = \sum_{p,s=1}^{P} a_{ip} \left( \sum_{q,r=1}^{P} a_{1q} a_{1r}{}^* c_{4,s}(p,q,r,s) \right) a_{js}^* \tag{2.64}$$

$$= \sum_{p=1}^{P} a_{ip} a_{jp}^* |a_{1p}|^2 \gamma_{4,s_p} \tag{2.65}$$

and

$$c^2{}_{ij} = \sum_{p,s=1}^{P} a_{ip} \left( \sum_{q,r=1}^{P} a_{1q} \exp^{-j2\pi \frac{d}{\lambda} \sin(\theta_q)} a_{1r}{}^* c_{4,s}(p,q,r,s) \right) a_{js}^* \tag{2.66}$$

$$= \sum_{p=1}^{P} a_{ip} a_{jp}^* \exp^{-j2\pi \frac{d}{\lambda} \sin(\theta_p)} |a_{1p}|^2 \gamma_{4,s_p} \tag{2.67}$$

where $a_{ij}$ represents the $ij$th element of $\mathbf{A}$ and $\{\gamma_{4,s_p}\}_{p=1}^{P}$ are the fourth-order cumulants (kurtosis) of the sources. In matrix form, these relations can be expressed, as

$$\begin{aligned} \mathbf{C}^1 &= \mathbf{A}\mathbf{F}\mathbf{A}^H \\ \mathbf{C}^2 &= \mathbf{A}\mathbf{\Phi}\mathbf{F}\mathbf{A}^H \end{aligned} \tag{2.68}$$

where the $P \times P$ $\mathbf{F} \triangleq diag\{\gamma_{4,s_1}|a_{11}|^2, \cdots, \gamma_{4,s_P}|a_{1P}|^2\}$ and $\mathbf{\Phi} \triangleq \text{diag}\{e^{-j2\pi\frac{d}{\lambda}\sin(\theta_1)}, \cdots, e^{-j2\pi\frac{d}{\lambda}\sin(\theta_P)}\}$. For different arrival angles, $rank(\mathbf{A}) = rank(\mathbf{\Phi}) = P$, and $\mathbf{D}$ is full-rank provided the sources have nonzero fourth-order cumulants and the first sensor has nonzero response to the incoming wavefronts.

(2) Note that these equations are in the same form as ESPRIT and Chiang and Nikias's ESPRIT-like method; however, as opposed to their method, there is no need for an identical copy of the array; only an identical response sensor pair is necessary for VESPA. Consequently, any version of ESPRIT or GEESE can be used to solve for $\mathbf{\Phi}$ by replacing $\mathbf{R}^{11}$ and $\mathbf{R}^{21}$ by $\mathbf{C}^1$ and $\mathbf{C}^2$, respectively.

Note, also, that there exists a very close link between $VC^3$ and VESPA. Although the way we chose $\mathbf{C}^1$ and $\mathbf{C}^2$ above seems to be not very obvious, there is a unique geometric interpretation to it. According to $VC^3$, as far as the bearing information is concerned, $\mathbf{C}^1$ is equivalent to the autocorrelation matrix of the array, and $\mathbf{C}^2$ is equivalent to the cross-correlation matrix between the array and its virtual copy (which is created by displacing the array by the vector that connects the second and the first sensors).

In addition to hardware savings, VESPA has the following advantages over second order-statistics based direction finding methods: (1) Direction finding is possible with uncalibrated arrays using VESPA by just adding a pair of identical sensors; (2) Array calibration and hence sensitivity problems associated with calibration mismatch are avoided; because, VESPA is a blind (self-calibrating) method; (3) VESPA is more robust to perturbations in the array sensor positions and responses than ESPRIT, because the need to maintain two entire identical arrays is eliminated; (3) When the noise component of the signal received by one of the guiding sensor pair elements is independent of the noise processes at the other sensors, VESPA can supress the noise regardless of its distribution [18]. In

practice, however, the noise does affect the standard derivations of the direction of arrival estimates.

### 2.3.1 Discussion

The fact that higher-order statistics have more arguments than covariances leads to more practical algorithms which have less restrictions on the array structure (for instance, the requirement of maintaining identical arrays for ESPRIT is reduced to only maintaining two identical sensors for VESPA). This fact also makes it possible to detect more sources than the number of sensors with higher-order statistics-based direction finding methods, i.e, the array aperture is effectively increased. Another advantage of using higher-order statistics-based methods over second-order methods is that the covariance matrix of the noise is not needed in most cases.

A common problem with all of the above higher-order statistics-based high-resolution direction finding methods is that these methods fail to estimate the DOAs correctly when there are coherent signals, which is the case for multipath propagation. Another problem, according to the recent study [6] of Cardoso and Moulines which present a comparative performance analysis of second- and fourth-order statistics based MUSIC methods, is that dynamic range of the source powers may be a factor limiting the performance of the fourth-order statistics based MUSIC. Our simulations and result of a real-data experiment indicate that high-dynamic range of source powers presents a problem for VESPA too. In this case, the resulting direction of arrival estimates are biased toward the most powerful source.

In Chapter 3, the case of coherent signals is considered; and, a subspace-based direction-finding method using fourth-order statistics is presented. In Chapter 6, an iterative direction finding algorithm is presented which works even when the source powers are widely different.

## 2.4 Appendix-Derivation of VESPA Equations

Here, we show the details of derivations of (2.65) and (2.67). Equation (2.65) focuses on $r_1(t)$, and is:

$$\begin{aligned}
c^1{}_{ij} &= \mathrm{cum}(r_1(t), r_1^*(t), r_i(t), r_j^*(t)) \\
&= \mathrm{cum}\left(\sum_{q=1}^{P} a_{1q}s_q(t), \sum_{r=1}^{P} a_{1r}^* s_r^*(t), \sum_{p=1}^{P} a_{ip}s_p(t), \sum_{s=1}^{P} a_{js}^* s_s^*(t)\right) \\
&\quad + \mathrm{cum}(n_1(t), n_1^*(t), n_i(t), n_j^*(t)) \\
&= \sum_{q=1}^{P}\sum_{r=1}^{P}\sum_{p=1}^{P}\sum_{s=1}^{P} a_{1q}a_{1r}^* a_{ip}a_{js}^* \mathrm{cum}(s_q(t), s_r^*(t), s_p(t), s_s^*(t)) \\
&= \sum_{p=1}^{P} a_{ip}a_{jp}^* |a_{1p}|^2 \gamma_{4,s_p}
\end{aligned} \tag{2.69}$$

where $1 \le i, j \le M$. In the above derivation cumulant properties **[CP1]**,**[CP3]**, **[CP5]** and **[CP6]** in [47] were used. We also used the fact that 4th-order cumulants of a Gaussian process are zero. The last line follows from the independence of the source signals and **[CP6]**, i.e.,

$$\mathrm{cum}(s_q(t), s_r^*(t), s_p(t), s_s^*(t)) = \begin{cases} \gamma_{4,s_p} & \text{if } q = r = p = s \\ 0 & \text{otherwise} \end{cases} \tag{2.70}$$

Since the first two sensors have identical response we have

$$r_2(t) = \sum_{p=1}^{P} a_{2p}s_p(t) = \sum_{p=1}^{P} a_{1p}e^{-j2\pi\frac{d}{\lambda}\sin(\theta_p)}s_p(t) \tag{2.71}$$

Equation (2.67) focuses on $r_1(t)$ and $r_2(t)$, and is

$$\begin{aligned}
&c_{ij}^2 \mathrm{cum}(r_2(t), r_1^*(t), r_i(t), r_j^*(t)) \\
&= \mathrm{cum}\left(\sum_{q=1}^{P} a_{1q}e^{-j2\pi\frac{d}{\lambda}\cos(\theta_q)}s_q(t), \sum_{r=1}^{P} a_{1r}^* s_r^*(t), \sum_{p=1}^{P} a_{ip}s_p(t), \sum_{s=1}^{P} a_{js}^* s_s^*(t)\right) \\
&\quad + \mathrm{cum}(n_2(t), n_1^*(t), n_i(t), n_j^*(t)) \\
&= \sum_{q=1}^{P}\sum_{r=1}^{P}\sum_{p=1}^{P}\sum_{s=1}^{P} a_{1q}a_{1r}^* a_{ip}a_{js}^* e^{-j2\pi\frac{d}{\lambda}\sin(\theta_q)} \mathrm{cum}(s_q(t), s_r^*(t), s_p(t), s_s^*(t))
\end{aligned}$$

$$= \sum_{p=1}^{P} a_{ip} a_{jp}^{*} e^{-j2\pi \frac{d}{\lambda} \sin(\theta_p)} |a_{1p}|^2 \gamma_{4,s_p} \tag{2.72}$$

where $1 \leq i, j \leq M$ and $c$ is the speed of propagation of the wavefronts.

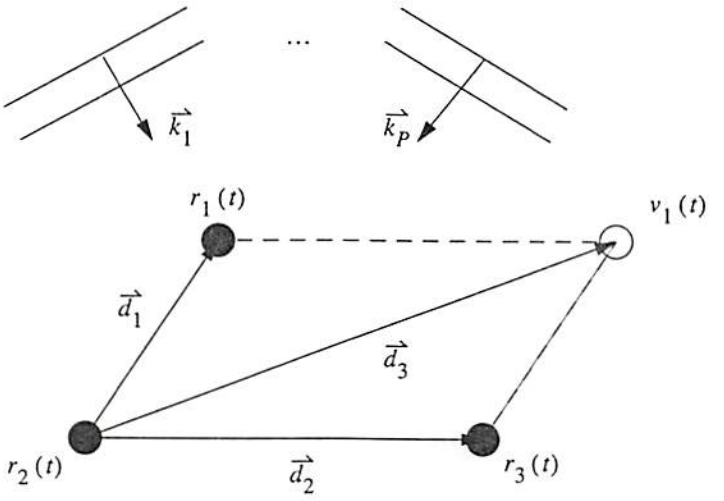


Figure 2.1: Demonstration of $VC^3$.

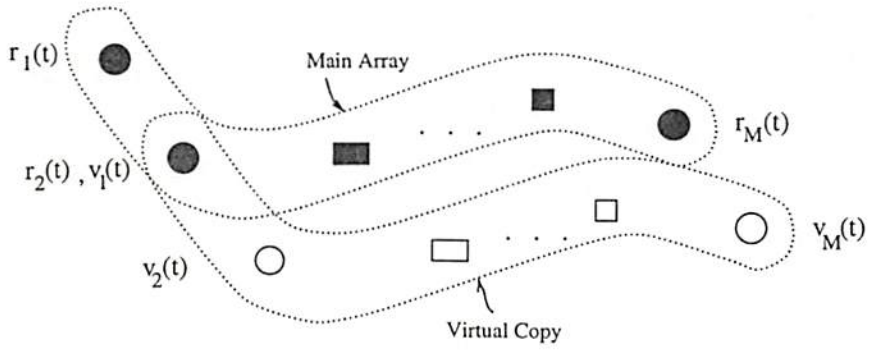


Figure 2.2: The main array and its virtual copy.

# Chapter 3

# Subspace-Based Direction Finding in Coherent Signals Case

When a signal source is close to a reflecting surface (e.g., a metallic object, building, sea surface, ground) the signal propagates through a multiplicity of paths. This phenomenon is known as *multipath* propagation. Multipaths originating from the same source are merely delayed and scaled copies of the direct path signal. In this case, when delays are short compared to the symbol duration, the source message does not change significantly, and the multipath signals are higly correlated (*coherent*). Coherent signals are also encountered in military communications when there are *smart jammers* which retrieve and retransmit signals.

In the case of coherent signals, existing subspace-based direction-finding methods, except for the WSF method [81] described in Chapter 2, fail. WSF method, on the other hand, requires a complicated multidimensional search, and it has several implementation problems, such as the need for accurate calibrations of the array and knowledge of the derivative of the steering vectors with respect to $\theta$. A variety of other solutions [15, 92, 25, 32, 71, 85, 58], were proposed to handle the coherency problem; however, these solutions are limited due to their assumptions. For example, if the array configuration is *uniform linear*, coherence can be handled using the *spatial smoothing method* of [71, 85] as a preprocessor to the usual second- and higher-order statistics methods; however, spatial smoothing is limited to uniform linear arrays and reduces the effective aperture size of the array; the

solution presented in [15, 92] requires computationally intense multidimensional search; and, [32] proposes using moving arrays. In [25] an attempt was made to generalize spatial smoothing to a class of very restrictive array geometries by using interpolated arrays; however, it was assumed that the array manifold is known, which requires array calibration. Porat and Friedlander present a modified version of their cumulant-based algorithm [58] to handle the case of coherent signals; however, their method is not practical; because, it requires selection of a highly redundant subset of fourth-order cumulants that contains $O(N^4)$ elements, and no guidelines exist for its selection; and, 2nd-, 4th- 6th- and 8th-order moments of the data are required.

In this chapter, we present an extension of VESPA for direction finding to the case of coherent sources. Our method [26], which we will refer to as *extended VESPA* throughout the chapter, is capable of resolving more signals than the second-order statistics-based spatial smoothing method, and is applicable to a larger class of arrays. A uniform linear subarray is needed; the rest of the array may have arbitrary and unknown response, and does not require calibration. In our method, the number of resolvable signals may exceed the number of sensors. On the other hand, the spatial smoothing method is limited to uniform linear arrays, and the number of resolvable signals is always less than the number of sensors.

In Section 3.1 we define the problem. A solution to the problem is presented in Section 3.2. Section 3.3 explains how the avaliable data can be used more efficiently. In Section 3.4, a theorem on non-Gaussian noise suppression is introduced. Results of simulation experiments are provided in Section 3.5. Conclusions are in Section 3.6.

## 3.1 Description of the Problem

Consider a scenario in which there are $G$ narrowband sources, $\{u_i(t)\}_{i=1}^{G}$. Suppose that each of these signals, $u_i(t)$ undergo frequency-flat multipath propagation producing a set of delayed and scaled replicas of itself, $\{s_{i,1}(t), \cdots, s_{i,p_i}(t)\}$ impinging on an M-element array from directions $\{\theta_{i,1}, \cdots, \theta_{i,p_i}\}$. In the sequel, the

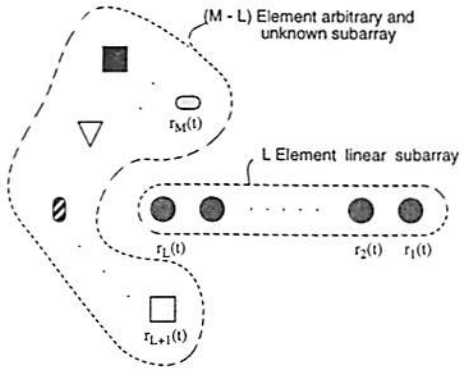


Figure 3.1: An example array configuration. There are $M$ sensors, $L$ of which are uniform linearly positioned; $r_1(t)$ and $r_2(t)$ are identical guiding sensors. Linear subarray elements are separated by $\Delta$.

collection of $p_i$ signals, $\{s_{i,1}(t), \cdots, s_{i,p_i}(t)\}$ which are coherent replicas of $u_i(t)$, will be referred to as the $i$th *group*. Let the total number of signals impinging on the array be $P$, that is $\sum_{i=1}^{G} p_i = P$. Our assumptions are: **A1)** The source signals, $\{u_i(t)\}_{i=1}^{G}$ are statistically independent, which is a valid assumption for physically separated sources; **A2)** The source signals have non-vanishing fourth-order cumulants; **A3)** The $M$ element array is composed of an $L$ element uniform linear subarray and an $M - L$ element subarray having arbitrary and unknown location and response (see Fig. 3.1); **A4)** The array is a non-ambiguous one, i.e. its response to a signal from a given direction is different from that due to another signal from a different direction; and, **A5)** The number of sources is less than the number of array elements (i.e., $G < M$). The reason for the linear subarray will be made clear below.

The signal received by the array at time $t$ is

$$\mathbf{r}(t) = \mathbf{A}\mathbf{s}(t) + \mathbf{n}(t) \tag{3.1}$$

where $\mathbf{r}(t) = [r_1(t), \cdots, r_M(t)]^T$, $\mathbf{A}$ is an $M \times P$ *unknown* steering matrix; $\mathbf{s}(t)$ is a $P \times 1$ signal vector, and $\mathbf{n}(t)$ is the independent measurement noise vector which can be Gaussian, non-Gaussian symmetrically distributed, or a mixture

of Gaussian and this type of non-Gaussian noise. We assume that $N$ snapshots taken at time points $t = 1, \cdots, N$ are available.

The coherence among the signals impinging on the array can be expressed by the following equation:

$$\mathbf{s}(t) = \begin{bmatrix} \mathbf{s}_1(t) \\ \mathbf{s}_2(t) \\ \vdots \\ \mathbf{s}_G(t) \end{bmatrix} = \begin{bmatrix} \mathbf{c}_1 & \mathbf{0} & \cdots & \mathbf{0} \\ \mathbf{0} & \mathbf{c}_2 & \cdots & \mathbf{0} \\ \vdots & \vdots & \ddots & \vdots \\ \mathbf{0} & \mathbf{0} & \cdots & \mathbf{c}_G \end{bmatrix} \begin{bmatrix} u_1(t) \\ u_2(t) \\ \vdots \\ u_G(t) \end{bmatrix} \triangleq \mathbf{Q}\mathbf{u}(t) \qquad (3.2)$$

where $\mathbf{s}_i(t) = [s_{i,1}(t), \cdots, s_{i,p_i}(t)]^T$ is a $p_i \times 1$ vector representing the coherent signals from the $i$th source, $u_i(t)$ $(1 \leq i \leq G)$; $\mathbf{c}_i = [c_{i,1}, \cdots, c_{i,p_i}]^T$ is a $p_i \times 1$ complex propagation vector for the $i$th source, which represents the amplitude and phase variations of each multipath and satisfies $\mathbf{s}_i(t) = \mathbf{c}_i u_i(t)$; and, $\mathbf{Q}$ is $P \times G$. The received signal vector, written in terms of the source signals, is:

$$\mathbf{r}(t) = \mathbf{A}\mathbf{Q}\mathbf{u}(t) + \mathbf{n}(\mathrm{t}) = \mathbf{B}\mathbf{u}(t) + \mathbf{n}(\mathrm{t}) \qquad (3.3)$$

where $\mathbf{B} \triangleq \mathbf{A}\mathbf{Q}$. Columns of $M \times G$ matrix $\mathbf{B}$ are called *generalized steering vectors.*

In this case, $rank(\mathbf{R}_s) = G < P$, and, hence $rank(\mathbf{R}) = G$ (see equation (2.2)). Consequently, Property 1 in Chapter 2 does not hold. Therefore, some of the signal eigenvectors diverge into the noise subspace. As a result, the covariance-based subspace direction finding methods described in Chapter 2 fail. If the array is *uniform linear*, then by applying the spatial smoothing method [71, 85], a new rank-$P$ matrix is obtained which can be used in place of $\mathbf{R}$ in any of these subspace methods; however, spatial smoothing is limited to uniform linear arrays and results in a less number of signals than that can be resolved with the same array under the absence of coherence. On the other hand, for VESPA, $rank(\mathbf{C}^1) = rank(\mathbf{C}^2) = G < P$ (see equation (2.68)), and, therefore, the diagonal elements of matrix $\mathbf{\Phi}$ which are obtained from VESPA are unknown functions of both the response of array and the propagation vectors. Consequently, when there are coherent signals, an explicit solution for the signal directions can not

be obtained from VESPA. In the next section, we extend VESPA to handle the coherent sources case.

## 3.2 New Solution

The solution proceeds in three steps.

### 3.2.1 Step 1: Estimate generalized steering vectors

Given two scalar processes $x_1(t)$ and $x_2(t)$ and an $M$-vector process $\mathbf{y}(t)$, we define $\text{cum}(x_1(t), x_2(t), \mathbf{y}(t), \mathbf{y}(t)^H)$ as the $M \times M$ matrix whose $ij$-th entry is $\text{cum}(x_1(t), x_2(t), y_i(t), y_j^*(t))$ where $y_i(t)$ and $y_j(t)$ are the $i$-th and $j$-th components of $\mathbf{y}(t)$, respectively. The $(m,n)$th element of $\mathbf{B}$ will be denoted by $b_{mn}$.

Let $r_1(t)$ and $r_2(t)$ represent signals recorded by a pair of sensors arbitrarily selected from the array, and suppose that the sensors are numbered accordingly, i.e., these sensors are numbered as the first and the second. First, the following fourth-order cumulant matrix is estimated from the data:

$$\begin{aligned}
\mathbf{C}_1 &\triangleq \text{cum}(r_1(t), r_1^*(t), \mathbf{r}(t), \mathbf{r}(t)^H) \\
&= \text{cum}\left(\sum_{m=1}^{G} b_{1m}u_m(t), \sum_{n=1}^{G} b_{1n}^* u_n^*(t), \sum_{i=1}^{G} \mathbf{b}_i u_i(t), \sum_{j=1}^{G} \mathbf{b}_j{}^H u_j^*(t), \right) \\
&\quad + \text{cum}(n_1(t), n_1^*(t), \mathbf{n}(t), \mathbf{n}^H(t)) \\
&= \sum_{m=1}^{G}\sum_{n=1}^{G}\sum_{i=1}^{G}\sum_{j=1}^{G} b_{1m}b_{1n}^* \mathbf{b}_i \mathbf{b}_j{}^H \text{ cum}(u_m(t), u_n^*(t), u_i(t), u_j^*(t)) \\
&= \sum_{i=1}^{G} \gamma_{4,u_i} |b_{1i}|^2 \mathbf{b}_i \mathbf{b}_i{}^H \\
&= \mathbf{B}\Lambda\mathbf{B}^H
\end{aligned} \tag{3.4}$$

where $\mathbf{b}_i$ is the $i$th column of $\mathbf{B}$, $\{\gamma_{4,u_i}\}_{i=1}^{i=G}$ are the fourth-order cumulants of the sources, and $\Lambda \triangleq diag(\gamma_{4,u_1}|b_{11}|^2, \cdots, \gamma_{4,u_G}|b_{1G}|^2)$. In the above derivation, cumulant properties **[CP1]**, **[CP3]**, **[CP5]** and **[CP6]** in Section 1.2.2 were used. Note that the cumulant of the additive Gaussian measurement noise is zero. The next to the last line of (3.4) follows from the independence of the source signals

and [CP6], i.e.,

$$\mathrm{cum}(u_m^*(t), u_n(t), u_i^*(t), u_j(t)) = \begin{cases} \gamma_{4,u_i} & \text{if } m = n = i = j \\ 0 & \text{otherwise} \end{cases} \tag{3.5}$$

Proceeding similarly, $\mathrm{cum}(r_2(t), r_1^*(t), \mathbf{r}(t), \mathbf{r}(t)^H)$ can be shown to be

$$\begin{aligned} \mathbf{C}_2 &\triangleq \mathrm{cum}(r_2(t), r_1^*(t), \mathbf{r}(t), \mathbf{r}(t)^H) \\ &= \sum_{i=1}^{G} \gamma_{4,u_i} b_{2i} b_{1i}^* \mathbf{b}_i \mathbf{b}_i^H \\ &= \mathbf{B}\mathbf{D}\mathbf{\Lambda}\mathbf{B}^H \end{aligned} \tag{3.6}$$

where $\mathbf{D} \triangleq diag(\frac{b_{21}}{b_{11}}, \cdots, \frac{b_{2G}}{b_{1G}})$.

Note that, due to assumption A4, $rank(\mathbf{B}) = G$ (i.e., full-rank) when the signals arrive at the array from different angles. Here, we assume that the first two sensors have nonzero responses to each group, i.e., the first two rows of $\mathbf{B}$ are all nonzero. Under this assumption and assumption A3, $\mathbf{D}$ and $\mathbf{\Lambda}$ are nonsingular. The case when the first two rows of $\mathbf{B}$ have zero entries is treated in Section 3.3.1.

Using (3.4) and (3.6) it is possible to estimate the matrix $\mathbf{D}$ and columns of $\mathbf{B}$ (i.e., the generalized steering vectors) each to within a complex constant.

The solution is based on the idea of rotational invariance of the underlying signal subspace which is the basis of the ESPRIT algorithm [66] and VESPA. In ESPRIT, the rotational invariance of the signal subspace is induced by the translational invariance of the array, i.e., an identical copy of the array which is displaced in the space is needed. On the other hand, in our cumulant-based algorithm, the same invariance is obtained without any need for an identical copy. In ESPRIT, the signal subspace is extracted from the eigendecomposition of the covariance matrix of the concatenated measurements from the main array and its copy. Here, the signal subspace is extracted from the singular value decomposition of the concatenated matrix of (3.4) and (3.6) which, in turn, gives $\mathbf{D}$ and the columns of $\mathbf{B}$, $\{\mathbf{b}_i\}_{i=1}^G$, each to within a complex constant.

A comparable result is not possible using just second-order statistics for arrays

having arbitrary shape and unknown response, because a spatial array covariance-matrix depends only on two arguments, whereas we need a statistic with at least three arguments to obtain matrices similar to (3.4) and (3.6). If, on the other hand, an array consists of two identical subarrays displaced in space, two covariance matrices can be obtained which have a structure similar to (3.4) and (3.6). In this case, in addition to the two arguments of the covariance matrix, one extra argument is present due to the fact that responses of identical but displaced arrays are identical up to a phase term, and, the phase term serves as the extra needed argument. Nevertheless, even in this case, ESPRIT can not be applied to these two covariance matrices if some of the incoming signals are coherent; because, the ranks of these matrices are then less than the number of incoming signals, which violates the rank condition of the ESPRIT problem. It is possible to restore the ranks of these matrices using the spatial smoothing method [71]; however, spatial smoothing is applicable only to uniform linear arrays. Consequently, existing second-order statistics based methods can not handle the coherent signals case with arrays having arbitrary and unknown geometries. Our method can.

In the Appendix, we show how the generalized steering vectors are estimated from (3.4) and (3.6) using the TLS ESPRIT algorithm.

In order to see the forest from the trees, we summarize the computational steps.

**Step 1:** From the $M \times 1$ array data, estimate the following $M \times M$ cumulant matrices:

$$\begin{aligned} \mathbf{C}_1 &\triangleq \operatorname{cum}(r_1(t), r_1^*(t), \mathbf{r}(t), \mathbf{r}^H(t)) \\ \mathbf{C}_2 &\triangleq \operatorname{cum}(r_2(t)^*, r_1^*(t), \mathbf{r}(t), \mathbf{r}^H(t)), \end{aligned} \tag{3.7}$$

and, stack these matrices into a $2M \times M$ matrix $\mathbf{C}$ as follows:

$$\mathbf{C} \triangleq \begin{bmatrix} \mathbf{C}_1 \\ \mathbf{C}_2 \end{bmatrix} \tag{3.8}$$

**Step 2:** Perform SVD of $\mathbf{C}$; keep the first $2M \times G$ submatrix of the left singular vectors of $\mathbf{C}$, where $G$ is the number of groups. Let this submatrix be $\mathbf{U}_1$.

**Step 3:** Partition $\mathbf{U}_1$ into two $M \times G$ matrices $\mathbf{U}_{11}$ and $\mathbf{U}_{12}$ as in (3.36).

**Step 4:** Perform SVD of $[\mathbf{U}_{11}, \mathbf{U}_{12}]$. Stack the last $G$ right singular vectors of $[\mathbf{U}_{11}, \mathbf{U}_{12}]$ into the $2G \times G$ matrix denoted $\mathbf{F}$.

**Step 5:** Partition $\mathbf{F}$ as $\mathbf{F} \triangleq \begin{bmatrix} \mathbf{F}_x \\ \mathbf{F}_y \end{bmatrix}$ where $\mathbf{F}_x$ and $\mathbf{F}_y$ are $G \times G$ .

**Step 6:** Perform eigendecomposition of $-\mathbf{F}_x\mathbf{F}_y^{-1}$; keep the eigenvalues. Let the eigenvector and eigenvalue matrices of $-\mathbf{F}_x\mathbf{F}_y^{-1}$ be $\mathbf{E}$ and $\mathbf{D}$, respectively.

**Step 7:** An estimate of $\mathbf{B}$ is obtained to within a diagonal matrix, as in (3.43).

Note that $r_1(t)$ and $r_2(t)$ can be chosen as any two sensor measurements in the array provided $\mathbf{D}$ and $\mathbf{\Lambda}$ in (3.4) and (3.6) are nonsingular. However, choosing $r_1(t)$ and $r_2(t)$ from the *linear subarray* leads directly to the DOA estimates at this step if the sources are statistically independent, because, in that case $G = P$, and $diag(\frac{b_{21}}{b_{11}}, \cdots, \frac{b_{2P}}{b_{1P}}) = \text{diag}\{e^{-j2\pi\frac{d}{\lambda}\sin(\theta_1)}, \cdots, e^{-j2\pi\frac{d}{\lambda}\sin(\theta_P)}\}$, which follows from the fact that linear subarray antennas have identical responses. Note that with the above choice of $r_1(t)$ and $r_2(t)$ (i.e., choosing $r_1(t)$ and $r_2(t)$ as identical-response sensor measurements), this step corresponds to VESPA. For the coherent case, however, the matrix $\mathbf{D}$ does not give the DOAs explicitly; but, the estimated generalized steering vectors can be used to find the DOAs, as explained in the next step.

### 3.2.2 Step 2: Spatial smoothing

Once we have estimated the generalized steering vectors $\{\mathbf{b}_i\}_{i=1}^{G}$, we can estimate the steering vector and, subsequently, the DOA of each received signal path. The general form of coherence between the received signals lets us express each generalized steering vector as a linear combination of steering vectors of *one* coherent group, *independent* of the other steering vectors, where the combination coefficients are the elements of the *unknown* complex propagation vector for that group. To see this, partition the matrices $\mathbf{B}$ and $\mathbf{A}$ as

$$\mathbf{B} = [\mathbf{b}_1, \cdots, \mathbf{b}_G], \tag{3.9}$$

$$\mathbf{A} = [\mathbf{A}_1, \cdots, \mathbf{A}_G], \tag{3.10}$$

where $\mathbf{b}_i$ is $M \times 1$, and the steering matrix for the $i$th group,

$$\mathbf{A}_i \triangleq [\mathbf{a}(\theta_{i,1}), \cdots, \mathbf{a}(\theta_{i,p_i})] \tag{3.11}$$

is $M \times p_i$. Additionally, $\theta_{i,m}$ represents the angle-of-arrival of the $m$th source in the $i$th coherent group with $1 \leq m \leq p_i$. Using the fact that the $i$th column of $\mathbf{Q}$ has $p_i$ nonzero elements, $\mathbf{B}$ can be expressed as

$$\mathbf{B} = \mathbf{AQ} = [\mathbf{A}_1\mathbf{c}_1, \cdots, \mathbf{A}_G\mathbf{c}_G]; \tag{3.12}$$

therefore, the $i$th column of $\mathbf{B}$, $\mathbf{b}_i$, is

$$\mathbf{b}_i = \mathbf{A}_i\mathbf{c}_i \tag{3.13}$$

where $i = 1, \cdots, G$.

Now, the problem of solving for steering vectors of the received signals is transformed into $G$ independent problems, each solving for the steering vectors of all the signal paths in each coherent group from the generalized steering vector of that group. To solve each of these new problems, each generalized steering vector $\mathbf{b}_i$ can be interpreted as a received signal for an array illuminated by $p_i$ coherent signals having a steering matrix $\mathbf{A}_i$, and covariance matrix $\mathbf{c}_i\mathbf{c}_i^H$. Then, the DOAs of each signal could be solved for by using a second-order-statistics-based subspace method such as MUSIC if the array is calibrated and if the rank of $\mathbf{c}_i\mathbf{c}_i^H$ is $p_i$; however, the array is not calibrated and $rank(\mathbf{c}_i\mathbf{c}_i^H) = 1$. Therefore, we propose to keep the part of each estimated generalized steering vector that corresponds to the *linear* part of the main array, and does not require calibration. By doing this, we will be able to incorporate spatial smoothing [71], [56] which, in turn, will *restore* the rank of $\mathbf{c}_i\mathbf{c}_i^H$ to $p_i$.

For this purpose, partition $\mathbf{b}_i$ as follows:

$$\mathbf{b}_i = \begin{bmatrix} \mathbf{b}_{L,i} \\ \mathbf{b}_{M-L,i} \end{bmatrix} = \begin{bmatrix} \mathbf{A}_{L,i} \\ \mathbf{A}_{M-L,i} \end{bmatrix} \mathbf{c}_i \qquad i = 1, \cdots, G \tag{3.14}$$

where $\mathbf{b}_{L,i}$ is the portion of $\mathbf{b}_i$ corresponding to the linear array of sensors (the

first $L$ elements of $\mathbf{b}_i$ for the array configuration in Fig.1), and $\mathbf{A}_{L,i}$ contains the first $L$ rows of $\mathbf{A}_i$. Now, $\mathbf{b}_{L,i}$ can be interpreted [26] as a received signal for an $L$ element uniform linear array that is illuminated by coherent signals from a *single* source whose propagation vector is $\mathbf{c}_i$. Note that the steering matrix of these coherent signals is $\mathbf{A}_{L,i}$. Treating $\mathbf{b}_{L,i}\mathbf{b}_{L,i}{}^H$ as the covariance matrix of the received signal, spatial smoothing can be applied to restore the rank of $\mathbf{b}_{L,i}\mathbf{b}_{L,i}{}^H$ to $p_i$ for $i = 1, \cdots, G$, and then, any second-order-statistics-based high-resolution method can be employed to find the DOAs. Note that the antenna patterns of the sensors in the uniform linear subarray, which are the same, are not required, i.e., calibration is not needed.

In order to derive the relationship between the number of array elements and maximum number of detectable signals by our method, the method of spatial smoothing [56], [71] is summarized next. Forward spatial smoothing for the $i$th group ($i = 1, \cdots, G$) starts by dividing the $L$-vector $\mathbf{b}_{L,i}$ into $K = L - S + 1$ overlapping subvectors of size $S$, $\mathbf{b}_{S,i}^k$ ($k = 1, \cdots, K$), with elements $\{b_{L,i}(k), \cdots, b_{L,i}(k+S-1)\}$. Partitioning $\mathbf{A}_{L,i}$ as

$$\mathbf{A}_{L,i} = \begin{bmatrix} \mathbf{A}_{S,i} \\ \mathbf{A}_{L-S,i} \end{bmatrix}, \tag{3.15}$$

in which $\mathbf{A}_{S,i}$ is $S \times p_i$, $\mathbf{b}_{S,i}^k$ can be expressed as (this is where use is made of the uniform linearity of the subarray)

$$\mathbf{b}_{S,i}^k = \mathbf{A}_{S,i}\mathbf{\Phi}_i{}^{(k-1)}\mathbf{c}_i \qquad k = 1, \cdots, K \qquad i = 1, \cdots, G, \tag{3.16}$$

where $\mathbf{\Phi}_i{}^{(k-1)}$ denotes the $(k-1)$ power of the $p_i \times p_i$ diagonal matrix

$$\mathbf{\Phi}_i = \mathrm{diag}\{e^{-jw_c\Delta sin\theta_{i,1}/c}, \cdots, e^{-jw_c\Delta sin\theta_{i,p_i}/c}\}, \tag{3.17}$$

in which $\theta_{i,m}$ represents the angle-of-arrival of the $m$th source in the $i$th coherent group, where $1 \leq m \leq p_i$, and $\Delta$ is the separation between the elements of the linear subarray under consideration. Consequently, for the $k$th subvector

$$\mathbf{b}_{S,i}^k\mathbf{b}_{S,i}^k{}^H = \mathbf{A}_{S,i}\mathbf{\Phi}_i{}^{(k-1)}\mathbf{c}_i\mathbf{c}_i{}^H\mathbf{\Phi}_i{}^{(k-1)^H}\mathbf{A}_{S,i}{}^H, \tag{3.18}$$

which, of course is rank-one.

Define the spatially smoothed matrix $\overline{\mathbf{b}_{S,i}\mathbf{b}_{S,i}{}^H}$ as the average of $\mathbf{b}_{S,i}^k\mathbf{b}_{S,i}^k{}^H$ over $k$ $(k = 1, \cdots, K)$ i.e.,

$$\begin{aligned}
\overline{\mathbf{b}_{S,i}\mathbf{b}_{S,i}{}^H} &= \tfrac{1}{K}\textstyle\sum_{k=1}^{K} \mathbf{b}_{S,i}^k\mathbf{b}_{S,i}^k{}^H \\
&= \mathbf{A}_{S,i}\underbrace{\left(\frac{1}{K}\sum_{k=1}^{K}\mathbf{\Phi}_i{}^{(k-1)}\mathbf{c}_i\mathbf{c}_i{}^H\mathbf{\Phi}_i{}^{(k-1)H}\right)}_{\triangleq\mathbf{R}_i}\mathbf{A}_{S,i}{}^H \\
&= \mathbf{A}_{S,i}\mathbf{R}_i\mathbf{A}_{S,i}{}^H
\end{aligned} \tag{3.19}$$

The matrix $\mathbf{R}_i$ can be expressed explicitly, as

$$\begin{aligned}
\mathbf{R}_i &= \tfrac{1}{K}\left[\mathbf{c}_i, \mathbf{\Phi}_i\mathbf{c}_i, \mathbf{\Phi}_i{}^2\mathbf{c}_i, \cdots, \mathbf{\Phi}_i{}^{(K-1)}\mathbf{c}_i\right]\begin{bmatrix} \mathbf{c}_i{}^H \\ (\mathbf{\Phi}_i\mathbf{c}_i)^H \\ (\mathbf{\Phi}_i{}^2\mathbf{c}_i)^H \\ \vdots \\ (\mathbf{\Phi}_i{}^{(K-1)}\mathbf{c}_i)^H \end{bmatrix} \\
&\triangleq \tfrac{1}{K}\mathbf{F}_i\mathbf{F}_i{}^H
\end{aligned} \tag{3.20}$$

where

$$\begin{aligned}
\mathbf{F}_i &= \begin{bmatrix} \mathbf{c}_i(1) & & \mathbf{0} \\ & \ddots & \\ \mathbf{0} & & \mathbf{c}_i(p_i) \end{bmatrix}\begin{bmatrix} 1 & v_{i,1} & v_{i,1}{}^2 & \cdots & v_{i,1}{}^{K-1} \\ 1 & v_{i,2} & v_{i,2}{}^2 & \cdots & v_{i,2}{}^{K-1} \\ \vdots & \vdots & \vdots & \ddots & \vdots \\ 1 & v_{i,p_i} & v_{i,p_i}{}^2 & \cdots & v_{i,p_i}{}^{K-1} \end{bmatrix} \\
&\triangleq \mathbf{C}_i\mathbf{V}_i
\end{aligned} \tag{3.21}$$

in which $v_{i,m} \triangleq e^{-jw_c\Delta sin\theta_{i,m}/c}$ with $1 \leq m \leq p_i$.

Under what conditions will the rank of $\mathbf{b}_{S,i}\mathbf{b}_{S,i}{}^H$ be restored to $p_i$? Note first that the rank of $\mathbf{R}_i$ is equal to the rank of $\mathbf{F}_i$, and, the rank of $\mathbf{F}_i$ is the same as that of $\mathbf{V}_i$. For the Vandermonde matrix $\mathbf{V}_i$, $\text{rank}(\mathbf{V}_i) = \min(p_i, K)$ [56]; hence, $\text{rank}(\mathbf{V}_i) = p_i$ if and only if $K \geq p_i$, i.e., if the number of subvectors used in spatial smoothing is greater than or equal to the number of coherent signals in the $i$th group. Thus, if $K = L - S + 1 \geq p_i$, or equivalently $L \geq p_i + S - 1$, then

$\text{rank}(\mathbf{R}_i) = p_i$. Additionally, if $S \geq p_i + 1$, the columns of $\mathbf{A}_{S,i}$ (which is $S \times p_i$) are linearly independent; and hence [see (3.19)] $\text{rank}(\overline{\mathbf{b}_{S,i}\mathbf{b}_{S,i}}^H) = p_i$. Combining both constraints on $L$, we obtain the following conditions on the length of the linear subarray, $L$ and the parameter $S$ under which the rank of $\mathbf{b}_{S,i}\mathbf{b}_{S,i}^H$ is restored to $p_i$ by $\overline{\mathbf{b}_{S,i}\mathbf{b}_{S,i}}^H$:

> $L$ must satisfy: $L \geq 2p_i$ if forward spatial smoothing is used; and, $L \geq 3p_i/2$ if both forward and backward smoothing are used [56]. This means that, if both methods are used, the linear subarray must have at least $3p_{max}/2$ elements where $p_{max}$ is the maximum number of multipaths in anyone of the $G$ groups. Given $L$ and $p_{max}$, the parameter $S$ must be selected such that $p_{max}+1 \leq S \leq L - p_{max}/2 + 1$.

### 3.2.3 Step 3: Extract DOAs

By applying any second-order-statistics-based subspace technique (e.g., root-MUSIC, etc.) to the pseudo-covariance matrix $\overline{\mathbf{b}_{S,i}\mathbf{b}_{S,i}}^H$, $i = 1, \cdots, G$, it is possible to estimate DOAs of up to $2L/3$ coherent signals in each group. As just noted, a linear subarray of minimum dimension $3p_{max}/2$ is needed.

### 3.2.4 Discussion

Since $\mathbf{B}$ is $M \times G$, the maximum number of groups, $G$, that can be resolved is $M-1$. Additionally, as we have just seen, it is possible to estimate DOAs of up to $2L/3$ coherent signals in each group. Consequently, the maximum total number of coherent sources that can be resolved by our method is $2(M-1)L/3$. If all sensors are in a uniform linear array, $(M = L)$, then a maximum of $2(M-1)M/3$ coherent sources can be resolved.

Note that in deriving our three-step method we did not restrict the entire array to be linear. Only an L-element part of it must be linear. In contrast, when the sources are coherent, spatial smoothing method of [56], [71] is limited to uniform linear arrays. In addition, while our method can resolve $2(L-1)L/3$ coherent signals, these methods can resolve at most $L-1$ signals using an $L$ element linear array.

Another point to note is that, if a coherent group contains more than $2L/3$ signals, only the DOA estimates of that group are affected, because, each group is treated *independently* in the second step of our method.

Finally, even if there are no multipaths, our method works, because, in this case, spatial smoothing does not affect the unity rank of $\mathbf{b}_{S,i}\mathbf{b}_{S,i}{}^H$, since there is only one signal in the $i$th group. Note that our method works for coherent or linearly correlated sources as well as independent sources. On the other hand, VESPA works only for the independent sources case. The tradeoff from a hardware standpoint is that our method requires a uniform linear subarray whose length depends on the number of multipaths in a coherent group, whereas VESPA requires two identical sensors. If one suspects any multipath will be present in the data, EVESPA must be used.

Next, in order to improve the generalized steering vector estimates, these estimates can be averaged; or, the principal component of the matrix with $j$th column, $\mathbf{b}_{ij}$ $(j = 1, \cdots, M^2(M-1)/2)$ can be chosen as an improved estimate of $\mathbf{b}_i$.

## 3.3 Efficient Use of Data

In this section, we show that our method can be modified to use the available data more efficiently.

### 3.3.1 Using Multiple Guiding Sensor Pairs

Just as when we chose the first two sensors as the guiding pair, the two pairs of sensors $(p, m)$ and $(q, m)$, $p \neq q$ also lead to two matrices, like (3.4) and (3.6), which are in ESPRIT form to estimate the generalized steering vectors $\{\mathbf{b}_{L,1}, \cdots, \mathbf{b}_{L,G}\}$. On the other hand, VESPA requires guiding sensor pair elements to have identical responses, because, VESPA is based on the fact that, in the incoherent case, responses of *identical* but displaced sensors are identical up to a phase constant which contains the angle of arrival information. Consequently, we have more degrees of freedom in our method than in VESPA. This observation suggests that the available data can be used efficiently by employing multiple guiding sensor

pairs in Step 1. To demonstrate this, consider the following cumulants which are generated by using the sensors $p$ and $m$ as the first guiding sensor pair, and $q$ and $m$ as the second guiding sensor pair

$$\mathbf{C}_{p,m} \triangleq \text{cum}(r_p(t), r_m^*(t), \mathbf{r}(t), \mathbf{r}^H(t)) = \mathbf{B}\mathbf{\Lambda}_{p,m}\mathbf{B}^H, \tag{3.22}$$

$$\mathbf{C}_{q,m} \triangleq \text{cum}(r_q(t), r_m^*(t), \mathbf{r}(t), \mathbf{r}^H(t)) = \mathbf{B}\mathbf{D}_{q,p}\mathbf{\Lambda}_{p,m}\mathbf{B}^H, \tag{3.23}$$

where, $\mathbf{B}$ is the generalized steering matrix, $\mathbf{\Lambda}_{p,m} \triangleq \text{diag}\{\gamma_{4,u_1} b_{p1} b_{m1}^*, \cdots, \gamma_{4,u_G} b_{pG} b_{mG}^*\}$, and $\mathbf{D}_{q,p} \triangleq \text{diag}\{\frac{b_{q1}}{b_{p1}}, \cdots, \frac{b_{qG}}{b_{pG}}\}$. The derivations of (3.22) and (3.23) are very similar to the derivations of (3.4) and (3.6).

Just as when we chose the first two sensors as the guiding pair, the two pairs of sensors $(m,p)$ and $(m,q)$, $p \neq q$ also lead to two matrices, as shown in (3.22) and (3.23), which are in ESPRIT form to estimate the generalized steering vectors $\{\mathbf{b}_1, \cdots, \mathbf{b}_G\}$. This observation is useful for two purposes. First, it suggests that the available data can be used efficiently by employing multiple guiding sensor pairs. Second, it provides a basis for a solution to a potential problem that is associated with the practical implementation of our method, as explained next.

In Section 3.2 the first two sensors were chosen as the guiding sensor pair, and it was assumed that the first two rows of $\mathbf{B}$ are all nonzero. The reason for this assumption is explained as follows. Suppose that the $i$th element $\mathbf{B}(1,i)$ in the first row of $\mathbf{B}$ is equal or close to zero. Then, $\mathbf{\Lambda}(1,i) = 0$ which causes $rank(\mathbf{C}) = G - 1$ (see (3.4), (3.6) and (3.8)), and consequently the number of independent sources appears to be one less than its actual value. As a result, all the sources but the $i$th will be separated. Similarly, each zero entry in the second row of $\mathbf{B}$ reduces $rank(\mathbf{C}_2)$ by one which, in turn, partially destroys the rotational invariance between the signal subspaces of $\mathbf{C}_1$ and $\mathbf{C}_2$. In these cases, the availability of multiple candidates for the guiding sensor pairs proves to be a useful solution. A simple selection procedure for the "right" sensor pairs in such cases is proposed next.

*A Simple Selection Procedure*: 1) Estimate the number of groups $G$ from the eigendecomposition of the array covariance matrix (sophisticated approaches such as MDL or AIC can be used here); 2) Check the rank of estimated $\mathbf{C}_{i,i}$ for $i =$

$1, \cdots, M$; and, prepare a list of values of $i$ for which the rank of the estimated $\mathbf{C}_{i,i} = G$. This is a list of all the "safe" indices, from which the indices $p$, $q$ and $m$ of $\mathbf{C}_{m,m}$ and $\mathbf{C}_{q,m}$ can be selected. The reason why we call this list "safe" is that for each value of $i$ in this list, the $i$th row of $\mathbf{B}$ must have all nonzero entries, because each zero entry in the $i$th row of $\mathbf{B}$ reduces the rank of $\mathbf{C}_{i,i}$ by one.

In general, we can choose the pair $(p, q)$ such that $p \neq q$ in $M(M-1)/2$ ways since interchanging $p$ and $q$ does not matter. In addition, $m$ can be chosen in $M$ ways. Therefore, the sensor pairs $(m, p)$ and $(m, q)$ can be chosen in $M^2(M-1)/2$ ways. Provided that these pairs are the "right" ones, for each choice there corresponds an ESPRIT problem defined by the two $M$x$M$ matrices $\mathbf{C}_{p,m}$ and $\mathbf{C}_{q,m}$. The solutions of these problems yield $M^2(M-1)/2$ estimates of each generalized steering vector $\mathbf{b}_i$ $(i = 1, \cdots, G)$. Next, in order to improve the generalized steering vector estimates, these estimates can be averaged; or, the principal component of the matrix with $j$th column, $\mathbf{b}_{ij}$ $(j = 1, \cdots, M^2(M-1)/2)$ can be chosen as an improved estimate of $\mathbf{b}_i$. Since the required computations for different choices of guiding sensor pairs are independent, they can be implemented in *parallel.*

### 3.3.2 Using Covariance Information

Sensor to sensor independence of the measurement noise lets us use the spatial covariance matrix of the array as side information to improve the generalized steering vector estimates and bearing estimates in our method. If it is known that the measurement noise is spatially white, the eigenvectors of the spatial covariance matrix corresponding to the smallest repeated eigenvalues span the noise subspace; and, the remaining eigenvectors define the signal subspace.

Although we can not identify the generalized steering vectors from the covariance matrix when coherence is present, we can improve our cumulant-based steering vector estimates by projecting them onto the signal subspace obtained from the spatial covariance matrix [16]. As explained in [16], the motivation behind this approach is that the variance of covariance estimates is lower than that of cumulant estimates for the same sample size. Note that this method is applicable only if the noise is white or the noise covariance matris is known.

If the goal is to estimate the DOAs, we proceed to improve our generalized steering vector estimates in extended-VESPA by:

1. Estimating the spatial covariance matrix corresponding to the uniform linear part of the array;

2. Identifying the signal subspace eigenvectors by eigenanalysis of the spatial covariance matrix;

3. Stacking the signal subspace eigenvectors into an $LxG$ matrix $\mathbf{E}_s$ (if there are $G$ coherent groups, the signal subspace is $G$ dimensional); and,

4. Projecting the cumulant-based generalized steering vector estimates $\{\mathbf{b}_{L,i}\}_{i=1}^{G}$ onto the signal subspace to obtain improved estimates $\{\mathbf{b}_{L,i,imp}\}_{i=1}^{G}$, i.e., $\mathbf{b}_{L,i,imp} = \mathbf{E}_s\mathbf{E}_s^H\mathbf{b}_{L,i}$. These improved generalized steering vector estimates are used in the spatial smoothing step of extended-VESPA.

### 3.3.3 Improving Generalized Steering Vector Estimates by Beamforming

The quality of bearing estimates in each coherent group depends on the accuracy of the corresponding generalized steering vector estimates. In Sections 3.2.2 and 3.2.3, we worked with the generalized steering vector estimates one at a time to extract the bearings of coherent signals in each group separately, and, when considering each group, we did not make use of the already existing generalized steering vector estimates of other groups. In this section we show that this latter information can be used to improve the estimate of the generalized steering vector of each individual group. This is achieved by suppressing the undesired groups using a suitable beamformer so that the transformed received signal contains only the desired group. The same procedure is repeated for each group and the transformed data is then processed as explained below. The transformations and subsequent processing can be implemented in parallel.

Suppose that the generalized steering matrix $\mathbf{B}$ is estimated in the first step of extended VESPA, and that we are interested in the $i$th group arrival angles ($i = 1, \cdots, G$). From the signal model, we have

$$\mathbf{r} = \mathbf{b}_i u_i(t) + \mathbf{B}_{u,i}\mathbf{u}_{u,i}(t) + \mathbf{n}(t) \tag{3.24}$$

where $M \times (G-1)$ matrix $\mathbf{B}_{u,i} \triangleq [\mathbf{b}_1, \cdots, \mathbf{b}_{i-1}, \mathbf{b}_{i+1}, \cdots, \mathbf{b}_G]$ and $(G-1)$-vector $\mathbf{u}_{u,i}(t) \triangleq [\mathbf{u}_1, \cdots, \mathbf{u}_{i-1}, \mathbf{u}_{i+1}, \cdots, \mathbf{u}_G]$. Both $\mathbf{B}_{u,i}$ and $u_{u,i}(t)$ are associated with the undesired groups.

Using the estimate $\hat{\mathbf{b}}_i$ obtained from the first step of extended VESPA, we can find two beamformer vectors $\mathbf{w}_{i1}$ and $\mathbf{w}_{i2}$ such that $\mathbf{w}_{i1}^H \hat{\mathbf{B}}_{u,i} = \mathbf{w}_{i2}^H \hat{\mathbf{B}}_{u,i} = \mathbf{0}$, and, $\mathbf{w}_{i1}^H \hat{\mathbf{b}}_i$ and $\mathbf{w}_{i2}^H \hat{\mathbf{b}}_i$ are nonzero. Two such vectors are obtained by picking any two of the left null space vectors of $\hat{\mathbf{B}}_{u,i}$. Since $\hat{\mathbf{b}}_i$ is independent of the columns of $\hat{\mathbf{B}}_{u,i}$, $\mathbf{w}_{i1}^H \hat{\mathbf{b}}_i$ and $\mathbf{w}_{i2}^H \hat{\mathbf{b}}_i$ are nonzero. Applying these beamformers to the received signal, we obtain two signals $\tilde{r}_1(t) = \mathbf{w}_{i1}^H \mathbf{r}(t)$ and $\tilde{r}_2(t) = \mathbf{w}_{i2}^H \mathbf{r}(t)$. Ideally, these transformations suppress the contributions of all groups but the desired group $u_i(t)$. Hence, $\tilde{r}_1(t) \approx \mathbf{w}_{i1}^H \mathbf{b}_i u_i(t) + \mathbf{w}_{i1}^H \mathbf{n}(t)$ and $\tilde{r}_2(t) \approx \mathbf{w}_{i2}^H \mathbf{b}_i u_i(t) + \mathbf{w}_{i2}^H \mathbf{n}(t)$. Let $c_{i1} \triangleq \mathbf{w}_{i1}^H \mathbf{b}_i$ and $c_{i2} \triangleq \mathbf{w}_{i2}^H \mathbf{b}_i$, so that $\tilde{r}_1(t) \approx c_{i1} u_i(t) + \mathbf{w}_{i1}^H \mathbf{n}(t)$ and $\tilde{r}_2(t) \approx c_{i2} u_i(t) + \mathbf{w}_{i2}^H \mathbf{n}(t)$.

Defining the cumulant vector $cum(\tilde{r}_1^*(t), \tilde{r}_1(t), \tilde{r}_1^*(t), \mathbf{r}(t))$ as the vector [1] with the $k$th entry as $cum(\tilde{r}_1^*(t), \tilde{r}_1(t), \tilde{r}_1^*(t), r_k(t))$, an improved estimate of $\mathbf{b}_i$ can now be obtained to within a complex constant from the following

$$\begin{aligned} cum(\tilde{r}_1^*(t), \tilde{r}_1(t), \tilde{r}_1^*(t), \mathbf{r}(t)) &\approx cum(c_{i1}{}^* u_i{}^*(t), c_{i1} u_i(t), c_{i1}{}^* u_i{}^*(t), \sum_{k=1}^{G} \mathbf{b}_k u_k(t)) \\ &= cum(c_{i1}{}^* u_i{}^*(t), c_{i1} u_i(t), c_{i1}{}^* u_i{}^*(t), \mathbf{b}_i u_i(t)) \\ &+ cum(c_{i1}{}^* u_i{}^*(t), c_{i1} u_i(t), c_{i1}{}^* u_i{}^*(t), \sum_{k \neq i}^{G} \mathbf{b}_k u_k(t)) \\ &= |c_{i1}|^2 c_{i1}{}^* \gamma_{4,i} \mathbf{b}_i \end{aligned} \tag{3.25}$$

where $\gamma_{4,i}$ is the fourth-order cumulant of the $i$th source, and we have used the independence of the signals and the additive Gaussian-noise, and **[CP1]**, **[CP3]**, **[CP5]**, **[CP6]** in Section 1.2.2. This improvement method will be referred to as BFBI1 (short for BeamForming-Based Improvement 1). A similar formulation was used in [19] where all signals but the desired one were assumed Gaussian, and therefore, they were suppressed by the cumulant operations.

In general, one can choose the beamformer vectors $\mathbf{w}_{i1}$ and $\mathbf{w}_{i2}$, which put nulls

[1] The reason why we have introduced $\tilde{r}_2$ will become clear later when we consider an ESPRIT-like formulation.

on all the undesired signals, in $M-G+1$ ways. Let those vectors be $\{\mathbf{w}_{ik}\}_{k=1}^{M-G+1}$, and $\tilde{r}_k(t) \triangleq \mathbf{w}_{ik}{}^H\mathbf{r}(t)$. Then, further smoothing of the estimate of $\mathbf{b}_i$ is possible by taking the principal component of the rank-one matrix whose $k$-th column is defined as $\mathbf{cum}(\tilde{r}_k^*(t), \tilde{r}_k(t), \tilde{r}_k^*(t), \mathbf{r}(t))$, $k = 1, \cdots, M-G+1$. This improvement method will be referred to as BFBI2. Note that an estimate of $\mathbf{b}_i$ can also be obtained from the correlation $E\{\tilde{r}_k^*(t)\mathbf{r}(t)\}$ in the high $SNR$ case; however, if the undesired sources are not suppressed perfectly, we need cumulants, as explained in the next paragraph.

Up to now, we assumed the undesired signals are suppressed perfectly so that we are left with only one source, and we could use the cumulant vector in (22); however, in practice, residual undesired signal terms are present in $\tilde{r}_1(t)$ and $\tilde{r}_2(t)$. In that case, the cumulant vector in (22) gives a weighted sum of generalized steering vectors of all the sources; therefore, it is better to use an ESPRIT-like formulation, as we did in the first step, which can handle multiple sources.

Let $\mathbf{d}_1 \triangleq \left[\mathbf{w}_{i1}{}^H\mathbf{b}_1, \cdots, \mathbf{w}_{i1}{}^H\mathbf{b}_G\right]$, and $\mathbf{d}_2 \triangleq \left[\mathbf{w}_{i2}{}^H\mathbf{b}_1, \cdots, \mathbf{w}_{i2}{}^H\mathbf{b}_G\right]$ where $\mathbf{w}_{i1}$ and $\mathbf{w}_{i2}$ are chosen as described above. Note that if perfect estimates of $\mathbf{b}_i$ were possible, all entries but $\mathbf{w}_{i1}{}^H\mathbf{b}_i$ of $\mathbf{d}_1$ and $\mathbf{w}_{i2}{}^H\mathbf{b}_i$ of $\mathbf{d}_2$ would be zero. Let us also define $\mathbf{C}_1 = cum(\tilde{r}_1^*(t), \tilde{r}_1(t), \mathbf{r}(t), \mathbf{r}^H(t))$ and $\mathbf{C}_2 = cum(\tilde{r}_1^*(t), \tilde{r}_2(t), \mathbf{r}(t), \mathbf{r}^H(t))$ as the $M \times M$ matrices whose $(m,n)$th elements, respectively, are $cum(\tilde{r}_1^*(t), \tilde{r}_1(t), r_m(t), r_n{}^*(t))$ and $cum(\tilde{r}_1^*(t), \tilde{r}_2(t), r_m(t), r_n{}^*(t))$. Using the notation $\mathbf{x}(k)$ for the $k$th element of a vector $\mathbf{x}$, a simple expression for $\mathbf{C}_1$ is derived, as

$$\begin{aligned}
\mathbf{C}_1 &= cum(\tilde{r}_1^*(t), \tilde{r}_1(t), \mathbf{r}(t), \mathbf{r}^H(t)) \\
&= cum(\sum_{k=1}^{G} \mathbf{d}_1(k)^* u_k{}^*(t), \sum_{k=1}^{G} \mathbf{d}_1(k) u_k(t), \sum_{k=1}^{G} \mathbf{b}_k u_k(t), \sum_{k=1}^{G} \mathbf{b}_k{}^H u_k{}^*(t)) \\
&= \sum_{k=1}^{G} |\mathbf{d}_1(k)|^2 \gamma_{4,k} \mathbf{b}_k \mathbf{b}_k{}^H \\
&= \mathbf{B}\mathbf{\Lambda}\mathbf{B}^H \qquad (3.26)
\end{aligned}$$

where $\mathbf{B} \triangleq [\mathbf{b}_1, \cdots, \mathbf{b}_G]$ and $\mathbf{\Lambda} \triangleq \mathrm{diag}\{|\mathbf{d}_1(1)|^2\gamma_{4,1}, \cdots, |\mathbf{d}_1(G)|^2\gamma_{4,G}\}$, and we used [**CP1**],[**CP3**],[**CP5**],[**CP6**] in Section 1.2.2. Note that if one assumes perfect nulling, in which case all $\mathbf{d}_1(k)$s but $\mathbf{d}_1(i)$ are zero, then $\mathbf{C}_1$ is theoretically rank-one.

Similarly, $\mathbf{C}_2$ can be shown to be

$$\begin{aligned}\mathbf{C}_2 &= \sum_{k=1}^{G} \mathrm{d}_1(k)^* \mathrm{d}_2(k) \gamma_{4,k} \mathbf{b}_k \mathbf{b}_k{}^H \\ &= \mathbf{B}\mathbf{\Phi}\mathbf{\Lambda}\mathbf{B}^H \end{aligned} \tag{3.27}$$

where $\mathbf{\Phi} \triangleq \mathrm{diag}\{\frac{\mathrm{d}_2(1)}{\mathrm{d}_1{}^*(1)}, \cdots, \frac{\mathrm{d}_2(G)}{\mathrm{d}_1{}^*(G)}\}$.

By applying ESPRIT to (3.26) and (3.27), we can obtain an improved estimate of $\mathbf{b}_i$, which is then used in *Steps* 2 and 3 of extended-VESPA in the same way as explained earlier. This improvement method will be referred to as BFBI3. Note that, because we are interested only in the part of $\mathbf{b}_i$ associated with the linear subarray in the second and third steps of extended VESPA, we could use only the linear part of the data to improve the linear part of $\mathbf{b}_i$. This is accomplished by applying the same procedure explained here, in which $\mathbf{r}$ and $\mathbf{B}$ are replaced by their linear parts, $\mathbf{r}_L$ and $\mathbf{B}_L$, respectively.

A flow-chart of this technique is given in Fig. 3.2.

## 3.4 Non-Gaussian Noise Suppression

**Theorem:** As in VESPA, in the presence of non-Gaussian signals, additive non-Gaussian noise suppression is possible with extended VESPA, if one of the sensors' measurement noise is independent of the measurement noises of other sensors of the array [17], [16].

**Proof:** Assume that the measurement noise of sensor $m$ is independent of the measurement noises of the other sensors. Using sensor $m$ and any other two sensors (say $p$ and $q$) in the array, extended VESPA can be applied as explained in Section 3.3.1. Extended VESPA starts with the estimation of the following two cumulant matrices:

$$\mathbf{C}_{p,m} \triangleq \mathrm{cum}(r_p(t), r_m^*(t), r_k(t), r_l^*(t)), \tag{3.28}$$

and

$$\mathbf{C}_{q,m} \triangleq \mathrm{cum}(r_q(t), r_m^*(t), r_k(t), r_l^*(t)), \tag{3.29}$$

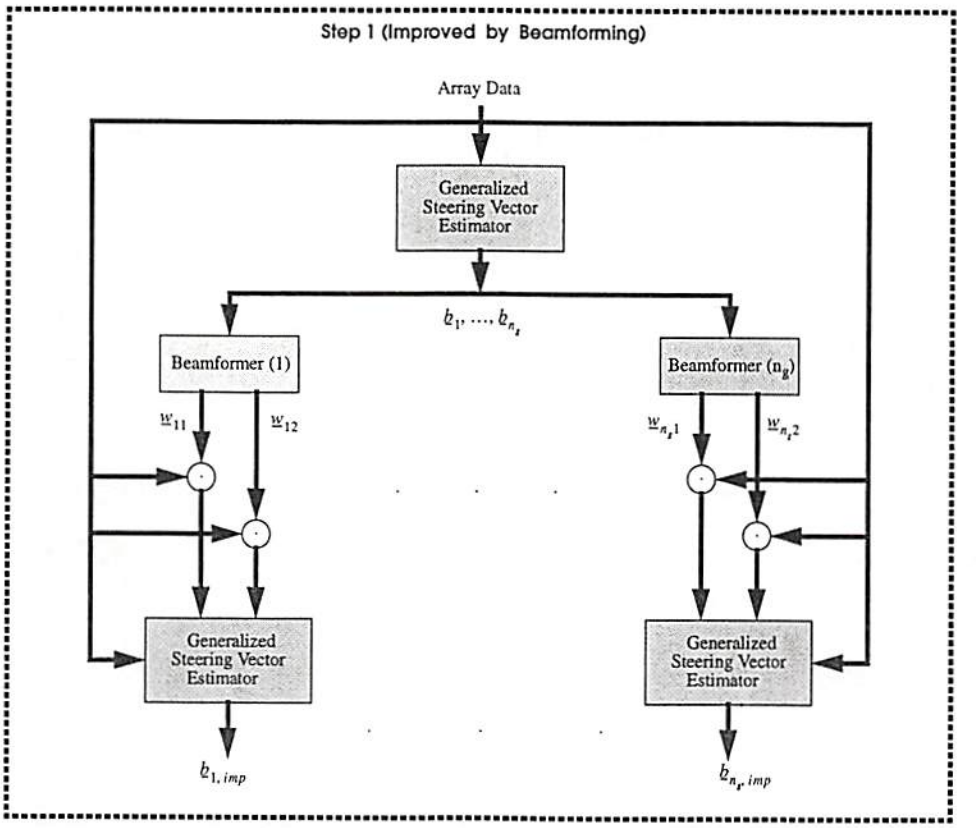


Figure 3.2: A flow-chart of the beamforming technique for improving generalized steering vector estimates.

for $k, l = 1, \cdots, M$, where $r_m(t)$, $r_p(t)$ and $r_q(t)$ denote the received signal by the sensors $m$, $p$ and $q$, respectively. Since, the received signal is the sum of the signals and measurement noise, and measurement noise is independent of the signals, each of the above cumulants is equal to the sum of cumulant of signals and cumulant of measurement noise by **[CP5]** in Section 1.2.2. However, by **[CP6]**, the cumulant of measurement noise is zero, because, the noise measured by the $m$th sensor is independent of the noises measured by the other sensors. Consequently, the above cumulants are theoretically noise free.

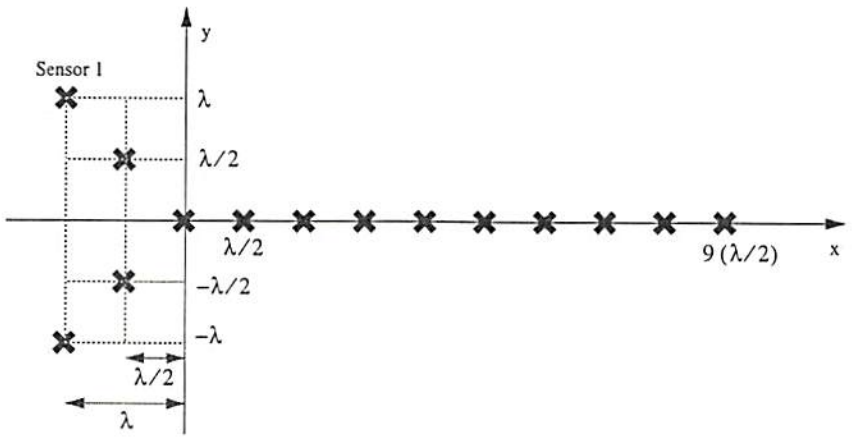


Figure 3.3: The array configuration used in the first experiment. The antenna elements are dipoles oriented by the angles given in the text.

## 3.5 Experimental Results

In this section we present results of some simulation experiments demonstrating our method.

### 3.5.1 Experiment 1: 14 sensors, 20 signals

We consider the array in Fig. 3.3. Each sensor in the array is a dipole antenna which has a response $\cos(\theta_j - \phi_i)$ to the $j$th signal where $\theta_j$ is its arrival angle and $\phi_i$ is the orientation of the $i$th dipole (see Fig. 3.4).

The orientations of the dipoles are chosen arbitrarily as $\{95^o, 85^o, 87^o, 92^o, 90^o, 90^o, 90^o, 90^o, 90^o, 90^o, 90^o, 90^o, 90^o, 90^o\}$. There are four groups, and each group contains a direct-path signal and four scaled and delayed replicas of the direct-path signal. The scaled and delayed replicas represent the multipaths. In this experiment there are 20 BPSK signals. Additive white Gaussian noise and a different $SNR$ is assumed for each direct-path signal. The direction of arrivals and propagation constants of the signals within each group relative to the direct-path and direct-path $SNR$s are chosen as follows, where unity propagation constants correspond to direct-path signals:

**Group 1**

DOAs: $\{40^o, 68^o, 80^o, 115^o, 130^o\}$,

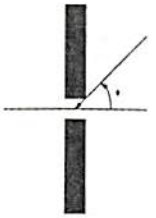

Figure 3.4: The response of the dipole antennas used in the experimental array.

Propagation Constants: $\{(0.2+0.8i), 1, (0.8-0.5i), (0.75+0.65i), (0.8-0.2i)\}$,
Direct-Path SNR: 20dB.

**Group 2**

DOAs: $\{50^o, 70^o, 90^o, 120^o, 135^o\}$,
Propagation Constants: $\{(0.9+0.3i), 1, (0.9-0.3i), (0.8+0.7i), 0.95\}$,
Direct-Path SNR: 18dB.

**Group 3**

DOAs: $\{45^o, 65^o, 85^o, 110^o, 125^o\}$,
Propagation Constants: $\{1, (0.8-0.7i), (0.7+0.7i), (0.65-0.8i), (0.9+0.1i)\}$,
Direct-Path SNR: 18dB.

**Group 4**

DOAs: $\{60^o, 85^o, 105^o, 118^o, 140^o\}$,
Propagation Constants: $\{(0.3-0.8i), (0.4+0.9i), (0.8+0.6i), (0.9+0.7i), 1\}$,
Direct-Path SNR: 19dB.

Taking the signals received by the rightmost two dipoles in Fig. 3.3 as $r_1(t)$ and $r_2(t)$, we applied our method to the scenario described above. 3000 snapshots were used to estimate the cumulant matrices. Both forward and backward spatial smoothing with MUSIC were used in the second and third steps of our method. Figure 3.5 shows the MUSIC spectrum for each coherent group obtained with our method for 100 Monte Carlo runs of the experiment. The sharp peaks in the

Table 3.1: Sample means $\mu$ and standard deviations $\sigma$ of the arrival angle estimates based on the 100 realizations of Experiment 1.

| | Groups | | | | | | | |
|---|---|---|---|---|---|---|---|---|
| | 1 | | 2 | | 3 | | 4 | |
| Path | $\mu$ | $\sigma$ | $\mu$ | $\sigma$ | $\mu$ | $\sigma$ | $\mu$ | $\sigma$ |
| 1 | 39.98 | 0.19 | 49.96 | 0.47 | 45.03 | 0.23 | 59.98 | 0.34 |
| 2 | 67.99 | 0.76 | 70.00 | 0.36 | 64.97 | 0.22 | 84.97 | 0.42 |
| 3 | 80.01 | 0.76 | 90.03 | 0.27 | 85.00 | 0.10 | 104.93 | 0.58 |
| 4 | 114.99 | 0.33 | 119.96 | 0.15 | 110.03 | 0.59 | 117.97 | 0.79 |
| 5 | 130.06 | 0.23 | 134.95 | 0.38 | 125.97 | 0.28 | 140.00 | 0.52 |

MUSIC spectrum give the arrival angle estimates. The actual arrival angles are also marked in Fig. 3.5. Observe that we are able to estimate all arrival angles, and the estimates are consistent.

In Table 3.1, the sample means and standard deviations of the arrival angle estimates based on the 100 realizations are given. These values should be compared with those given above, to see that our method performs well.

Note that we have a total of 20 sources and a 10 sensor linear subarray. Covariance based methods, including the spatial smoothing, fail for this case, because, the number of signals is larger than the number of sensors.

### 3.5.2 Experiment 2: Effect of data length

In this experiment we investigate the effect of number of snapshots on the performance of our method. The same antenna array and signal model as in Experiment 1 were used. The arrival angles and propagation constants were chosen the same whereas direct-path SNRs were fixed at $20dB$. We increased the number of snapshots by steps of 250 in the range $[500, 3000]$. Taking the rightmost two dipoles in Fig. 3.3 as $r_1(t)$ and $r_2(t)$, we applied our method. Both forward and backward spatial smoothing with Root-MUSIC were used in the second and third steps of our method. We ran our method for 30 Monte Carlo realizations of the experiment, at each value of number of snapshots. Figure 3.6 shows the sample standard deviations as a function of number of snapshots. As seen from the figure, standard deviations decrease as the sample size is increased.

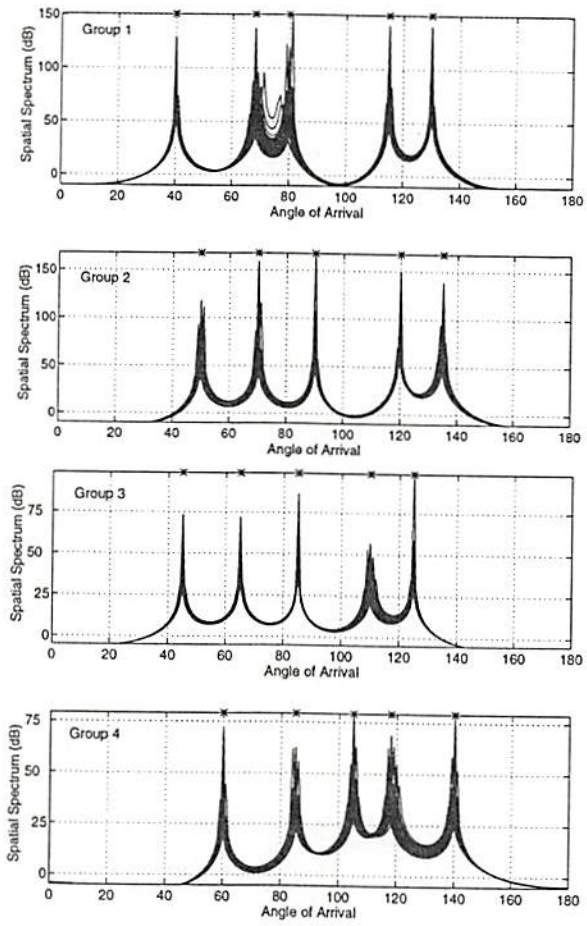


Figure 3.5: MUSIC spectrum estimates for each coherent group obtained with our method for 100 runs of the first experiment. The actual arrival angles are marked with the symbol "*".

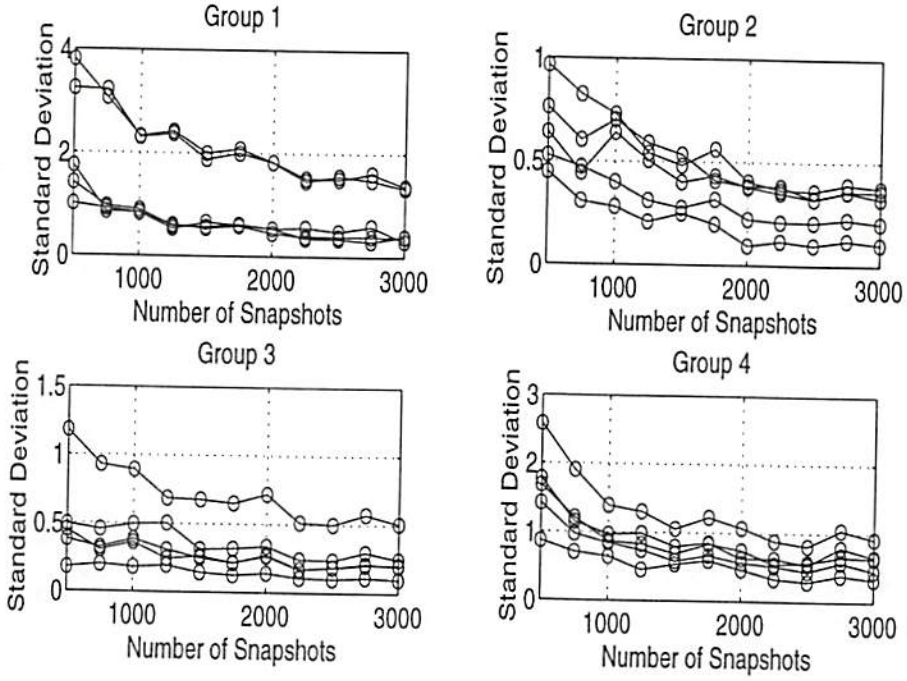


Figure 3.6: Sample standard deviations [in degrees] of angle estimates obtained with extended-VESPA for each signal as a function of number of snapshots based on 30 realizations of Experiment 2. "o" signs indicate data points.

### 3.5.3 Experiment 3: Using covariance information

In this experiment we show that projecting the generalized steering vector estimates onto the signal subspace obtained from the spatial array covariance matrix yields better angle estimates than those obtained from the basic version of our cumulant-based direction-finding algorithm. This improvement method was proposed in Section 3.3.2.

For this purpose, we assumed the same signal scenario as in Experiment 1. There are four independent groups and five signals in each group. We applied our basic algorithm for 100 different realizations of Experiment 1; for each realization we also applied the method described in Section 3.3.2 in order to get improved angle estimates, i.e., we projected the generalized steering vector estimates onto the signal space obtained from the spatial covariance matrix corresponding to the linear subarray. The number of snapshots was 2000. For both methods we calculated the root-mean-square errors (rmse) for each angle estimate which is defined as $rmse = \sqrt{\frac{1}{N}\sum_{n=1}^{N}(\theta_{est,n} - \theta)^2}$ where $\theta$ and $\theta_{est,n}$ are the actual value of the arrival angle and its estimated value for the $n$th realization, respectively. The results are given in Table 3.7. Observe that, for low SNRs, our projection method gives better angle estimates than the basic version of our cumulant-based direction-finding algorithm. As SNR increases, both versions tend to give equal performance. One concludes, therefore, that using the covariance information yields better results in low SNR cases.

### 3.5.4 Experiment 4: Improvement by BFBI3, 2 groups

The purpose of employing the beamformer that is described in Section 3.3.3 in the first step of improved extended VESPA is to minimize the cross-term effects in the cumulant estimates which are present due to multiple groups. Although different groups are statistically independent, cross-term effects are present because a finite number of samples are used in estimating the cumulants. In this experiment, we substantiate our earlier claim that the cross-term effects are reduced by suppressing other groups when working with each group, one at a time. We again consider the 14-element array in Fig. 3; but, for simplicity we assumed

two groups, each containing five coherent signals, with the following propagation constants and arrival angles:

**Group 1**

DOAs: $\{45^o, 70^o, 90^o, 100^o, 120^o\}$,

Propagation Constants: $\{0.3 - 0.8i, 0.4 + 0.9i, 0.8 + 0.6i, 0.9 + 0.7i, 1\}$.

**Group 2**

DOAs: $\{50^o, 65^o, 80^o, 93^o, 110^o\}$,

Propagation Constants: $\{0.9 + 0.3i, 10.9 - 0.3i, 0.8 + 0.7i, 1\}$.

The signals with unit propagation constants correspond to direct paths. We assumed AWG noise, and 2500 snapshots were used. Whereas the direct path SNR of the second group was fixed at 10dB, the first group SNR was variable and was increased by 2dB steps in the range from 0 to 20dB. For each value of the first group SNR, we performed a 100 run Monte Carlo experiment by running both extended-VESPA and its improved version. For the improved version, we used BFBI3.

Fig. 3.7 displays the RMSEs for the second group arrival angles as a function of the first group SNR, for both regular and extended-VESPA with BFBI3 improvement. The second group was assumed the desired one for BFBI3. As Fig. 3.7 shows, the RMSEs curves for both versions of extended VESPA follow the same path up to 10dB, after which the RMSE performance of regular extended-VESPA deteriorates while the improved version gives better estimates.

These observations support our earlier claims: when the first group's signal powers are lower than those of the second group, cross-terms in the second group's cumulant estimates due to the first group are negligible (see the region for SNR less than 10 dB in Fig. 3.7. Consequently, using BFBI3 to suppress the impact of first group does not reduce RMSEs of the second group's arrival angles. On the other hand, when the first group's signal powers are much higher than those of the second group (when SNR is greater than 10dB), the cross-terms present in the second group's cumulant estimates due to the first group are powerful. They result in poor sample estimates, and hence, degrade the RMSE performance of the regular extended-VESPA estimates. In this case, the improved version of extended VESPA suppresses the first group's signals, and, therefore, reduces the

cross terms as expected (see Fig. 3.7 for SNR greater than 10dB). This in turn, results in better cumulant estimates and hence better DOA estimates.

Fig. 3.8 displays the RMSEs for the first group arrival angles as a function of the first group SNR, for both regular and extended-VESPA with BFBI3 improvement. The first group was assumed the desired one for BFBI3. As expected, the RMSEs decrease as the first group SNR increases. When the first group SNR is less than the second group SNR (the region for which SNR is less than 10dB in Fig. 3.8), the improved method gives slightly better estimates. The reason is that, in this region, suppressing the second group eliminates the cross terms in the first group's cumulant estimates due to the second group. As the first group SNR increases, impact of cross terms due to the second group reduces; therefore, both methods give equally good estimates.

### 3.5.5 Experiment 5: BFBI1 versus BFBI3

In this experiment, we compare the beamforming improvement methods BFBI1 and BFBI3, which are described in Section 3.3.3. The performance measure used for comparison is the mean-squared error. We also compare both methods to the regular version of extended-VESPA. Note that the BFBI1 does not require the extra eigendecomposition that BFBI3 does, and hence is computationally much simpler than BFBI3.

The signal scenario is as in Experiment 1. There are four groups each containing five signals. The propagation constants and arrival angles are given in Experiment 1. The direct path SNR for each group was increased simultaneously by 2dB steps in the range $-10$ to 30dB for all groups. For each value of SNR, we performed a 100 run Monte-Carlo experiment by running both extended-VESPA and its two improved versions: BFBI1 and BFBI3. The root-mean-squared errors (RMSEs) obtained by the three methods for the first group signals are plotted as a function of SNR in Fig.3.9. Observe that the BFBI3 has the lowest RMSE among the three methods over a useful range of SNR values. In this experiment, the minimum required SNR for accurate estimation of DOAs with all of these three methods seems to be between $-10$ and 0dB, below which neither of the three methods give reliable estimates since RMSEs are unacceptably high. For

SNR greater than a threshold value, BFBI1 has about the same MSE performance as BFBI3, which is better than the performance of regular extended-VESPA. At an even higher SNR value, all three methods seem to have equal performances.

Conclusions to be drawn from this experiment are: (1) Use BFBI1 for high SNR cases, since it is computationally much simpler than BFBI3; and, (2) For higher SNRs, neither cumulant-based beamforming method yields much improvement over regular extended-VESPA. Another interesting point to note is, as seen from Fig. 3.9, for some groups, below an SNR threshold, BFBI1 may yield even worse results than the regular extended-VESPA. This is because BFBI1 assumes that all groups, except the desired one, are perfectly suppressed, which is only true if the generalized steering vector estimates are estimated without error. For low SNRs, the sample cumulants, which are used to obtain the generalized steering vector estimates, are corrupted by lots of additive noise; therefore, the vector-based improvement method may actually deteriorate the original generalized steering vector estimates. On the other hand, BFBI3 overcomes this problem by taking the principal component of a suitably defined cumulant-matrix, at the expense of computational load. Consequently, *BFBI3 always yields the best MSE performance in the useful range of SNR values; therefore, it is recommended for low SNRs.*

No simulations have been included for BFBI2 because BFBI3 is a better alternative than BFBI2 from an accuracy standpoint.

## 3.6 Conclusions

We have shown that, using cumulants, subspace-based direction-finding is possible in the coherent signals case. A uniform linear subarray is needed; the rest of the array may have arbitrary and unknown response, and does not require calibration. We have also shown that it is possible to detect more targets than sensors, which is an impossible task to accomplish using covariance-based subspace methods with arbitrary arrays, even in the case of *known* array response and *incoherent* signals.

Unlike some of the proposed cures for handling coherence, our method requires *no* array calibration or search procedure, and, unlike existing covariance-based

spatial smoothing, for our method the array does not have to be entirely linear. Only some part of the array must be linear and the number of its elements determines the maximum number of resolvable signals in each coherent group.

The entire array is fully exploited by our method, which results in increased aperture. To be more specific, the total number of sensors determines the number of resolvable coherent groups. As shown in Section refns, the presence of four arguments in the cumulants we are using enables us to first estimate the generalized steering vectors for each group. After estimating the generalized steering vectors, we use spatial smoothing as a post processing scheme on each individual generalized steering vector to find the directions; therefore, an increased effective aperture is obtained. Since covariances only have two arguments, a formulation to estimate the generalized steering vectors similar to Step 1 of our procedure is not possible for them; therefore, covariance-based methods can not handle sources on a group by group basis, which results in a reduced number of resolvable targets when they are used.

We have also developed several methods to improve direction-of-arrival estimates obtained by extended-VESPA. Among these methods, the subspace-based beamforming improvement method, BFBI3, is found to offer the most significant improvement for low SNRs. For high SNRs, we suggest using extended-VESPA without the improvement methods.

Extended-VESPA can replace existing covariance-based processing in a given array without requiring any modification in the associated hardware, provided the given array includes a linear subarray. Since independent groups are treated individually, processing can be parallelized to reduce the computing time.

## 3.7 Appendix-Obtaining Generalized Steering Vectors

Define a new $2M \times M$ matrix $\mathbf{C}$ by concatenating $\mathbf{C}_1$, $\mathbf{C}_2$ as follows

$$\mathbf{C} \triangleq \begin{bmatrix} \mathbf{C}_1 \\ \mathbf{C}_2 \end{bmatrix} = \begin{bmatrix} \mathbf{B} \\ \mathbf{BD} \end{bmatrix} \mathbf{\Lambda B}^H \triangleq \mathbf{S\Lambda B}^H. \tag{3.30}$$

The singular value decomposition of $\mathbf{C}$ yields

$$\mathbf{C} = [\mathbf{U}_1, \mathbf{U}_2] \begin{bmatrix} \mathbf{\Sigma} & \mathbf{0} \\ \mathbf{0} & \mathbf{0} \end{bmatrix} \mathbf{V}^H \tag{3.31}$$

where $\mathbf{\Sigma} \triangleq \text{diag}(\sigma_1, \cdots, \sigma_G)$; $\mathbf{U}_1 \triangleq [\mathbf{u}_1, \cdots, \mathbf{u}_G]$ and $\mathbf{U}_2 \triangleq [\mathbf{u}_{G+1}, \cdots, \mathbf{u}_{2M}]$. It follows therefore that

$$\mathbf{C}^H \mathbf{U}_2 = \mathbf{0}, \tag{3.32}$$

or, equivalently

$$\mathbf{B}\mathbf{\Lambda}^* \mathbf{S}^H \mathbf{U}_2 = \mathbf{0}. \tag{3.33}$$

Since $\mathbf{B}\mathbf{\Lambda}^*$ is full-rank, (3.33) implies $\mathbf{S}^H\mathbf{U}_2 = \mathbf{0}$. Using the fact that $\mathbf{U}_1$ is orthogonal to $\mathbf{U}_2$, it follows that

$$\text{span}(\mathbf{S}) = \text{span}(\mathbf{U}_1). \tag{3.34}$$

Therefore, there exists a nonsingular $G \times G$ matrix $\mathbf{T}$ such that

$$\mathbf{U}_1 = \mathbf{S}\mathbf{T} \tag{3.35}$$

or, such that

$$\begin{bmatrix} \mathbf{U}_{11} \\ \mathbf{U}_{12} \end{bmatrix} = \begin{bmatrix} \mathbf{B} \\ \mathbf{B}\mathbf{D} \end{bmatrix} \mathbf{T} \tag{3.36}$$

where we partitioned $\mathbf{U}_1$ exactly the same way as $\mathbf{S}$, i.e., into two $M \times G$ matrices $\mathbf{U}_{11}$ and $\mathbf{U}_{12}$. Equation (3.36) establishes the signal subspace and its rotationally-invariant counterpart. Note that this rotational invariance is obtained without requiring translational invariance of the array, as opposed to ESPRIT.

Having obtained this invariance, we follow the same steps of ESPRIT in which we use the first $G$ left singular vectors of the concatenated matrix of the cumulant matrices $\mathbf{C}_1$ and $\mathbf{C}_2$ instead of signal eigenvectors of the covariance matrix of an ESPRIT array.

Equation (3.36) shows that $\mathbf{U}_{11}$ and $\mathbf{U}_{12}$ share a common columnspace of dimension $G$; therefore, $\text{rank}([\mathbf{U}_{11}, \mathbf{U}_{12}]) = G$. This last result implies [66] there

exists a $2G \times G$ matrix $\mathbf{F} \triangleq \begin{bmatrix} \mathbf{F}_x \\ \mathbf{F}_y \end{bmatrix}$ which is rank-$G$ such that

$$\begin{aligned} \mathbf{0} &= [\mathbf{U}_{11}, \mathbf{U}_{12}]\mathbf{F} \\ &= \mathbf{U}_{11}\mathbf{F}_x + \mathbf{U}_{12}\mathbf{F}_y \\ &= \mathbf{B}\mathbf{T}\mathbf{F}_x + \mathbf{B}\mathbf{D}\mathbf{T}\mathbf{F}_y, \end{aligned} \tag{3.37}$$

Since $\mathbf{B}$ is full-rank, (3.38) results in

$$\mathbf{0} = \mathbf{T}\mathbf{F}_x + \mathbf{D}\mathbf{T}\mathbf{F}_y, \tag{3.38}$$

which is equivalent to

$$-\mathbf{F}_x\mathbf{F}_y^{-1} = \mathbf{T}^{-1}\mathbf{D}\mathbf{T}, \tag{3.39}$$

Equation (3.39) implies that the eigenvalues of $-\mathbf{F}_x\mathbf{F}_y^{-1}$ must be equal to the diagonal elements of $\mathbf{D}$. To estimate the diagonal elements of $\mathbf{D}$, we, therefore, need a matrix $\mathbf{F}$ which satisfies (3.38). Such a matrix can be obtained by performing a singular value decomposition of the $M \times 2G$ matrix $[\mathbf{U}_{11}\mathbf{U}_{12}]$. Since $[\mathbf{U}_{11}\mathbf{U}_{12}]$ is rank $G$, the last $G$ right singular vectors of $[\mathbf{U}_{11}\mathbf{U}_{12}]$ can be selected as $\mathbf{F}$.

Using (3.35) and (3.39), columns of the steering matrix $\mathbf{B}$ can be obtained to within a constant as follows. Let $\mathbf{E}$ be the eigenvector matrix of $-\mathbf{F}_x\mathbf{F}_y^{-1}$. From (3.39), it follows that $\mathbf{E} = (\mathbf{Z}\mathbf{T})^{-1}$ where $\mathbf{Z}$ is an arbitrary diagonal matrix with nonzero entries. Therefore, multiplying (3.35) by $\mathbf{E}$, we find that

$$\mathbf{U}_1\mathbf{E} = \mathbf{S}\mathbf{T}(\mathbf{Z}\mathbf{T})^{-1} = \mathbf{S}\mathbf{Z}^{-1}, \tag{3.40}$$

and, using the partitioning of (3.36) in (3.40), we find that

$$\mathbf{U}_{11}\mathbf{E} = \mathbf{B}\mathbf{Z}^{-1} \tag{3.41}$$

and

$$\mathbf{U}_{12}\mathbf{E}\mathbf{D}^{-1} = \mathbf{B}\mathbf{Z}^{-1}, \tag{3.42}$$

where $\mathbf{D}$ was estimated as explained previously. Finally, an improved estimate of

$\mathbf{B}$ is obtained to within a diagonal matrix by averaging these results, as follows:

$$\mathbf{B}\mathbf{Z}^{-1} = \frac{1}{2}\left(\mathbf{U}_{11}\mathbf{E} + \mathbf{U}_{12}\mathbf{E}\mathbf{D}^{-1}\right). \tag{3.43}$$

Table 3.2: Root-mean-squared errors obtained in Experiment 3 for: (a) Group 1, (b) Group 2, (c) Group 3, (d) Group 4. The variables $rmse_1$ and $rmse_2$ refer to root-mean-squared errors obtained using two different versions of our DF method, the basic version and the improved version. The latter is obtained by projecting the generalized steering vector estimates onto the signal subspace obtained from the estimated spatial covariance matrix of the linear subarray, respectively. The results were based on 2000 snapshots and 100 realizations, and are given for SNR levels of [10, 5, 0, -5, -10] dB.

(a)

| $SNR$ | $Angle$ | 130 | 115 | 80 | 68 | 40 |
|---|---|---|---|---|---|---|
| -10 | $rmse_1$ | 4.08 | 7.90 | 12.11 | 7.49 | 12.04 |
| | $rmse_2$ | 3.50 | 6.89 | 10.05 | 6.83 | 9.98 |
| -5 | $rmse_1$ | 2.38 | 2.35 | 3.24 | 2.67 | 3.07 |
| | $rmse_2$ | 2.16 | 2.10 | 2.82 | 2.63 | 2.29 |
| 0 | $rmse_1$ | 1.13 | 1.01 | 2.31 | 2.34 | 0.96 |
| | $rmse_2$ | 1.01 | 0.99 | 2.30 | 2.33 | 0.81 |
| 5 | $rmse_1$ | 0.75 | 0.69 | 2.21 | 2.08 | 0.75 |
| | $rmse_2$ | 0.73 | 0.68 | 2.19 | 2.07 | 0.74 |
| 10 | $rmse_1$ | 0.55 | 0.61 | 1.83 | 1.78 | 0.54 |
| | $rmse_2$ | 0.54 | 0.61 | 1.83 | 1.77 | 0.53 |

(b)

| $SNR$ | $Angle$ | 135 | 120 | 90 | 70 | 50 |
|---|---|---|---|---|---|---|
| -10 | $rmse_1$ | 4.52 | 7.38 | 10.33 | 9.30 | 9.98 |
| | $rmse_2$ | 2.81 | 7.73 | 9.60 | 8.58 | 8.36 |
| -5 | $rmse_1$ | 1.33 | 1.98 | 5.32 | 4.68 | 3.39 |
| | $rmse_2$ | 1.19 | 1.82 | 4.31 | 4.01 | 2.86 |
| 0 | $rmse_1$ | 0.83 | 1.05 | 1.74 | 1.77 | 1.18 |
| | $rmse_2$ | 0.78 | 1.03 | 1.73 | 1.76 | 1.16 |
| 5 | $rmse_1$ | 0.50 | 0.23 | 0.30 | 0.41 | 0.53 |
| | $rmse_2$ | 0.49 | 0.22 | 0.29 | 0.41 | 0.52 |
| 10 | $rmse_1$ | 0.44 | 0.20 | 0.25 | 0.36 | 0.42 |
| | $rmse_2$ | 0.43 | 0.19 | 0.25 | 0.37 | 0.41 |

(c)

| $SNR$ | $Angle$ | 125 | 110 | 85 | 65 | 45 |
|---|---|---|---|---|---|---|
| -10 | $rmse_1$ | 5.17 | 7.37 | 6.52 | 9.45 | 8.49 |
| | $rmse_2$ | 1.95 | 4.17 | 4.27 | 3.18 | 5.33 |
| -5 | $rmse_1$ | 1.09 | 1.96 | 1.60 | 1.11 | 1.37 |
| | $rmse_2$ | 0.63 | 1.09 | 0.29 | 0.47 | 0.65 |
| 0 | $rmse_1$ | 0.45 | 0.72 | 0.15 | 0.31 | 0.40 |
| | $rmse_2$ | 0.44 | 0.74 | 0.16 | 0.32 | 0.40 |
| 5 | $rmse_1$ | 0.33 | 0.68 | 0.11 | 0.11 | 0.24 |
| | $rmse_2$ | 0.33 | 0.67 | 0.11 | 0.24 | 0.27 |
| 10 | $rmse_1$ | 0.31 | 0.66 | 0.11 | 0.23 | 0.24 |
| | $rmse_2$ | 0.31 | 0.67 | 0.11 | 0.23 | 0.24 |

(d)

| $SNR$ | $Angle$ | 140 | 118 | 105 | 85 | 60 |
|---|---|---|---|---|---|---|
| -10 | $rmse_1$ | 8.29 | 10.06 | 12.39 | 11.90 | 9.17 |
| | $rmse_2$ | 3.29 | 5.52 | 6.47 | 5.66 | 4.48 |
| -5 | $rmse_1$ | 2.19 | 2.51 | 4.49 | 4.30 | 2.98 |
| | $rmse_2$ | 1.65 | 2.47 | 1.93 | 1.76 | 1.29 |
| 0 | $rmse_1$ | 1.08 | 1.46 | 1.87 | 1.69 | 1.16 |
| | $rmse_2$ | 1.02 | 1.54 | 1.05 | 0.76 | 0.55 |
| 5 | $rmse_1$ | 0.94 | 1.44 | 0.90 | 0.66 | 0.49 |
| | $rmse_2$ | 0.89 | 1.37 | 0.88 | 0.66 | 0.49 |
| 10 | $rmse_1$ | 0.89 | 1.30 | 0.81 | 0.66 | 0.49 |
| | $rmse_2$ | 0.88 | 1.30 | 0.81 | 0.65 | 0.49 |

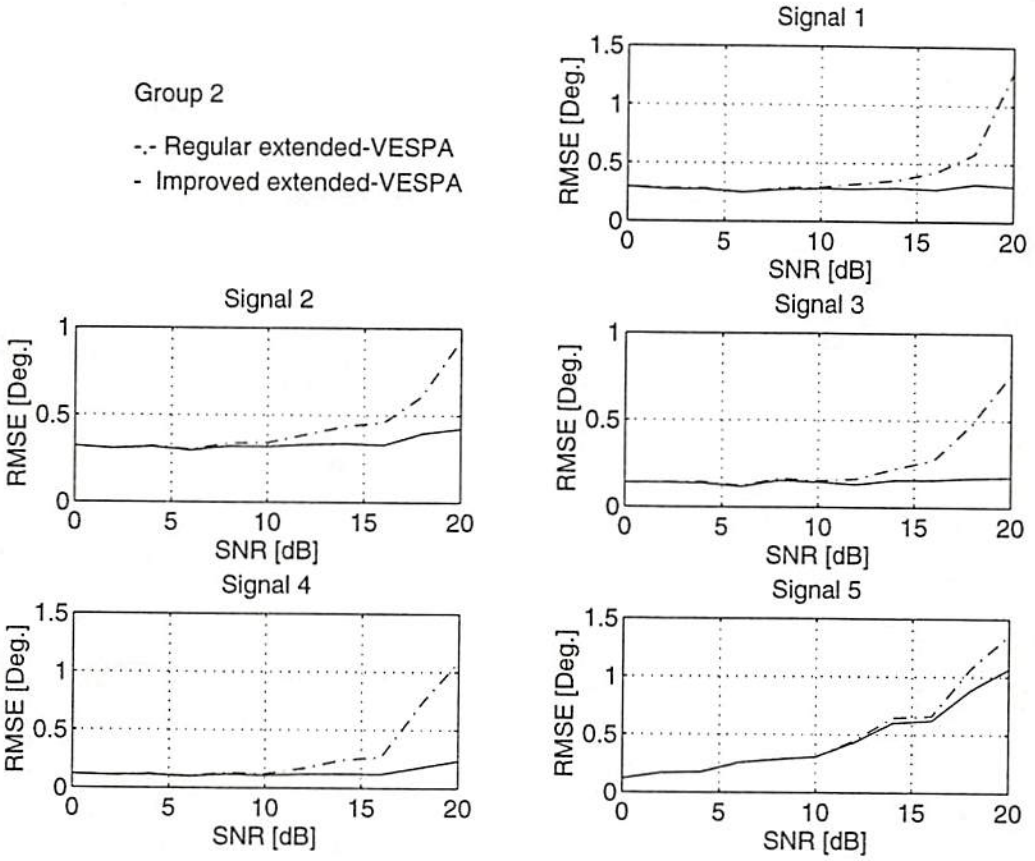


Figure 3.7: Root-mean-squared errors (RMSEs) for the arrival angle estimates of the second group obtained in Experiment 4 as a function of the first group SNR. The ordering of the signals are the same as in the text.

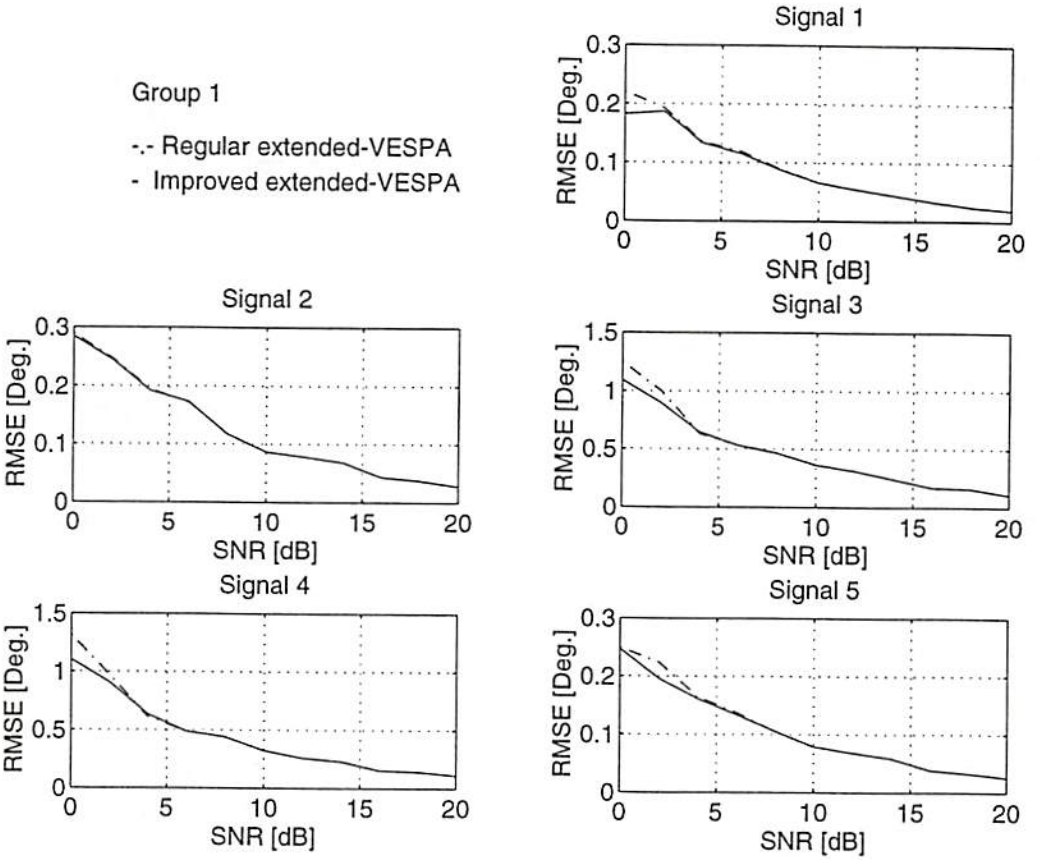


Figure 3.8: Root-mean-squared errors (RMSEs) for the arrival angle estimates of the first group obtained in Experiment 4 as a function of first group SNR. The ordering of the signals are the same as in the text.

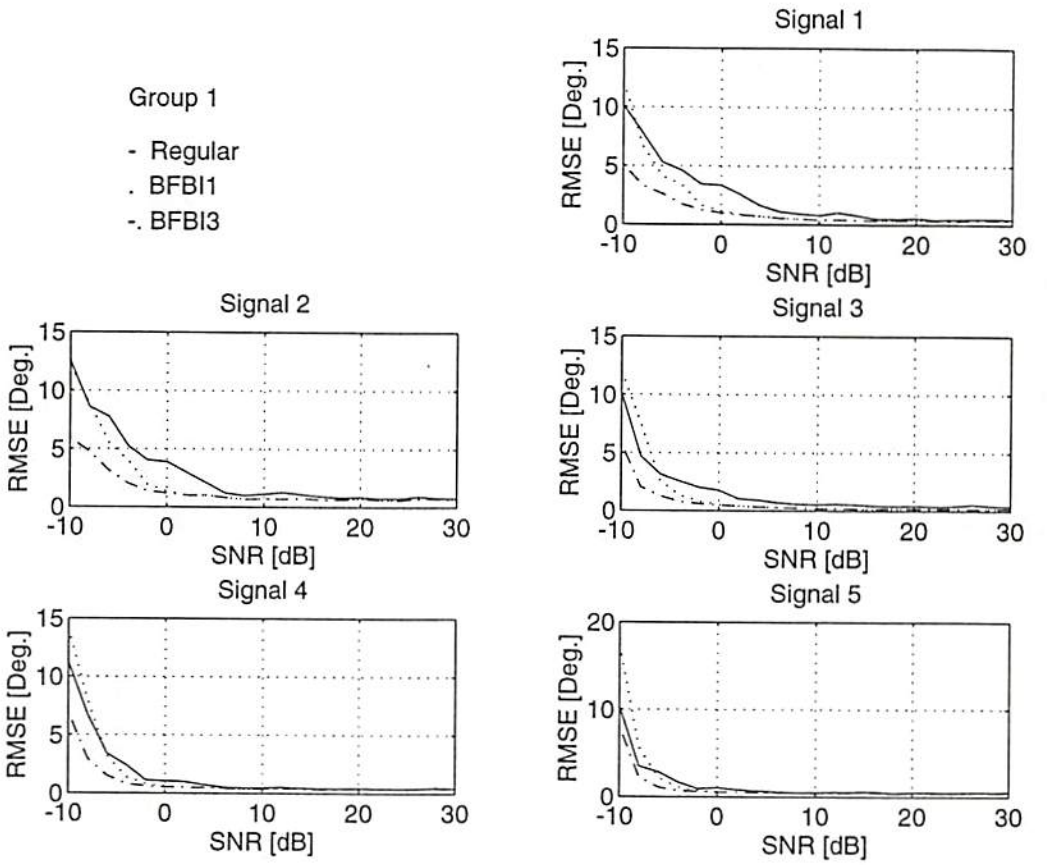


Figure 3.9: Root-mean-squared errors (RMSEs) for the arrival angle estimates of the first group obtained in Experiment 5. BFBI1 and BFBI3 refer to the cumulant subspace-based and vector-based improvement methods, respectively. The ordering of the signals are the same as in the text.

# Chapter 4

# Blind Beamforming for Coherent Signals

By beamforming we mean the process of combining the sensor outputs of an array with suitable weight vectors such that desired signals are recovered subject to an optimality criterion. In this chapter, we address the *blind* beamforming problem for coherent signal environments assuming no knowledge about the array structure or response. Before presenting our approach, we first discuss the limitations of the existing covariance-based beamforming methods for this problem.

There are a number of second-order statistics based criteria that have been proposed for obtaining the optimum beamforming weight vector that combines the array sensor measurements to recover desired signals while supressing interferences. These criteria lead to the same general form for the optimum weight vector [48], i.e., $\mathbf{w}_{opt} = c\mathbf{R}^{-1}\mathbf{a}(\theta_d)$ where $\mathbf{R}$ is the spatial covariance matrix of the received signal $\mathbf{r}(t)$, $\mathbf{a}(\theta_d)$ is the array response in the desired direction (look-direction), and $c$ is a constant whose value depends on the criterion used. In the special case of MVDR [5], the array output power is minimized subject to a unity look-direction gain constraint, $\mathbf{w}_{opt}^H\mathbf{a}(\theta_d) = 1$, which results in $1/c = \mathbf{w}_{opt}^H\mathbf{R}^{-1}\mathbf{w}_{opt}$. It is clear that the *array response* in the desired signal direction must either be known or estimated to implement the optimum beamformer. If the array response or geometry is unknown, as in the blind beamforming problem, it is necessary to calibrate the array to obtain the response information; however, array calibration

is a very costly procedure. Calibration can be avoided and the array response can be estimated using ESPRIT [66]; however, ESPRIT requires translationally equivalent subarrays, which is often an impractical constraint, and, as for other subspace-based methods, ESPRIT fails in the coherent signals case. Even if the response function of the array is known or array is calibrated, due to perturbations in the geometry and the response of the array, the response in the desired direction may be different than its calculated value. Therefore it becomes important to use the estimated values of the array response for fine tuning to the received signals. There are a number of so-called property-restoring methods such as the adaptive CMA [72] that use second-order statistics and rely on certain known properties of the source signals; however, the signals extracted by property-restoring methods do not necessarily have the same waveform as the actual source signals.

The optimum beamformer using second-order statistics tends to cancel the desired signal and it fails to perform optimally when there are signals coherent with the desired signal [63]. Moreover, it tends to cancel the desired signal in the output [70]. A detailed explanation of signal cancellation phenomenon can be found in [70]. Several methods have appeared in [2], [56], [70], [71], [77] to overcome the signal cancellation problem when coherent interferers are present. The methods of [2], [56], [70], [71] are limited to uniform linear arrays; [77] requires some specific array configuration. None of these methods are directly applicable to the blind beamforming problem due to their implicit constraints on the array structure.

For a blind beamformer, on the other hand, the presence of coherent multipaths does not make any difference. In other words, the case of coherent multipath signals is identical to that of independent signals with no multipath; because, as shown in Section 4.1, each coherent multipath from a given source causes only a reparameterization of the steering vector of that source.

In the cumulant-based processing framework, the blind recovery problem has received increased research interest. Adaptive solutions based on optimization of various cumulant-based criteria, or solutions depending on eigendecomposition of suitably defined cumulant matrices were proposed [80], [8], [68], [ [7], and references therein]. In these methods, second order statistics are used to whiten

the signal part of the received signals prior to applying cumulant-based post processing, which is the main drawback, because the covariance matrix of the noise needs to be estimated or known a priori. Besides, these methods have limitations. For example, the eigendecomposition-based method in [7] fails when there are sources having identical kurtosis, i.e. sources of the same type. An alternative is to use only higher than second-order cumulants. An iterative approach using only fourth-order cumulants were suggested by Cardoso [see [7], and references therein]. In the fourth-order cumulant method of Dogan and Mendel [19], it was assumed that the independent interfering signals are Gaussian, whereas the sole desired signal is non-Gaussian. Cumulants were used to suppress the Gaussian interferences and noise, so that one is left only with the desired signal statistics.

Here, we assume a more general scenario where there may be multiple desired signal sources and interferences. Smart jammers can also be modeled as multipaths. Our assumptions are: **A1)** The desired sources are statistically independent among themselves, and independent of the other sources; and, all of the source signals may be subject to multipath propagation. **A2)** Frequency-flat multipath propagation; **A3)** The desired source signals must have nonzero kurtosis, but no such assumption is made about interferences–if their cumulants are zero, they are already suppressed by the virtue of cumulants; if not, they will be rejected by an optimum beamformer; and, **A4)** The array is a non-ambiguous one, i.e. its response to a signal from a given direction is different from that due to another signal from a different direction. Our approach does not require any knowledge about the array.

The organization of this chapter is as follows: We formulate the problem in Section 4.1. In Section 4.2, a solution is proposed. Experimental results supporting our conclusions and demonstrating our method are provided in Section 4.3. Finally, conclusions are presented in Section 4.4.

## 4.1 Formulation of the Problem

Consider a signal scenario in which there are several narrow-band sources and interferences. Suppose that these signals undergo frequency-flat multipath propagation producing several sets of delayed and scaled replicas, which are received by an $M$ element array having *arbitrary* and *unknown response* and *geometry.* Let a total of $P$ signals $\{s_1(t), \cdots, s_P(t)\}$, from $G$ independent and narrow-band sources, $u_i(t)$, with $p_i$ multipath signals for each source ($\sum_{i=1}^{G} p_i = P$), impinge upon the array. It is assumed that the number of sources is less than the number of array elements (i.e., $G < M$). The $i$th group contains multipaths of the $i$th source and 'smart' jammers which are coherent with the $i$th source. The array measurements are corrupted by additive Gaussian noise whose spatial correlation structure is unknown. We assume that $N$ snapshots taken at time points $t = 1, \cdots, N$ are available. With these assumptions, the signal received by the array at time $t$ is

$$\mathbf{r}(t) = \mathbf{A}\mathbf{s}(t) + \mathbf{n}(t) \tag{4.1}$$

where $\mathbf{r}(t) = [r_1(t), \cdots, r_M(t)]^T$, $\mathbf{A}$ is an $M \times P$ *unknown* steering matrix; $\mathbf{s}(t)$ is a $P \times 1$ signal vector, and $\mathbf{n}(t)$ is the independent measurement noise vector which can be Gaussian, non-Gaussian symmetrically distributed, or a mixture of Gaussian and this type of non-Gaussian noise.

Expressing the coherence among the signals as in (3.2), the received signal vector, written in terms of the source signals is:

$$\mathbf{r}(t) = \mathbf{A}\mathbf{Q}\mathbf{u}(t) + \mathbf{n}(\mathrm{t}) = \mathbf{B}\mathbf{u}(t) + \mathbf{n}(\mathrm{t}) \tag{4.2}$$

Our objective is to recover the signals $\{u_i(t)\}_{i=1}^{G}$ without any information about the array structure.

## 4.2 Proposed Solution

Our solution proceeds in three main steps: (1) Estimate the generalized steering vectors; (2) Using the estimated generalized steering vectors in the previous step,

design beamformers to recover each signal one at a time; and, (3) Correct the constellation rotation. Since all of the signals are estimated one at a time regardless of which signals are desired, temporal structures of the signals can be used to differantiate one from the other.

### 4.2.1 Step 1: Estimation of Generalized Steering Vectors

The generalized steering vectors $\{\mathbf{b}_1, \cdots, \mathbf{b}_G\}$ are estimated following Step 1 of Chapter 3. Any pair of "right" sensor measurements can be used in (3.4) and (3.6). The ideas presented in Sections 3.3.1 and 3.3.3 can be used here to improve the generalized steering vector estimates.

### 4.2.2 Step 2: Optimum Beamforming

Using the generalized steering vector estimates $\{\hat{\mathbf{b}}_1, \cdots, \hat{\mathbf{b}}_G\}$ obtained in the previous step, and second-order statistics, we can design optimum beamformers to recover the source signals $\{u_i(t)\}_{i=1}^G$ to within a complex constant, one at a time, as follows. The received signal at time point $t$ can be expressed as

$$\mathbf{r}(t) = \mathbf{b}_i u_i(t) + \mathbf{B}_{i,int}\mathbf{u}_{i,int}(t) + \mathbf{n}(t) \tag{4.3}$$

where $i = 1, \cdots, G$; all the source signals except $u_i(t)$ are treated as interferences; $\mathbf{b}_i$ is the generalized steering vector of $u_i(t)$ and $\mathbf{B}_{i,int} = [\mathbf{b}_1, \cdots, \mathbf{b}_{i-1}, \mathbf{b}_{i+1}, \cdots, \mathbf{b}_G]$ is the generalized steering matrix of the other sources, $\mathbf{u}_{i,int}(t) = [u_1, \cdots, u_{i-1}, u_{i+1}, \cdots, u_G]^T$.

Using (4.3), the spatial array covariance matrix can be written as:

$$\mathbf{R} = \sigma_i^2 \mathbf{b}_i \mathbf{b}_i^H + \mathbf{R}_{i,int} \tag{4.4}$$

where $\sigma_i^2 = E\{u_i(t)u_i(t)^*\}$, and $\mathbf{R}_{i,int}$ is the array covariance matrix of all other sources except $u_i(t)$ and includes the noise.

A number of different criteria for optimum recovery of the signals $\{u_i(t)\}_{i=1}^G$ lead to the same beamformer structure which is given by $\mathbf{w}_i = c\mathbf{R}^{-1}\mathbf{b}_i$, where $\mathbf{R}$ is the array covariance matrix, and the constant $c$ depends on the criterion

being used. The minimum-variance distortionless-response (MVDR) beamformer weight vector is obtained by minimizing the array output power $E\{|\mathbf{w}_i{}^H\mathbf{r}(t)|^2\} = \mathbf{w}_i{}^H\mathbf{R}\mathbf{w}_i$ subject to the unity gain (distortionless response) constraint $\mathbf{w}_i\mathbf{b}_i = 1$ for the desired signal. We denote this weight vector as $\mathbf{w}_{i,mvdr}$. The solution for $\mathbf{w}_{i,mvdr}$ is [48]:

$$\mathbf{w}_{i,mvdr} = c_{i,mvdr1}\mathbf{R}^{-1}\mathbf{b}_i \tag{4.5}$$

where $c_{i,mvdr1} = \frac{1}{\mathbf{b}_i^H\mathbf{R}^{-1}\mathbf{b}_i}$.

The maximum signal-to-interference-plus-noise ratio (SINR) beamformer weight vector is obtained as follows: the signal power at the array output is given by $E\{|\mathbf{w}_i{}^H\ \mathbf{b}_i u_i(t)|^2\} = \sigma_i^2|\mathbf{w}_i{}^H\mathbf{b}_i|^2$. The interference-plus-noise power is $E\{|\mathbf{w}_i{}^H (\mathbf{B}_{i,int}\mathbf{u}_{i,int} + \mathbf{n}(t))|^2\} = \mathbf{w}_i{}^H\mathbf{R}_{i,int}\mathbf{w}_i$. SINR is defined as

$$SINR(\mathbf{w}_i) = \sigma_i^2\frac{|\mathbf{w}_i{}^H\mathbf{b}_i|^2}{\mathbf{w}_i{}^H\mathbf{R}_{i,int}\mathbf{w}_i} \tag{4.6}$$

Applying the Cauchy inequality to (4.6), we find that

$$SINR(\mathbf{w}_i) = \sigma_i^2\frac{|\left(\mathbf{R}_{i,int}^{1/2}\mathbf{w}_i\right)^H\left(\mathbf{R}_{i,int}^{-1/2}\mathbf{b}_i\right)|^2}{\mathbf{w}_i{}^H\mathbf{R}_{i,int}\mathbf{w}_i} \leq \sigma_i^2\mathbf{b}_i^H\mathbf{R}_{i,int}^{-1}\mathbf{b}_i \triangleq SINR_{max} \tag{4.7}$$

where equality is achieved if and only if

$$\mathbf{w}_{i,SINR} = c_{i,SINR1}\mathbf{R}_{i,int}^{-1}\mathbf{b}_i \tag{4.8}$$

in which $c_{i,SINR1}$ is a nonzero constant.

$\mathbf{w}_{i,SINR}$ in (4.8) can be expressed in terms of the available array covariance matrix $\mathbf{R}$, by first rearranging (4.4), as

$$\mathbf{R}_{i,int} = \mathbf{R} - \sigma_i^2\mathbf{b}_i\mathbf{b}_i^H, \tag{4.9}$$

and, then applying the Matrix Inversion Lemma to (4.9), and, then computing (4.8), as

$$\mathbf{w}_{i,SINR} = c_{i,SINR1}\mathbf{R}_{i,int}^{-1}\mathbf{b}_i$$

$$
\begin{aligned}
&= c_{i,SINR1}\left[\mathbf{R}^{-1} - \mathbf{R}^{-1}\mathbf{b}_i(\mathbf{b}_i^T\mathbf{R}^{-1}\mathbf{b}_i - \sigma_i^{-2})^{-1}\mathbf{b}_i^T\mathbf{R}^{-1}\right]\mathbf{b}_i \\
&= c_{i,SINR1}\mathbf{R}^{-1}\mathbf{b}_i\left[\mathbf{I} - (\mathbf{b}_i^T\mathbf{R}^{-1}\mathbf{b}_i - \sigma_i^{-2})^{-1}\mathbf{b}_i^T\mathbf{R}^{-1}\mathbf{b}_i\right] \\
&= c_{i,SINR1}\mathbf{R}^{-1}\mathbf{b}_i(\mathbf{b}_i^T\mathbf{R}^{-1}\mathbf{b}_i - \sigma_i^{-2})^{-1}\left[\mathbf{b}_i^T\mathbf{R}^{-1}\mathbf{b}_i - \sigma_i^{-2} - \mathbf{b}_i^T\mathbf{R}^{-1}\mathbf{b}_i\right] \\
&= \frac{-c_{i,SINR1}\sigma_i^2}{\mathbf{b}_i^T\mathbf{R}^{-1}\mathbf{b}_i - \sigma_i^{-2}}\mathbf{R}^{-1}\mathbf{b}_i \\
&= c_{i,SINR2}\mathbf{R}^{-1}\mathbf{b}_i, \qquad (4.10)
\end{aligned}
$$

where $c_{i,SINR2} \triangleq \frac{-c_{i,SINR1}\sigma_i^2}{\mathbf{b}_i^T\mathbf{R}^{-1}\mathbf{b}_i - \sigma_i^{-2}}$.

Finally, the source signals $\{u_i(t)\}_{i=1}^G$ are each recovered to within a complex constant by replacing $\mathbf{b}_i$, in the above optimum beamformers by its estimate $\hat{\mathbf{b}}_i$, obtained in Step 1, and replacing $\mathbf{R}$ by its sample estimate, so that

$$\hat{u}_i(t) = \mathbf{w}_i{}^H\mathbf{r}(t) \qquad (4.11)$$

where $i = 1, \cdots, G$, and $\mathbf{w}_i$ is either $\mathbf{w}_{i,SINR}$ or $\mathbf{w}_{i,mvdr}$.

Step 2 can be done in parallel for all $G$ sources.

### 4.2.3 Step 3: Constellation Rotation Correction

In the first step of our source recovery algorithm, the generalized steering vectors for each source are estimated to within a complex constant [see (3.43)]. Using these estimates in the above beamformers results in source estimates which are rotated arbitrarily from their original constellations. Since the choice of optimum decision regions depends on the signal constellation, a method is needed to recover the actual constellation. In this section we show how this can be done for one-dimensional signal constellations; the two-dimensional case can be corrected using cumulants.

Let $u_i(t)$ be the one-dimensional signal of interest, and $\hat{u}_i(t)$ be its perfect estimate to within a complex constant $ce^{j\theta}$, i.e., $\hat{u}_i(t) = ce^{j\theta}u_i(t)$. The constant $c$ accounts for both the arbitrary scaling and the signal power so that $u_i(t)$ is normalized to have unit power. Noting that $u_i(t)$ is real, the following hold:

$$\Re\{\hat{u}_i(t)\} = c\cos\theta u_i(t), \qquad \Im\{\hat{u}_i(t)\} = c\sin\theta u_i(t). \qquad (4.12)$$

The correlations

$$E\{\Re\{\hat{u}_i(t)\}^2\} = c^2\cos^2\theta, \qquad E\{\Im\{\hat{u}_i(t)\}^2\} = c^2\sin^2\theta, \tag{4.13}$$

and

$$E\{\Re\{\hat{u}_i(t)\}\Im\{\hat{u}_i(t)\}\} = c^2\cos\theta\sin\theta \tag{4.14}$$

can be estimated from the beamformer output $\hat{u}_i(t)$. Using these results, $\theta$ and $c$ can be obtained as

$$\hat{c} = \sqrt{E\{\Re\{\hat{u}_i(t)\}^2\} + E\{\Im\{\hat{u}_i(t)\}^2\}} \tag{4.15}$$

and

$$\hat{\theta} = \arctan\left(\frac{E\{\Re\{\hat{u}_i(t)\}\Im\{\hat{u}_i(t)\}\}}{E\{\Re\{\hat{u}_i(t)\}^2\}}\right) \tag{4.16}$$

Finally, the actual constellation of $u_i(t)$ can be recovered, to within a sign ambiguity, as

$$u_i(t) = \frac{1}{\hat{c}}e^{-j\hat{\theta}}\hat{u}_i(t) \tag{4.17}$$

where $i = 1, \cdots, G$. The sign ambiguity comes from the fact $u_i(t)$ and $-u_i(t)$ have equal powers. However, it is possible to overcome the sign ambiguity problem by attaching a known sequence to each signal before transmitting, and comparing the demodulated sequence with the orginal sequence at the receiver side.

## 4.3 Simulation Experiments

### 4.3.1 Experiment 1

The scenario consists of three independent binary phase shift keyed (BPSK) sources which are subject to multipath propagation, and arrive at the array in Fig. 4.1 from four, two and three different directions, respectively. The arrival directions and propagation constants were chosen arbitrarily as: [50°, 70°, 90°, 100°] and [1, $-0.8 + j0.2$, $-0.3 - j0.7$, $0.6 + j0.6$]; [60°, 80°] and [1, $-0.1 + j0.8$]; and, [45°, 65°, 85°] and [1, $0.5 - j0.6$, $0.7 + j0.4$]. Unity propagation constants belong to direct paths, and direct path SNRs equal 10dB. The array

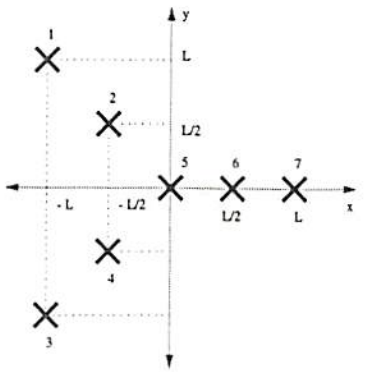


Figure 4.1: The array geometry used in the first experiment; $L$ is the wavelength.

elements were assumed to be arbitrarily rotated dipole antennas. The array response to a signal from angle $\theta$ is given by [1, $\cos(\theta - 85^o)e^{-j\pi(\sin(\theta)+\cos(\theta))}$, $\cos(\theta - 87^o)e^{-j\pi 4\sin(\theta)}$, $\cos(\theta - 92^o)e^{-j\pi(\sin(\theta)+\cos(\theta))}$, $\cos(\theta - 80^o)e^{-j\pi(2\sin(\theta)+2\cos(\theta))}$, $\cos(\theta - 75^o)e^{-j\pi(2\sin(\theta)+3\cos(\theta))}$, $\cos(\theta - 95^o)e^{-j\pi(2\sin(\theta)+4\cos(\theta))}$]. 3000 snapshots were taken. The problem of interest is to recover each source message, one at a time.

We tested our cumulant-based beamforming method, which assumes no information about the array geometry or response, and the classical MVDR beamformer for which we had to assume that arrival angles of the desired signals (the direct paths from each source) and the array response in those directions are perfectly known. The beamformer outputs from both methods are presented in Fig. 4.2. Observe that, whereas cumulant-based beamformer outputs are localized around 1 and $-1$, the MVDR beamformer fails to recover the source messages. The MVDR beamformer fails because of signal cancellation. Spatial smoothing, as explained in Section 2.2.3, is a remedy to signal cancellation in the MVDR beamformer for coherent signals; however, spatial smoothing is applicable only to uniform linear arrays, whereas the array in this experiment is a nonuniform one.

This experiment supports our earlier claim that multiple coherent signals received by an array of arbitrary geometry and unknown response can be recovered by our cumulant-based optimum blind beamformer.

### 4.3.2 Experiment 2

In this experiment we compare our method to an MVDR beamformer using the spatial smoothing method [71] (S-MVDR). Since spatial smoothing is limited to uniform linear arrays, we restrict ourselves here to this case although our method is applicable to any array. We assume that two coherent 3000 bit BPSK signals of equal power and of zero relative phase impinge upon a ten-element uniform linear array.

First, we assumed that the two signals arrive from broadside from closely-spaced directions $\{90°, 95°\}$ (measured with respect to the endfire). For this scenario, we tested both our method, and the classical-MVDR (C-MVDR) and smoothed-MVDR (S-MVDR) beamformers. In our cumulant-based blind beamformer, we used the first two sensors in the $0°$ direction as the guiding pair, and our rotation-correction algorithm. For the C-MVDR beamformer, we must assume that the desired signal direction is either known or estimated; therefore, assuming the desired signal is the one arriving from $90°$, we designed the C-MVDR beamformer. For the S-MVDR beamformer we used a subarray of length 6 (subarray length$= L/2 + 1, L = 10$) for backward and forward smoothing. The outputs of these three beamformers for the desired signal at 0, 10 and 20 dB SNRs with fixed noise power are shown in Figure 4.3 a-c. As seen, the C-MVDR beamformer fails. On the other hand, S-MVDR beamformer recovers the signals as SNR is increased; however, for equal SNRs, our cumulant-based beamformer is always better than the S-MVDR beamformer.

Second, we assumed that the two signals arrive from closely spaced directions $\{0°, 5°\}$ near endfire. Reddy *et al* [63] have shown that, for this case, spatial smoothing loses its decorrelating power for moderate smoothing lengths and therefore results in increased signal cancellation as SNR is increased. In our cumulant-based method we used the pairs $(r_1(t), r_1(t))$ and $(r_1(t), r_2(t))$ where $r_1(t)$ and $r_2(t)$ are the first two sensor measurements in the $0°$ direction. Assuming the desired signal direction is $0°$, we designed the C-MVDR beamformer. For the S-MVDR beamformer we used the same smoothing as before. Figures 4.4 a-c show outputs of the three beamformers for 0, 10 and 20 dB SNRs with fixed noise power. The presence of coherence helps the C-MVDR and S-MVDR beamformers

at low SNRs, but, these beamformers deteriorate as SNR is increased [63]. On the other hand, comparison of the first column of Fig. 4.4 with the other two columns indicates that our method is always better than the S-MVDR beamformer at equal SNRs, and that our method improves as SNR is increased, because our method combines coherent signal powers effectively instead of trying to decorrelate them.

### 4.3.3 Experiment 3

We evaluate the output signal-to-interference-plus-noise-ratio (SINR) performance of our cumulant-based beamformer and compare it to those of the classical-MVDR (C-MVDR), smoothed-MVDR (S-MVDR) and an MVDR beamformer (E-MVDR) which uses the exactly known generalized steering vector of the desired signal. Note that due to the multipaths, in reality, it is impossible to know the generalized steering vectors prior to processing even if the array is perfectly known or calibrated; hence the E-MVDR beamformer is rather a hypothetical one which is designed as a benchmark for our cumulant-based beamformer.

Assuming the same signal scenario and C-MVDR, S-MVDR and cumulant-based beamformers as in Experiment 2, and using the new E-MVDR beamformer, we performed: 1) Two 10-point Monte-Carlo experiments for the case of broadside arrivals, for SNR=10 dB and 0 dB. The output SINR for S-MVDR, E-MVDR and our cumulant based beamformer are plotted in Figs. 4.5 and 4.6 for each of these SNRs. The cumulant-based beamformer performs best even for very small number of snapshots, and converges to the maximum possible output SINR value quickly. The difference in the large-snapshot output SINR between cumulant-based and S-MVDR is around 19dB at SNR=10 dB and 12 dB at SNR=0 dB. More interestingly, the cumulant-based beamformer outperforms the E-MVDR that uses the exact value of the generalized steering vector of the desired signal. Note that the only difference between our cumulant-based beamformer and the E-MVDR is that whereas the E-MVDR uses the exact values of the generalized steering vectors, our beamformer uses the estimated values of them. The simulation results show that our blind beamformer "tunes" to the data better than the E-MVDR; 2) Two 10-point Monte-Carlo experiments for the case of endfire arrivals, for SNR=10 dB and 0 dB. The output SINR for S-MVDR, E-MVDR

and our cumulant based beamformer are plotted in Figs. 4.7 and 4.8 for each of the SNRs. The cumulant based beamformer performs best even for very small number of snapshots, such as 50, and converges to the maximum possible output SINR value quickly. The difference in the large-snapshot output SINR between cumulant-based and S-MVDR is around 11 dB at SNR=10 dB and 2.5 dB at SNR=0 dB. Again, the cumulant-based beamformer outperforms the E-MVDR.

In this experiment, the output SINRs of the classical-MVDR beamformer were very low, therefore, we do not display them with the other three beamformers here. These results suggest that not very many snapshots are needed before excellent performance is obtained with our new beamformer.

Finally, note that, whereas the smoothed-MVDR beamformer can utilize only the smoothing subarray, our method uses the entire array, i.e., our method uses a larger aperture.

### 4.3.4 Experiment 4

In this experiment we compare our blind beamforming method to the spatial smoothing-based MVDR beamformer in terms of resolvable number of signals. We demonstrate that our beamformer can separate sources even if the total number of incoming signals is more than the number of sensors, and show that spatial smoothing fails to separate the sources in this case. Since spatial smoothing is limited to uniform linear arrays, we restrict ourselves here to this case, although our method is applicable to any array having arbitrary and unknown response. We assume four independent BPSK signals of equal power and 3000 bits long which are subject to multipath propagation resulting in coherent signals. The array is assumed to be a 10-element uniform linear array with omnidirectional components. The four source signals arrive at the array from two, three, four and five different directions, respectively. Note that the total number of signals impinging on the array is 14 which is more than the number of sensors. The signal arrival angles and propagation constants were chosen as: $[55^o, 30^o]$ and $[1, 0.7 + j0.6]$; $[40^o, 90^o, 60^o]$ and $[1, 0.6 - j0.7, 0.5 + j0.8]$; $[70^o, 80^o, 120^o, 100^o]$ and $[1, 0.8 + j0.5, 0.7 + j0.6, 0.5 + j0.6]$; $[110^o, 65^o, 130^o, 140^o, 150^o]$ and $[1, 0.6 + j0.6, 0.7 - j0.7, 0.5 + j0.6, 0.8 - j0.6]$.

Table 4.1: Bit error rates ($BER$s) obtained in Experiment 4. $BER_{cum}$ and $BER_{smth}$ refer to bit error rates obtained using our cumulant-based method and smoothed-MVDR method, respectively.

| | SNR=10dB | | SNR=0dB | | SNR=-5dB | |
|---|---|---|---|---|---|---|
| Source No | $BER_{cum}$ | $BER_{smth}$ | $BER_{cum}$ | $BER_{smth}$ | $BER_{cum}$ | $BER_{smth}$ |
| 1 | 0 | 0 | 0 | 0.0013 | 0.0010 | 0.0397 |
| 2 | 0 | 0.5000 | 0 | 0.4687 | 0.0030 | 0.3900 |
| 3 | 0 | 0.2087 | 0 | 0.1937 | 0.0080 | 0.2173 |
| 4 | 0 | 0.2277 | 0 | 0.2123 | 0 | 0.2087 |

For this scenario, we tested our cumulant-based beamformer and smoothed-MVDR beamformer. In our method, we used the first two sensors in the end-fire direction as the guiding pair, and our rotation correction algorithm. In the smoothed MVDR beamformer we had to assume that the desired signal directions are either known or are estimated, because MVDR depends on the array response in the desired signal direction; therefore, we assumed that, for each source, the desired signal is the direct path and its arrival angle is known. Note that, for our method, angle-of-arrival information is not needed. For the smoothed-MVDR beamformer we used a subarray of length 6 (subarray length= $L/2+1, L = 10$), for backward and forward smoothing. Figures 4.9-4.10 show outputs of both beamformers for 10 and $-5$ dB SNRs. Observe that the smoothed-MVDR method fails while our method can separate all of the four sources successfully. The bit error rates (BERs) obtained by employing a threshold detector at the output of both beamformers are given in Table 4.1. Note that our cumulant-based method results in either zero or very small BERs for the SNRs used in the experiment.

## 4.4 Conclusions

We have developed a cumulant-based optimum *blind* beamformer for recovery of independent sources in the presence of coherent multipath propagation, which is applicable to any *arbitrary* array configuration; it does not require *any knowledge* about array response, and relies *solely* on the measurements. There is no need to estimate the directions of arrival. Our approach is based on the observation that

using cumulants of received signals, two matrices can be formed which conform to the ESPRIT architecture. In this approach, multipath powers are effectively utilized instead of decorrelated.

The two matrices permit us to estimate the generalized steering vectors for each source blindly. Then, a number of cumulant-based beamformers can be designed whose optimality have already been shown in the second-order statistics framework. Note that since the steering vectors are estimated from the data, the beamformer is tuned to the data, thereby avoiding sensitivity problems associated with mismatch in the assumed steering vectors, which occurs in the case of covariance-based processing. A comparable result using just second-order statistics does not exist for the the blind beamforming problem. Both Gaussian and non-Gaussian noises with unknown statistics can be suppressed as long as they are independent of the signals of interest. Simulation results have verified our theoretical work.

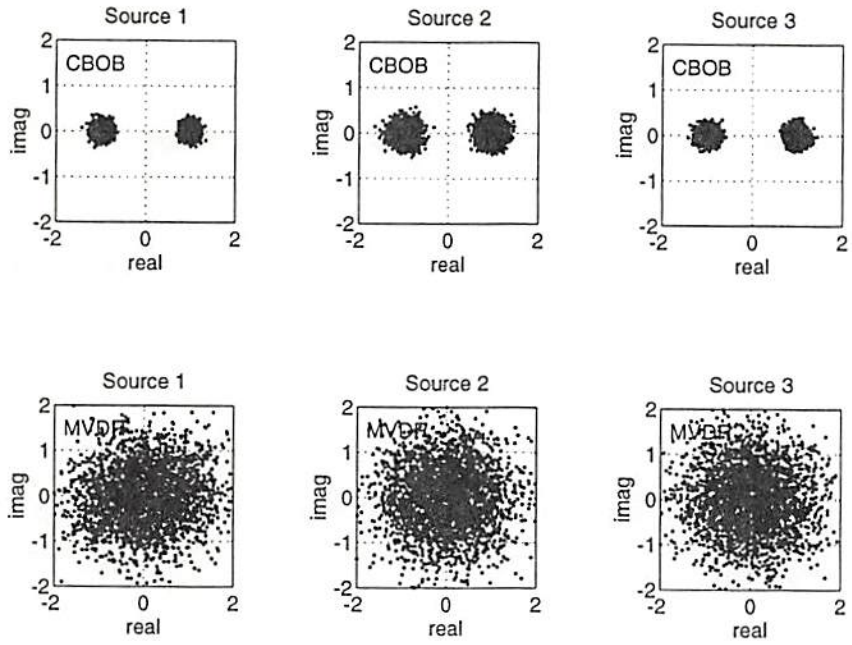


Figure 4.2: Cumulant-based and MVDR beamformer outputs for Experiment 1. SNR=10dB. "CBOB" refers to cumulant-based optimum beamformer.

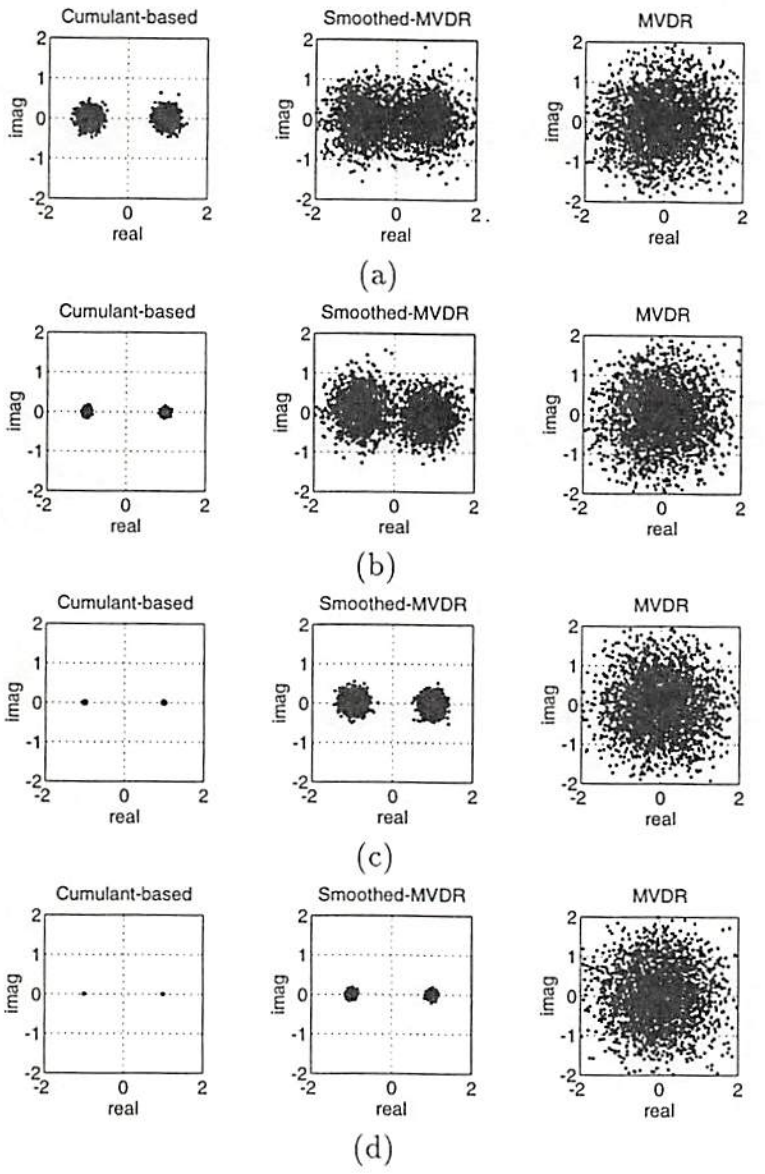


Figure 4.3: Various beamformer outputs for two coherent signals near broadside from closely spaced directions $\{90^o, 95^o\}$ at (a) SNR=$0dB$, (b) SNR=$10dB$, (c) SNR=$20dB$, (d) SNR=$30dB$.

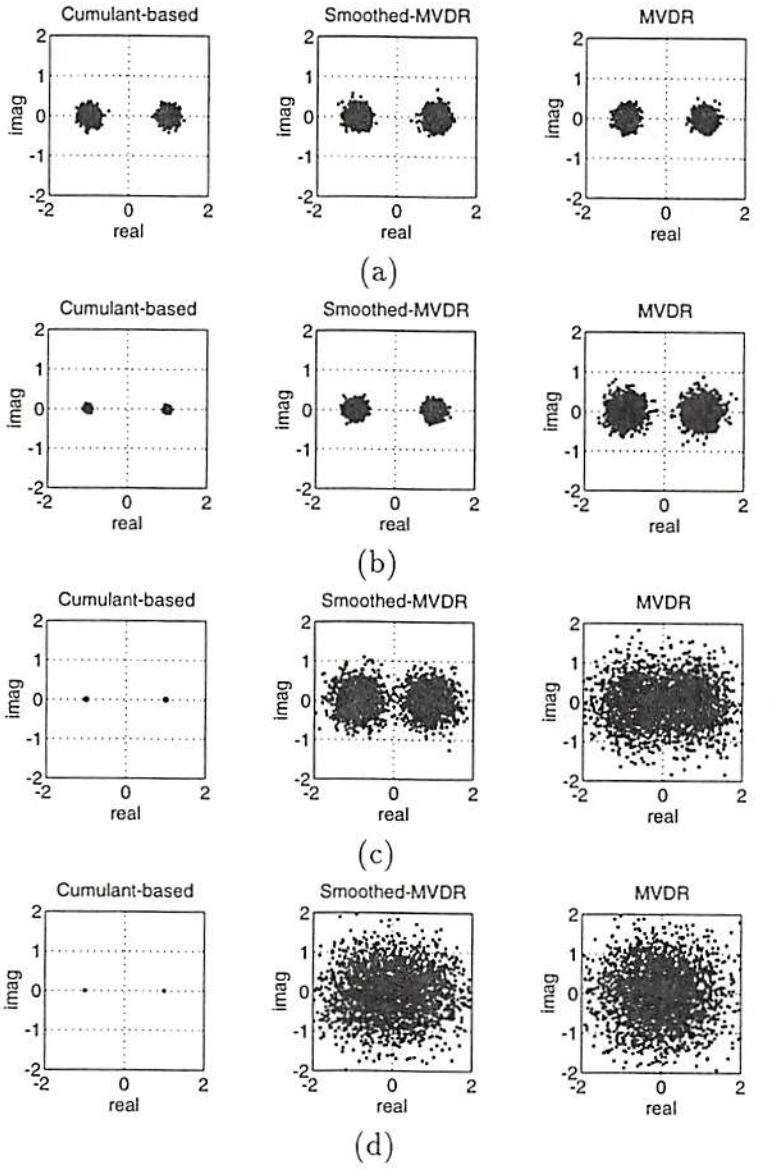


Figure 4.4: Various beamformer outputs for two coherent signals near endfire from closely spaced directions $\{0^o, 5^o\}$ at (a) SNR=0$dB$, (b) SNR=10$dB$, (c) SNR=20$dB$, (d) SNR=30$dB$.

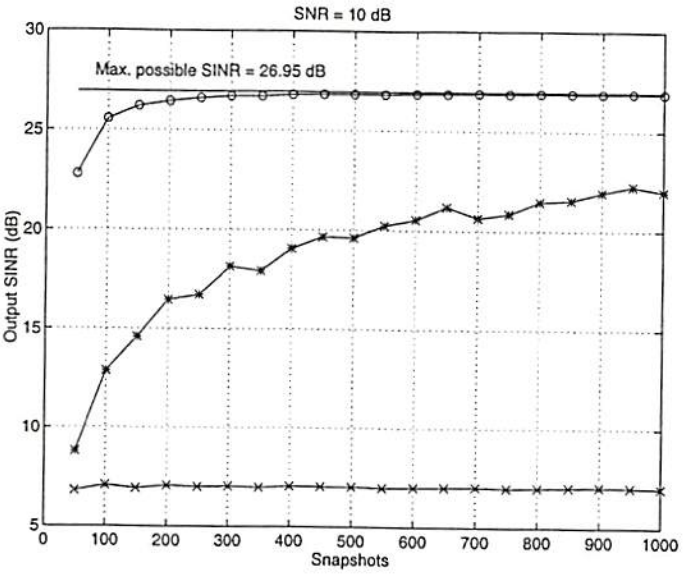


Figure 4.5: Output SINR of S-MVDR, E-MVDR and our cumulant-based beamformer as a function of number of snapshots obtained from 10 Monte-Carlo runs. SNR=10dB. Signals are received from broadside. "o" denotes the cumulant-based beamformer; "x" denotes the S-MVDR beamformer; "*" denotes the E-MVDR beamformer.

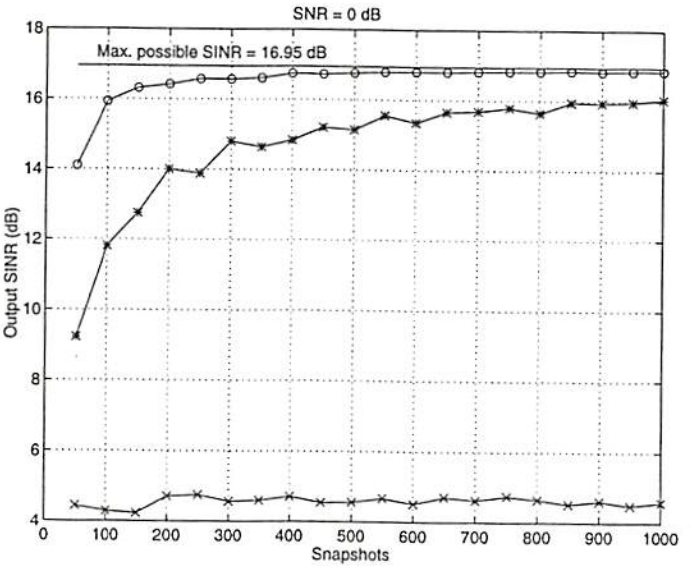


Figure 4.6: Output SINR of S-MVDR, E-MVDR and our cumulant-based beamformer as a function of number of snapshots obtained from 10 Monte-Carlo runs. SNR=0dB. Signals are received from broadside. "o" denotes the cumulant-based beamformer; "x" denotes the S-MVDR beamformer; "*" denotes the E-MVDR beamformer.

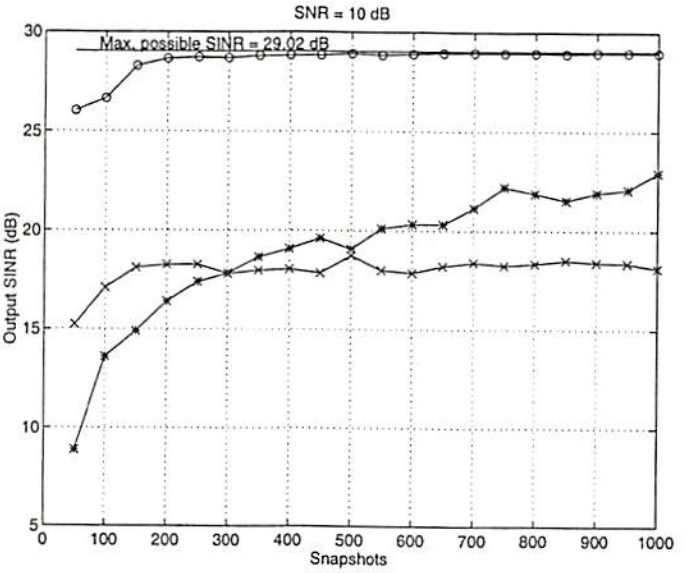


Figure 4.7: Output SINR of S-MVDR, E-MVDR and our cumulant-based beamformer as a function of number of snapshots obtained from 10 Monte-Carlo runs. SNR=10dB. Signals are received from endfire. "o" denotes the cumulant-based beamformer; "x" denotes the S-MVDR beamformer; "*" denotes the E-MVDR beamformer.

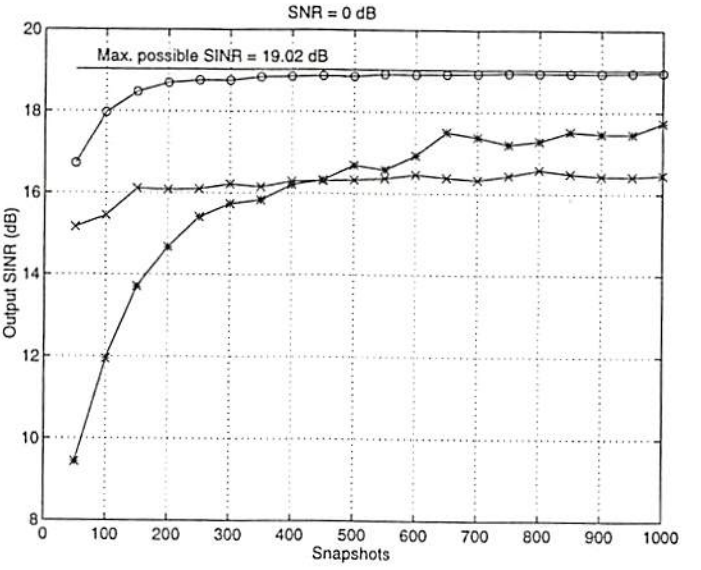


Figure 4.8: Output SINR of S-MVDR, E-MVDR and our cumulant-based beamformer as a function of number of snapshots obtained from 10 Monte-Carlo runs. SNR=0dB. Signals are received from endfire. "o" denotes the cumulant-based beamformer; "x" denotes the S-MVDR beamformer; "*" denotes the E-MVDR beamformer.

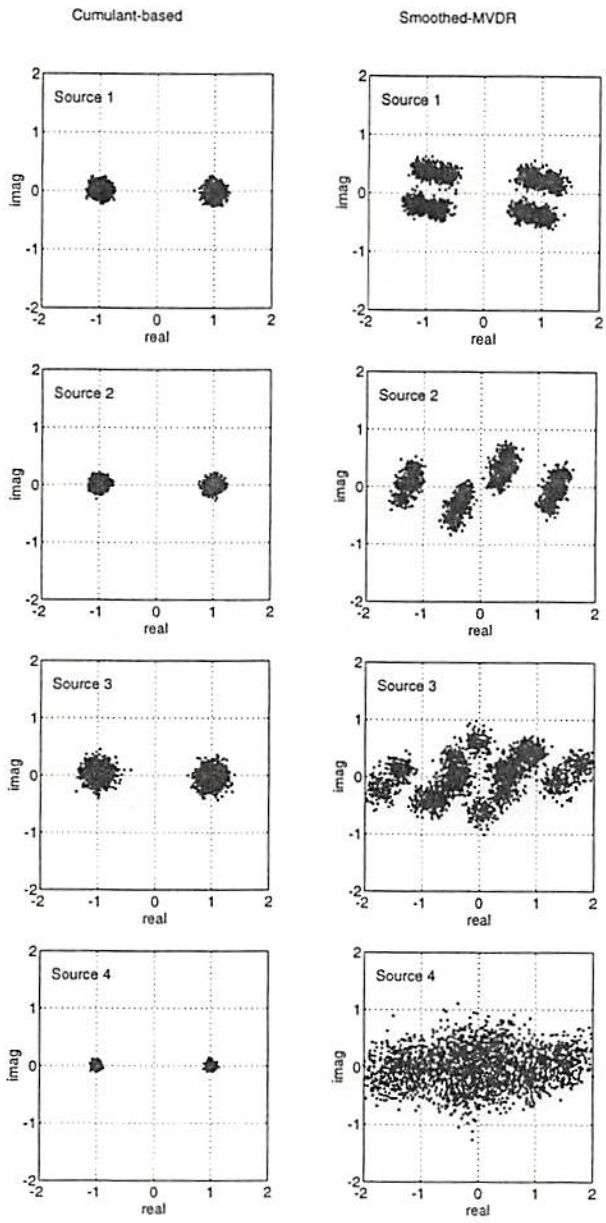


Figure 4.9: Cumulant-based (first column) and smoothed-MVDR (second column) beamformer outputs for the fourth experiment. SNR=10dB.

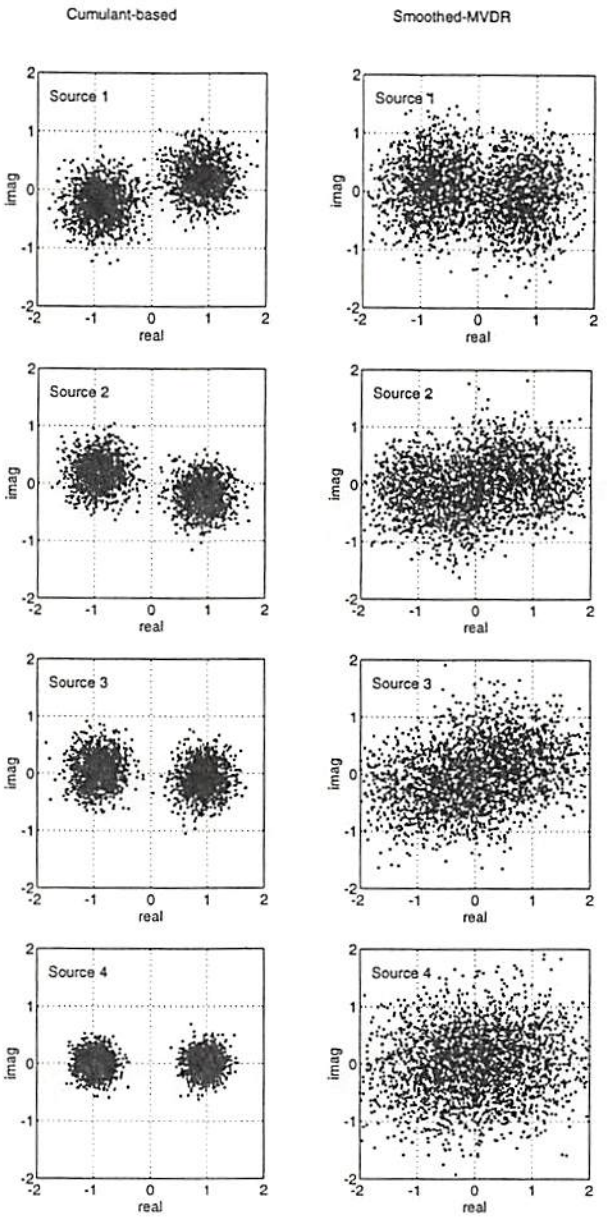


Figure 4.10: Cumulant-based (first column) and smoothed-MVDR (second column) beamformer outputs for the fourth experiment. SNR=−5dB.

# Chapter 5

# Beamspace and Iterative Virtual ESPRIT

Preprocessing array data prior to applying high-resolution direction finding algorithms has been shown to offer numerous benefits such as enhanced resolution, improved performance in colored noise, reduced sensitivity to sensor perturbations and reduced computation. Preprocessing, which is also referred to as *beamspace* transformation, involves suitably projecting the array data (of, say, dimension $M$) into several subspaces (called *subbands*) of lower or equal dimension (say $N$). Then, each subband data is processed to obtain DOAs and source signals in the same way as if it were received from a pseudoarray of size $N$. By doing this, the gain of the beampattern outside each spatial sector can be reduced, thereby filtering out signals located outside the sector. Apart from these advantages, a beamspace transformation results in a reduced parameter space, which brings a cubic decrease in computational complexity, because, an eigendecomposition requires computations on the order of $M^3$ for $M$ sensors.

Maximum-likelihood direction finding in beamspace was considered by Xu and Buckley [88]. Lee and Wengrovitz [39] have shown that beamspace processing can significantly reduce the SNR resolution threshold of the MUSIC algorithm and they have derived the associated optimum beamspace transformation. Zoltowski *et al* [94] presented a beamspace root-MUSIC algorithm. All of these methods assume *calibrated* arrays. ESPRIT, on the other hand, which does not require

calibration and relies on the shift invariance structure of the array, is difficult to implement in beamspace, because the shift invariance is lost during a beamspace transformation. A beamspace version of ESPRIT was developed, however, by Xu *et al* [89], who showed that if the beamspace transformation has the same invariance as the array shift invariance, then the lost invariance can be restored. Such requirements restrict the usefulness of desired beamformers, which is a limitation of covariance-based processing. In contrast, the availability of more than two arguments in cumulants can make beamspace processing possible with *arbitrary* beamspace transformations.

In this chapter, we present a beamspace version of the virtual-ESPRIT algorithm (VESPA) [17] that retains the most desirable property of VESPA, namely, that there is no need for an identical copy of the array; only an identical response sensor pair is required. The proposed beamspace-VESPA works with arbitrary transformations. Using the beamspace approach, we have also developed an iterative VESPA. Iterative VESPA can handle highly dynamic range of signal powers as opposed to VESPA. This problem was noted by Cardoso and Moulines in [6].

In Section 5.1 we formulate the problem. We present our beamspace VESPA and iterative VESPA in Sections 5.2 and 5.3, respectively. Simulation experiments that demonstrate the beamspace VESPA and a real data experiment that demonstrate the iterative VESPA are presented in Section 5.4. Section 5.5 concludes the chapter.

## 5.1 Formulation of the Problem

Suppose we have an $M$ element antenna array which contains a pair of identical sensors, and that $P$ statistically independent narrowband sources $\{s_p(t)\}_{p=1}^{P}$ are impinging on the array from directions $\{\theta_p\}_{p=1}^{P}$. We assume that: (1) the array structure is arbitrary except that it must have two antennas having identical responses; and, (2) the array is *uncalibrated*, i.e., its response is unknown. The problem is to estimate $\{\theta_p\}_{p=1}^{P}$ and to recover the sources $\{s_p(t)\}_{p=1}^{P}$ blindly.

The received signal is given by

$$\mathbf{r}(t) = \mathbf{A}\mathbf{s}(t) + \mathbf{n}(t) \tag{5.1}$$

where $\mathbf{A} = [\mathbf{a}_1, \cdots, \mathbf{a}_P]$ is an $M \times P$ unknown steering matrix; $\mathbf{s}(t)$ is the $P$-vector of the sources; $\mathbf{n}(t)$ is additive Gaussian noise independent of the signals, with unknown auto-correlation.

Suppose that the array data is projected to a beamspace by a transformation matrix, $\mathbf{T}$, of dimension, $N \times M$ $(N \leq M)$, as follows:

$$\tilde{\mathbf{r}}(t) = \mathbf{T}\mathbf{r}(t) = \mathbf{T}\mathbf{A}\mathbf{s}(t) + \mathbf{T}\mathbf{n}(t) = \tilde{\mathbf{A}}\mathbf{s}(t) + \tilde{\mathbf{n}}(t) \tag{5.2}$$

Note that the beamspace data $\tilde{\mathbf{r}}(t)$ can be interpreted as received from an $N$-element array having the $N \times P$ steering matrix $\tilde{\mathbf{A}}$. The arrival angles $\{\theta_p\}_{p=1}^{P}$ can be estimated using covariance-based ESPRIT if the beamspace steering matrix $\tilde{\mathbf{A}}$ has a displacement invariance. However, even if the steering matrix $\mathbf{A}$ has a displacement invariance, this property *does not necessarily hold* for $\tilde{\mathbf{A}}$ when an *arbitrary* beamspace transformation $\mathbf{T}$ is employed; it only holds for *specific* transformations [89]. Consequently, covariance-based ESPRIT *can not be used* with arbitrary beamspace transformations. In contrast, we will show that the availability of more than two arguments in cumulants makes beamspace direction finding possible with *arbitrary* beamspace transformations.

## 5.2 Beamspace VESPA

Without loss of generality, let the two identical response sensors be the first two sensors in the array, and denote the measurements from these sensors by $r_1(t)$ and $r_2(t)$, which are given by

$$r_1(t) = \sum_{p=1}^{P} a_{1p}\, s_p(t) \tag{5.3}$$

$$r_2(t) = \sum_{p=1}^{P} a_{1p}\, e^{-j\frac{2\pi d}{\lambda}\sin\theta_p}\, s_p(t) \tag{5.4}$$

where $a_{mn}$ denotes the $(m,n)$th element of $\mathbf{A}$, and $d$ is the distance between the identical response sensors. We assume that the first two sensors have nonzero responses to the incoming signals.

Our beamspace VESPA is:

**Step 1:** First we estimate the following fourth-order cumulant matrix using the element-space identical sensor measurements and beamspace data together:

$$\begin{aligned}\mathbf{C}_1 &\triangleq \text{cum}(r_1(t), r_1^*(t), \tilde{\mathbf{r}}(t), \tilde{\mathbf{r}}(t)^H) \\ &= \sum_{p=1}^{P} \gamma_{4,p} |a_{1p}|^2 \tilde{\mathbf{a}}_p \tilde{\mathbf{a}}_p^H \\ &= \tilde{\mathbf{A}} \mathbf{\Lambda} \tilde{\mathbf{A}}^H \end{aligned} \tag{5.5}$$

where $\tilde{\mathbf{r}}(t) = \mathbf{Tr}(t)$; $\tilde{\mathbf{A}} = [\tilde{\mathbf{a}}_1, \cdots, \tilde{\mathbf{a}}_P]$; $\{\gamma_{4,p}\}_{p=1}^P$ are the (non-zero) fourth-order cumulants of the sources; and, $\mathbf{\Lambda} \triangleq diag\{|a_{11}|^2\gamma_{4,1}, \cdots, |a_{1P}|^2\gamma_{4,P}\}$. Equation (5.5) was derived using cumulant properties [CP1], [CP3],[CP5], [CP6] in [47]. Note that the fourth-order cumulant of the additive Gaussian measurement noise is zero.

Next, we estimate:

$$\begin{aligned}\mathbf{C}_2 &\triangleq \text{cum}(r_2(t), r_1^*(t), \tilde{\mathbf{r}}(t), \tilde{\mathbf{r}}(t)^H) \\ &= \sum_{p=1}^{P} \gamma_{4,p} |a_{1p}|^2 \, e^{-j\frac{2\pi d}{\lambda}\sin\theta_p} \, \tilde{\mathbf{a}}_p \tilde{\mathbf{a}}_p^H \\ &= \tilde{\mathbf{A}} \mathbf{\Phi} \mathbf{\Lambda} \tilde{\mathbf{A}}^H \end{aligned} \tag{5.6}$$

where $\mathbf{\Phi} \triangleq diag\{e^{-j\frac{2\pi d}{\lambda}\sin\theta_1}, \cdots, e^{-j\frac{2\pi d}{\lambda}\sin\theta_P}\}$.

Having estimated the matrices $\mathbf{C}_1$ and $\mathbf{C}_2$, the arrival angles and the source signals can be obtained as follows.

**Step 2:** Stack $\mathbf{C}_1$ and $\mathbf{C}_2$ into a $2N \times N$ matrix $\mathbf{C}$ as follows:

$$\mathbf{C} \triangleq \begin{bmatrix} \mathbf{C}_1 \\ \mathbf{C}_2 \end{bmatrix} \tag{5.7}$$

and, perform the SVD of $\mathbf{C}$; keep the first $2N \times P$ submatrix of the left singular vectors of $\mathbf{C}$. Let this submatrix be $\mathbf{U}_1$.

**Step 3:** Partition $\mathbf{U}_1$ into two $N \times P$ matrices $\mathbf{U}_{11}$ and $\mathbf{U}_{12}$.

**Step 4:** Perform the SVD of $[\mathbf{U}_{11}, \mathbf{U}_{12}]$. Stack the last $P$ right singular vectors of $[\mathbf{U}_{11}, \mathbf{U}_{12}]$ into the $2P \times P$ matrix denoted $\mathbf{F}$.

**Step 5:** Partition $\mathbf{F}$ as $\mathbf{F} \triangleq \begin{bmatrix} \mathbf{F}_x \\ \mathbf{F}_y \end{bmatrix}$ where $\mathbf{F}_x$ and $\mathbf{F}_y$ are $P \times P$ .

**Step 6:** Perform the eigendecomposition of $-\mathbf{F}_x\mathbf{F}_y^{-1}$. The eigenvalue matrix gives $\mathbf{\Phi} \triangleq diag\{e^{-j\frac{2\pi}{d}\sin\theta_1}, \cdots, e^{-j\frac{2\pi}{d}\sin\theta_P}\}$ from which the arrival angles are readily obtained. Let the eigenvector matrix of $-\mathbf{F}_x\mathbf{F}_y^{-1}$ be $\mathbf{E}$.

**Step 7:** For signal recovery, an estimate of $\tilde{\mathbf{A}}$ is obtained to within a diagonal matrix, as $\tilde{\mathbf{A}} = \frac{1}{2}(\mathbf{U}_{11}\mathbf{E} + \mathbf{U}_{12}\mathbf{E}\mathbf{\Phi}^{-1})$. Columns of $\tilde{\mathbf{A}}$ can be used to recover the sources by MVDR [5] beamformers as follows:

$$s_p(t) = \frac{\tilde{\mathbf{a}}_p^H \tilde{\mathbf{R}}^{-1}}{\tilde{\mathbf{a}}_p^H \tilde{\mathbf{R}}^{-1} \tilde{\mathbf{a}}_p} \tilde{\mathbf{r}}(t) \quad p = 1, \cdots, P \tag{5.8}$$

where $\tilde{\mathbf{a}}_p$ is the $p$-th column of $\tilde{\mathbf{A}}$, and $\tilde{\mathbf{R}}$ is the sample beamspace array covariance matrix, $\tilde{\mathbf{R}} = \frac{1}{N}\sum_{t=1}^{N} \tilde{\mathbf{r}}(t)\tilde{\mathbf{r}}(t)^H$.

Note that the above steps are the same as VESPA, except that the third and fourth arguments in $\mathbf{C}_1$ and $\mathbf{C}_2$ are chosen from the beamspace data. We can also use beamspace data as the scalar arguments of (5.5) and (5.6) in place of the element-space data. In this case, we again follow the above steps; however, the eigenvalue matrix in **Step 6** does not give the correct arrival angles, because, this time, the first two beamspace arguments in the new matrix used in place of (5.6) don't necessarily have the displacement-invariance structure as in (5.4). However, the arrival angles can be obtained using the estimate $\tilde{\mathbf{A}}$ found in **Step 7**; this is achieved by first obtaining $\mathbf{A}$ as $\mathbf{A} = \mathbf{T}^{\#}\tilde{\mathbf{A}}$ where $\#$ stands for pseudoinverse operation, and then dividing the responses of the two identical sensors. Again, columns of $\tilde{\mathbf{A}}$ are used to recover the sources, as in (5.8). This approach is demonstrated in Experiment 1.

## 5.3 Iterative VESPA (IVESPA)

Like all subspace-based methods, VESPA relies on sample statistics of the array measurements which suffer from cross terms due to the presence of multiple sources. When some of the sources have very small powers and cumulants compared to those of other sources, undesirable cross terms are present in the sample statistics of the weak sources due to the other sources for small numbers of samples. In this case, VESPA fails to accurately localize the weak sources. In practice, this case occurs when the source signals have different constellations and significantly different powers. Note that the denser the source signal constellation becomes, the smaller the cumulant of the signal becomes, because the signal looks more Gaussian. For example, fourth-order cumulants of unit-power BPSK, 4QAM and 16QAM signals are -2, -1 and -0.68, respectively. In addition, sources having small powers are deemphasized during the calculation of sample higher-order statistics, because higher than second-order powers of the data are computed.

The presence of source signals having widely separated powers and cumulants can be detected in VESPA by comparing signal singular values of the array cumulant matrix after the separation of the signal and noise subspaces. Note that separation of the signal and noise subspaces requires that the number of sources are detected accurately. If presence of such sources is detected VESPA can not be used. For this case, we propose a new beamspace-based approach, the *iterative VESPA* which also works even if the source powers are not separated. Most importantly, iterative VESPA does not require estimating the number of sources. Therefore, we suggest replacing VESPA by iterative VESPA when extra computational load is acceptable.

Iterative VESPA is as follows:

**Step 1:** Estimate

$$\begin{aligned} \mathbf{C}_1 &\triangleq \mathrm{cum}(r_1(t), r_1^*(t), \mathbf{r}(t), \mathbf{r}(t)^H) \\ \mathbf{C}_2 &\triangleq \mathrm{cum}(r_2(t), r_1^*(t), \mathbf{r}(t), \mathbf{r}(t)^H) \end{aligned} \tag{5.9}$$

where $r_k$ is the $k$th component of $\mathbf{r}(t)$. If the signal subspace singular values of

$\mathbf{C}_1$ are very separated, then, for $i = 1, \cdots, P$:

**Step 2:** If $i = 1$, go to Step 4. Otherwise, form a modified signal, $\mathbf{r}_i(t) = \mathbf{N}_{i-1}\mathbf{r}_{i-1}(t)$ where $\mathbf{N}_{i-1}$ is the left null-space matrix of the steering vector $\mathbf{a}_{i-1}$ of the most powerful source obtained from VESPA at the previous step ($\mathbf{N}_1 = \mathbf{I}$, $\mathbf{r}_1(t) = \mathbf{r}(t)$). Doing so suppresses the most powerful source in $\mathbf{r}_i(t)$.

**Step 3:** Estimate the following two $(M-i+1) \times (M-i+1)$ cumulant matrices:

$$\mathbf{C}_{i1} \triangleq \text{cum}(r_{i1}(t), r_{i1}^*(t), \mathbf{r}_i(t), \mathbf{r}_i(t)^H) \tag{5.10}$$

$$\mathbf{C}_{i2} \triangleq \text{cum}(r_{i2}(t), r_{i1}^*(t), \mathbf{r}_i(t), \mathbf{r}_i(t)^H) \tag{5.11}$$

where $r_{ik}(t)$ is the $k$th element of $(M-i+1)$-vector $\mathbf{r}_i(t)$.

**Step 4:** Assuming only one source is present, find the modified steering vector $\mathbf{b}_i$ of that source following the procedure in the Appendix.

**Step 5:** Compute $\mathbf{a}_i = pinv(\mathbf{N}_{i-1})\mathbf{b}_i$, where $pinv$ denotes pseudoinverse.

**Step 6:** Use the elements of $\mathbf{a}_i$ corresponding to the identical response pair of sensors to find the direction $\phi_i$ of the $i$th source. This is done as follows:

Let the identical response pair be the $m$-th and $(m+1)$th sensors. Then the responses of these sensors to the $i$-th wavefront, i.e. the $m$-th and $m+1$-th elements of $\mathbf{a}_i$, are in the form $a_{im} = c_i$ and $a_{i(m+1)} = c_i e^{-j\frac{2\pi d}{\lambda}\sin\phi_i}$, where $d$ is the separation between the $m$-th and $(m+1)$th sensors. Consequently, $\phi_i$ can be found from $a_{im}$ and $a_{i(m+1)}$.

**Step 7:** Recover the $i$th source using $\mathbf{a}_i$ in an MVDR [5] beamformer.

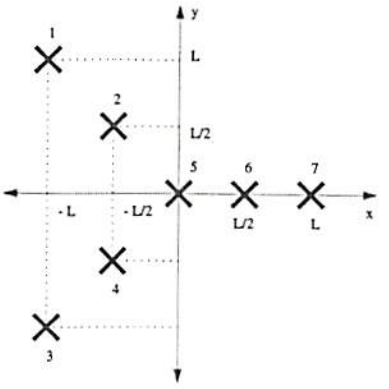


Figure 5.1: The Y-array used in Experiments 1 and 2. $L$ is the wavelength.

## 5.4 Simulation Experiments

### 5.4.1 Experiment 1: Separation of two closely spaced sources using Beamspace VESPA

We assume two 4QAM sources with 3dB and 60dB SNRs impinging on an array of 7 sensors from directions $20^o$ and $25^o$. The array consists of dipole antennas having different orientations and configured as in Figure 5.1. Each dipole has a response $\cos(\theta)$ where $\theta$ is the angle measured in the counter-clockwise direction from the y-axis. If the antenna has an orientation of $\alpha$, the response becomes $\cos(\theta - \alpha)$. The orientations of the antennas were selected arbitrarily as [$2^o$, $4^o$, $6^o$, $8^o$, $0^o$, $0^o$, $0^o$]. The measurements are corrupted by additive circularly symmetric white Gaussian noise. 2000 snapshots were taken. Note that the array does not have a displacement structure that can be exploited by ESPRIT. Figure 5.2 shows the covariance-based MUSIC spectrum obtained for 50 realizations by assuming the array manifold is known. Observe that the peak corresponding to the 3dB source is not as clear as that corresponding to the 60dB source.

Using the 6th and 7th sensors as the identical sensor pair, we applied VESPA to this scenario. VESPA assumes no apriori information about the array response except that the 6th and 7th sensors have identical response. Table 5.1 shows the means and standard deviations of the angle estimates obtained from element space VESPA for 50 realizations. It is seen that VESPA estimates are biased toward the

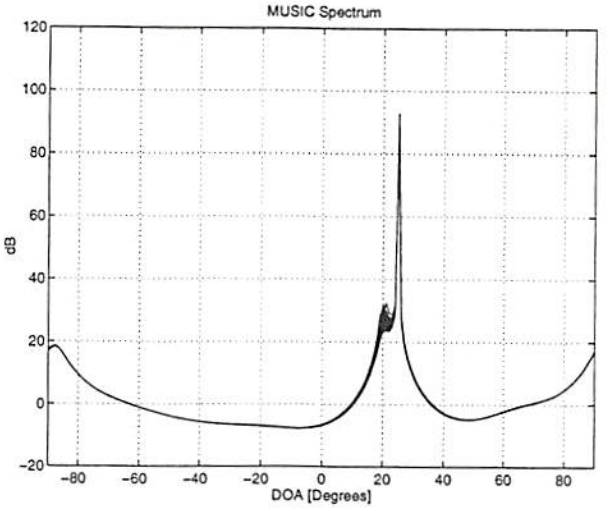


Figure 5.2: MUSIC Spectrum obtained for 50 realizations of Experiment 1.

most powerful source and fails to estimate the arrival angle of the weak source.

For the beamspace-VESPA, we used the following $2 \times 7$ transformation matrix:

$$\mathbf{T} = \mathbf{D}_s{}^{-1}\mathbf{E}_s{}^{H} \tag{5.12}$$

where $\mathbf{E}_s$ is the $7 \times 2$ signal subspace eigenvector matrix and $\mathbf{D}_s$ is the corresponding eigenvalue matrix obtained from the sample array covariance matrix. The element space data was projected to the beamspace as in (5.2). Let the beamspace measurement vector be expressed as $\tilde{\mathbf{r}} = [\tilde{r}_1, \tilde{r}_2]^T$. Then we estimate the $2 \times 2$ cumulant matrices $\mathbf{C}_1 = \text{cum}(\tilde{r}_1(t), \tilde{r}_1^*(t), \tilde{\mathbf{r}}(t), \tilde{\mathbf{r}}(t)^H)$ and $\mathbf{C}_2 = \text{cum}(\tilde{r}_2(t), \tilde{r}_1^*(t), \tilde{\mathbf{r}}(t), \tilde{\mathbf{r}}(t)^H)$. The $2 \times 2$ beamspace steering matrix $\tilde{\mathbf{A}}$ is obtained following **Steps 2-7**. As explained earlier, the arrival angles are obtained using the estimated beamspace steering matrix. For this purpose, we first obtain the $7 \times 2$ element space steering matrix $\mathbf{A}$ as follows:

$$\mathbf{A} = \mathbf{T}^{\#}\tilde{\mathbf{A}}. \tag{5.13}$$

Finally, the arrival angles are obtained as follows:

$$\theta_1 = \sin^{-1}(\angle(\frac{\mathbf{A}(6,1)}{\mathbf{A}(7,1)})/\pi) \tag{5.14}$$

$$\theta_2 = \sin^{-1}(\angle(\frac{\mathbf{A}(6,2)}{\mathbf{A}(7,2)})/\pi) \tag{5.15}$$

The means and standard deviations of the arrival angle estimates obtained from beamspace-VESPA for 50 realizations are given in Table 5.1 . It is seen that the arrival angles are estimated correctly despite the 57dB power difference between the sources.

Table 5.1: The means and standard deviations of the arrival angle estimates obtained from element space VESPA and beamspace-VESPA for 50 realizations.

| | VESPA | | Beam-VESPA | |
|---|---|---|---|---|
| | Mean | St. Dev. | Mean | St. Dev. |
| $\theta_1 = 20^o$ | 24.93 | 0.10 | 20.74 | 0.98 |
| $\theta_2 = 25^o$ | 25.05 | 0.09 | 25.01 | 0.01 |

### 5.4.2 Experiment 2: VESPA versus Beamspace VESPA for separation of two closely spaced sources

In this experiment, we compare VESPA and Beamspace VESPA when there are two, closely spaced 4QAM sources, one very strong and the other very weak. We used the same 7-element Y-array as in Experiment 1. The two sources impinge on the array from directions $20^o$ and $23^o$. The power of the source at $20^o$ was fixed at 70dB, whereas the power of the source at $23^o$ was varied in the range $0 - 50$dB. Measurements were corrupted by additive circularly-symmetric white Gaussian noise. 2500 snapshots were used. Recall that this array does not have a displacement structure that can be exploited by ESPRIT.

We conducted a 20-run Monte-Carlo experiment on this data and compared VESPA and Beamspace VESPA. Using the 6th and 7th sensors as the identical sensor pair, we applied VESPA to this scenario for 20 realizations. VESPA assumes no apriori information about the array response except that the 6th and 7th sensors have identical response. For the Beamspace VESPA, we used the same $2 \times 7$ transformation as in Experiment 1 and followed the same steps for the same 20 realizations.

The sample means and standard deviations of the arrival angle estimates obtained from both methods are plotted in Figs. 5.3 and 5.4 as a function of the power of the source at $23^o$. It is seen that, when this source is weak, VESPA estimates are biased toward the most powerful source at $20^o$, and VESPA fails to estimate the bearing of the weak source at $23^o$. As the power of the source at $23^o$ increases, VESPA tends to estimate its bearing better. On the other hand, when the source powers are very different, the Beamspace VESPA can estimate the source bearings fairly well except for a small bias for the weak source. It is also observed from Fig. 5.3 that, for this particular choice of the beamspace transformation, as the source powers get closer, the Beamspace VESPA estimates become more biased.

### 5.4.3 Experiment 3: Beamspace VESPA for reduction of computations

In general, the resolution of DOA estimates increases with the number of array elements; however, the drawback is a cubic increase in the computational load, because, the major computational complexity of VESPA is due to the singular value decomposition which requires $O(M^3)$ computations. Beamspace VESPA was introduced as a way to reduce computational complexity. An important part of beamspace VESPA is the design of a useful beamspace transformation. In this experiment, we present a transformation for a uniform linear array, which is suitable when the user has a general idea about which sector of the space the targets are in. The experimental results show that the resolution of beamspace VESPA with this transformation is nearly identical to that of elementspace VESPA, whereas the computations are reduced approximately by a factor of 8.

An $L = 10$ element ULA with half-wavelength spacing is used in the simulations. There are two independent BPSK sources at $-0.5^o$ and $0.5^o$ with respect to broadside. The source powers are equal, and are varied in the range $0-18$dB with respect to the additive white circularly symmetric Gaussian noise power. Note that the sources are separated by $1^o$ which is nearly one-tenth of the Rayleigh separation, $11.5^o$ [Rayleigh separation$= sin^{-1}(2/L)$]. For the design of the beamspace transformation, the sources were assumed known to be in a $45^o$ sector centered at

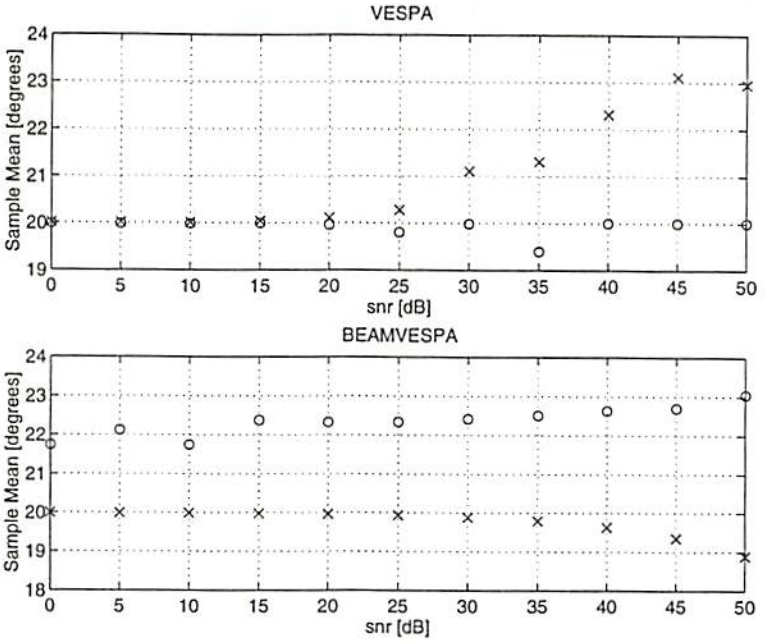


Figure 5.3: The sample means of the arrival angle estimates obtained from element space VESPA and Beamspace VESPA for 20 realizations, as a function of the power of the source at 23°.

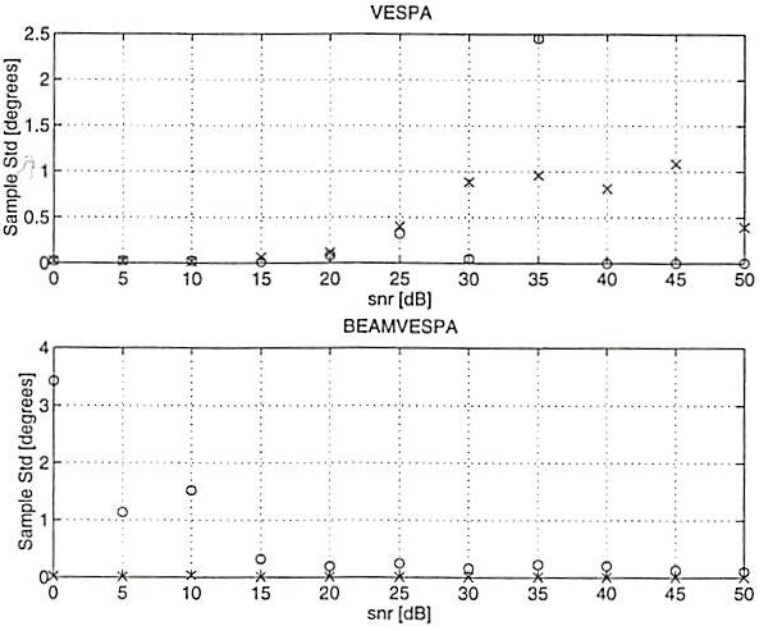


Figure 5.4: The sample standard deviations of the arrival angle estimates obtained from element space VESPA and Beamspace VESPA for 20 realizations, as a function of the power of the source at 23°.

the broadside.

The rows $\mathbf{t}_i$ of a $5 \times 10$ beamspace transformation matrix $\mathbf{T}$, (or, in other words, the beams) were chosen as follows:

$$\mathbf{t}_i = [1, exp(j\pi u_i), exp(j2\pi u_i), \cdots, exp(j(L-1)\pi u_i)] \tag{5.16}$$

where $u_i = 2i/L$ and $i = -2, -1, 0, 1, 2$. Then the data was transformed to beamspace as $\mathbf{r}_b(t) = \mathbf{T}\mathbf{r}(t)$. With this transformation, each element $r_{bi}(t)$ becomes the discrete-time Fourier transform (DFT) of the measurement vector $\mathbf{r}(t)$ evaluated at frequency $u_i = sin(\theta_i)$ $(-1 \leq u_i \leq 1)$, where $\theta_i$ is the pointing direction of the $i$th beam. The response of each beam is a $sin(u_i)/u_i$ function centered at the corresponding pointing direction, and has nulls at both sides of $u_i$, at points spaced $\delta u = 2/L$ radians (Rayleigh separation) away from the pointing direction and each other. A DFT beamformer like this was used by Zoltowski *et al* [94]. With these values, the five beams, altogether, cover a $47^o$ sector from $-23.5^o$ to $23.5^o$, centered at the broadside.

We conducted a 50-run Monte Carlo simulation using VESPA and beamspace VESPA on the elementspace data and transformed data, respectively. We used the $10 \times 10$ cumulant matrix pair $cum(r_1^*, r_1, \mathbf{r}, \mathbf{r}^H)$ and $cum(r_2^*, r_1, \mathbf{r}, \mathbf{r}^H)$ for VESPA; and, the $5 \times 5$ pair $cum(r_1^*, r_1, \mathbf{r}_b, \mathbf{r}_b^H)$ and $cum(r_2^*, r_1, \mathbf{r}_b, \mathbf{r}_b^H)$ for beamspace VESPA. Note that the SVD of the latter pair of matrices requires 8 times less computations than that of the former, because the dimensions of the latter pair of cumulants are half that of the former. We display the means and standard deviations of the DOA estimates obtained with both methods in Table 5.2, as a function of source SNRs. It is observed that the resolution of beamspace VESPA with this transformation is nearly identical to that of elementspace VESPA in this range of SNR values, as mentioned earlier.

Further reduction in the computational load is possible by choosing a smaller sector of interest. For example, choosing a $23^o$ sector from $-11.5$ to $11.5^o$, which is achieved with 3 beams using $i = 1, 0, -1$, results in a reduction of $(10/3)^3$ in computations when compared with VESPA; however, this choice requires more a priori information about the locations of the sources. Table 5.3 shows the sample means and standard deviations obtained for this case.

Table 5.2: Sample means and standard deviations of the bearing estimates obtained with elementspace VESPA and beamspace VESPA as a function of SNR, when 5 beams were used.

| | Sample Mean | | | |
|---|---|---|---|---|
| | VESPA | | Beamspace VESPA | |
| SNR [dB] | Signal 1 | Signal 2 | Signal 1 | Signal 2 |
| 18 | -0.501 | 0.495 | -0.500 | 0.494 |
| 15 | -0.492 | 0.488 | -0.493 | 0.489 |
| 12 | -0.496 | 0.498 | -0.497 | 0.499 |
| 9 | -0.485 | 0.520 | -0.487 | 0.513 |
| 6 | -0.516 | 0.488 | -0.505 | 0.496 |
| 3 | -0.580 | 0.575 | -0.625 | 0.539 |
| | Sample Std | | | |
| | VESPA | | Beamspace VESPA | |
| SNR [dB] | Signal 1 | Signal 2 | Signal 1 | Signal 2 |
| 18 | 0.032 | 0.046 | 0.032 | 0.046 |
| 15 | 0.057 | 0.041 | 0.058 | 0.043 |
| 12 | 0.091 | 0.076 | 0.096 | 0.079 |
| 9 | 0.123 | 0.151 | 0.138 | 0.157 |
| 6 | 0.247 | 0.231 | 0.245 | 0.264 |
| 3 | 0.438 | 0.462 | 0.526 | 0.562 |

Table 5.3: Sample means and standard deviations of the bearing estimates obtained with elementspace VESPA and beamspace VESPA as a function of SNR, when 3 beams were used.

| | Sample Mean | | | |
|---|---|---|---|---|
| | VESPA | | Beamspace VESPA | |
| SNR [dB] | Signal 1 | Signal 2 | Signal 1 | Signal 2 |
| 18 | -0.499 | 0.507 | -0.498 | 0.506 |
| 15 | -0.492 | 0.488 | -0.493 | 0.489 |
| 12 | -0.495 | 0.496 | -0.497 | 0.499 |
| 9 | -0.509 | 0.513 | -0.513 | 0.514 |
| 6 | -0.481 | 0.497 | -0.470 | 0.455 |
| 3 | -0.581 | 0.675 | -0.531 | 0.807 |
| | Sample Std | | | |
| | VESPA | | Beamspace VESPA | |
| SNR [dB] | Signal 1 | Signal 2 | Signal 1 | Signal 2 |
| 18 | 0.042 | 0.042 | 0.041 | 0.042 |
| 15 | 0.057 | 0.041 | 0.058 | 0.043 |
| 12 | 0.096 | 0.081 | 0.095 | 0.083 |
| 9 | 0.106 | 0.127 | 0.107 | 0.161 |
| 6 | 0.178 | 0.212 | 0.253 | 0.274 |
| 3 | 0.521 | 0.487 | 0.571 | 0.787 |

### 5.4.4 Experiment 4: Real data processing with VESPA and Iterataive VESPA

In this experiment, we demonstrate IVESPA and compare it with VESPA by means of the following experiment, using a set of data provided by our sponsor, CRASP [1].

Three signals of 1000 symbols each are generated. The signal types are BPSK, BPSK and 16QAM, and they occupy a bandwidth of 350 KHz. These signals were used to modulate a wavefront simulator designed to approximate uniform plane waves impinging upon an 8-element uniform linear array with an element spacing of one half wavelength at 900 MHz. The arrival directions are: BPSK1 at $6.3^o$, BPSK2 at $25.2^o$ and 16QAM at $40^o$. The 900 MHz 8-channel measurements were downconverted and sampled at 5.12 MHz.

The eigenvalues of the estimated $8 \times 8$ array covariance matrix are as follows:

$$10^4 * [6.25, 0.47, 0.03, 0.00, 0.00, 0.00, 0.00, 0.00] \tag{5.17}$$

First, VESPA was applied to this data. VESPA starts by choosing a guiding sensor pair and estimating two cumulant matrices. In our case, any two of the sensor measurements can be used as the guiding sensor pair since the array is uniform and linear. We used the first two sensors for this purpose, and estimated the following fourth-order cumulants:

$$\begin{aligned} \mathbf{C}_1 &\triangleq \text{cum}(r_1(t), r_1^*(t), \mathbf{r}(t), \mathbf{r}(t)^H) \\ \mathbf{C}_2 &\triangleq \text{cum}(r_2(t), r_1^*(t), \mathbf{r}(t), \mathbf{r}(t)^H) \end{aligned} \tag{5.18}$$

Before applying the rest of the VESPA steps we first checked the singular values of $\mathbf{C}_1$ and $\mathbf{C}_2$; e.g., the singular values of $\mathbf{C}_1$ are found to be:

$$10^8 * [3.73, 0.06, 0.004, 0.00, 0.00, 0.00, 0.00, 0.00] \tag{5.19}$$

Observe that the the second and third signal singular values which belong to

[1] Center for Research on Applied Signal Processing

the second BPSK source and the 16QAM source, respectively, are very small compared to the first singular value, which belongs to the first BPSK signal. One reason why the singular values of the cumulant matrix are more separated than the eigenvalues of the covariance matrix is that, the computation of fourth-order cumulant estimates requires fourth powers of the data, and these increase faster than the second powers for high signal levels. Yet another reason is the difference between the fourth-order cumulants of equal-power BPSK and 16QAM signals, as mentioned in Section 5.3. Applying VESPA, we obtained the following angle estimates:

$$6.37^{o}, 6.30^{o}, 7.43^{o} \tag{5.20}$$

which shows that VESPA is biased towards the most powerful source.

Second, we applied IVESPA to this data, and obtained the following angle estimates:

$$6.34^{o}, 25.86^{o}, 40.59^{o} \tag{5.21}$$

It is seen that the arrival angles are estimated correctly with IVESPA.

Finally, we show that as the sample size is increased, VESPA gives accurate estimates. To show this, we simulated the same real data experiment in the computer paying particular attention to the signal conditions. We increased the sample size by 500 steps in this range, and for each sample size, we ran both VESPA and IVESPA on the simulated data for 10 realizations of the experiment. The averaged direction-of-arrival estimates obtained from VESPA and the actual values of DOAs are plotted as a function of data length in Figure 5.5. It is observed that for short data lengths VESPA fails to give reliable estimates; however, as the data length increases, the estimates converge to their actual values. On the other hand, IVESPA worked fine for all the values of the data length.

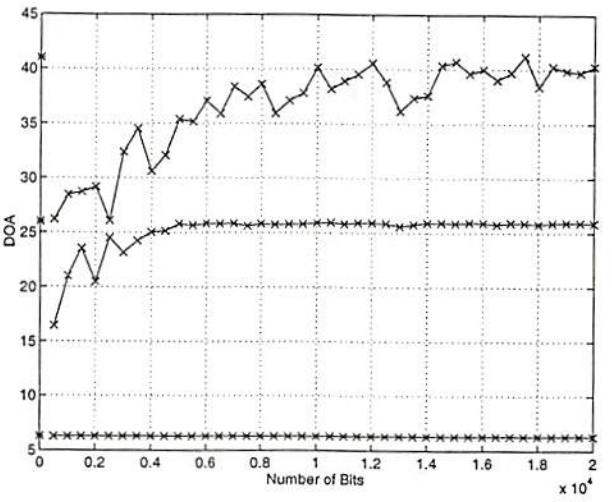


Figure 5.5: Average value of the direction-of-arrival estimates obtained from 10 realizations of VESPA as the data length is varied. The actual values of the directions-of-arrival are marked as "*" on the plot.

## 5.5 Conclusions

We have presented the beamspace VESPA and the iterative VESPA for direction finding and waveform recovery of narrowband signals. The Beamspace VESPA works with arbitrary and unknown arrays provided there is an identical response sensor pair in the array. The proposed method is applicable to arbitrary beamspace transformations as opposed to its covariance-based counterpart, beamspace-ESPRIT. Experimental results demonstrating the method were also presented.

Iterative VESPA is more general than VESPA and is applicable also to cases where VESPA is applicable. IVESPA has the following advantages over VESPA: 1) It can handle the case where the data length is short and some of the sources have very small powers and higher-order statistics compared to others, in which case VESPA needs more data to localize the weak sources; 2) Detection of number of sources is not required for IVESPA; 3) It can be applied to uncalibrated and arbitrary-shape arrays provided the array has two sensors having identical response–the same requirement as in VESPA; and, 4) IVESPA can replace VESPA when extra computations are acceptable. Results of a real data experiment demonstrating the method are presented.

## 5.6 Appendix-A procedure for estimating the arrival angle and steering vector of the most dominant source

A modified form of TLS ESPRIT [66] for one source:

**Step 1:** Stack $\mathbf{C}_{i1}$ and $\mathbf{C}_{i2}$ into a $2(M-i+1)\times(M-i+1)$ matrix $\mathbf{C}$ as follows:

$$\mathbf{C} \triangleq \begin{bmatrix} \mathbf{C}_{i1} \\ \mathbf{C}_{i2} \end{bmatrix} \tag{5.22}$$

and, perform the SVD of $\mathbf{C}$; keep the first left singular $2(M-i+1)$-vector of $\mathbf{C}$. Let this vector be $\mathbf{u}_1$.

**Step 2:** Partition $\mathbf{u}_1$ into two $(M-i+1)$-vectors $\mathbf{u}_{11}$ and $\mathbf{u}_{12}$.

**Step 3:** Perform the SVD of $[\mathbf{u}_{11}, \mathbf{u}_{12}]$; keep the last right singular vector of $[\mathbf{u}_{11}, \mathbf{u}_{12}]$. Let this 2-vector be $\mathbf{f}$.

**Step 4:** Partition $\mathbf{f}$ as $\mathbf{f} \triangleq \begin{bmatrix} f_x \\ f_y \end{bmatrix}$.

**Step 5:** An estimate of the modified steering vector of the source is obtained to within a scalar, as $\mathbf{b}_i = \mathbf{u}_{11} - \frac{f_y}{f_x}\mathbf{u}_{12}$.

# Chapter 6

# Polarization and Direction of Arrival Estimation with Minimally-Constrained Arrays

It is advantageous to use diversely polarized signals and antennas for several reasons. Diversity in signal polarization can be used to improve the receiver performance. Multiple signals arriving from close directions can be resolved on the basis of their polarizations when diversely polarized antennas are used. If the receiver antenna polarization is matched with that of the incoming wave, the induced power in the receiver is maximized. Otherwise, there is a polarization mismatch, which, in the worst case may cause a zero signal power in the receiver; this lets two signals having orthogonal polarizations share the same frequency without interfering with each other, or an undesired signal can be nulled out by an antenna having orthogonal polarization.

The problems of estimating directions of arrival and polarization parameters of multiple cochannel signals has been considered in various works [23, 34, 91, 40, 44]. In the framework of second-order statistics, Ferrara and Parks [23] extended the ML, MUSIC, and adapted angular response (AAR) algorithms, which were designed for identically polarized arrays, to diversely polarized arrays. Ziskind and Wax [91] developed a different version of the ML method for diversely polarized arrays. A smoothed version of MUSIC and Pencil-MUSIC was given by Hua [34]

to handle coherent signals, and a performance analysis was presented by Cheng and Hua [10]. Swindlehurst and Viberg used a subspace fitting algorithm for angle and polarization estimation. In all of these methods, however, it was assumed that the array manifold is either *known* or obtained through array calibration. In [40], Li and Compton used ESPRIT [66] to estimate direction of arrival and polarization paramaters of multiple signals. ESPRIT is computationally efficient and the undesirable procedures of array calibration and multidimensional-search are totally avoided and the parameters of interest are obtained directly; however, ESPRIT is applicable only to antenna arrays having a special structure called *displacement invariance.* As a consequence, in Li and Compton's method, to estimate parameters of at most $M-1$ signals, it is required that the array be a 2M element ULA consisting of $M$-pairs of crossed dipoles. In the higher-order statistics framework, the virtual-ESPRIT algorithm for direction finding [17] has removed the restriction of having to have an identical copy of the array, while retaining the computational advantages of ESPRIT; instead of two identical arrays, only a subarray having two sensors that have identical response is required.

In this chapter, it is shown that, using fourth-order statistics, both directions of arrival and polarization parameters of at most $M-1$ multiple cochannel signals can be estimated using any $M$-element array having $M-3$-elements that are of *arbitrary* and *unknown* response and geometry, and a subarray consisting of *three* short dipole antennas displaced in space and configured in a certain fashion. This way the constraint on the array configuration is minimized. For a totally linear array, our method requires 50% less hardware than Li and Compton's.

In Section 6.1, the problem is formulated. We propose a solution in Section 6.2. The overall computational procedure is presented in Section 6.3. Section 6.4 provides four simulation experiments. Conclusions are presented in Section 6.5.

## 6.1 Formulation of the Problem

Suppose there are $P$ elliptically polarized signals $\{s_1(t), \cdots, s_P(t)\}$ from statistically independent non-Gaussian sources, impinging on a planar array of $M$ antennae from directions $\{\phi_1, \cdots, \phi_P\}$ in the same plane as the array. Let $\mathbf{r}(t)$ be

the $M$-vector representing the signal received by the antenna array. Then $\mathbf{r}(t)$ is expressed by the measurement equation

$$\mathbf{r}(t) = \mathbf{A}\mathbf{s}(t) + \mathbf{n}(t) = \sum_{p=1}^{P} \mathbf{a}_p s_p(t) + \mathbf{n}(t) \tag{6.1}$$

where $\mathbf{A} = [\mathbf{a}_1, \cdots, \mathbf{a}_P]$ is an $M \times P$ steering matrix whose columns represent the (unknown) responses of the subarray to the incoming wavefronts, $\mathbf{s}(t)$ is the $P$-vector of the sources signals $\{s_i(t)\}_{i=1}^{P}$. We make the following assumptions about the model in (6.1): 1. $\{s_i(t)\}_{i=1}^{P}$ are non-Gaussian, statistically independent, and have non-zero fourth-order cumulants; 2. $\mathbf{n}(t)$ is a Gaussian noise process that may have arbitrary and unknown cross-statistics, and is statistically independent of $\mathbf{s}(t)$; and, 3. The columns of $\mathbf{A}$ are linearly independent for the given direction of arrival and polarization parameters. This nonambiguity assumption is common in array processing.

The array is assumed to be composed of two subarrays, one having a *regular* geometry, and the other having an *arbitrary* and *unknown* response and geometry. The regular subarray will be designed such that it contains a *minimum* number of elements required to estimate the angle and polarization parameters of interest. Later, we show such a regular subarray consists of *three* short dipole antennas. First, we introduce the polarization concept.

Polarization of a transverse electromagnetic (TEM) wave is characterized by the ellipse traced by the extremity of its electric field vector [49] as time progresses. The electric field must be observed along its direction of propagation. Polarization is classified as linear, circular, or elliptical. If the electric field vector as a function of time is always directed along a line, the field is said to be linearly polarized. Linear and circular polarizations are special cases of elliptical polarization. A typical polarization ellipse is shown in Fig. 6.1.

The polarization ellipse is defined by two constants, namely the ellipticity angle $\alpha$ and the orientation angle $\beta$. For a given polarization, specified by $\alpha$ and $\beta$, the electric field vector can be written [49] as

$$\mathbf{e} = E_\phi \, \mathbf{e}_\phi + E_\theta \, \mathbf{e}_\theta \tag{6.2}$$

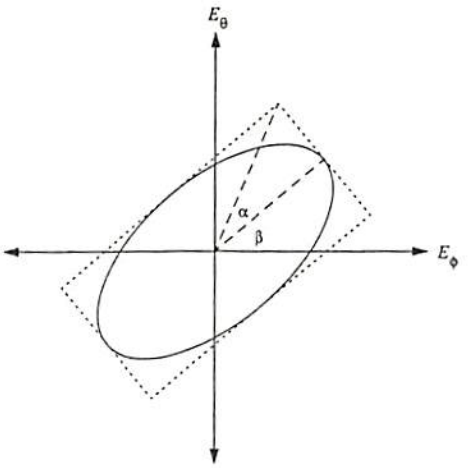


Figure 6.1: A typical polarization ellipse.

where the horizontal and vertical components, $E_\phi$ and $E_\theta$ are given by

$$E_\phi = E\cos\gamma,\ E_\theta = E\sin\gamma\, e^{j\eta} \tag{6.3}$$

in which $E$ is the electric field amplitude, and $\gamma$ and $\eta$ are the following functions of $\alpha$ and $\beta$

$$\begin{aligned} \cos 2\gamma &= \cos 2\alpha\, \cos 2\beta, \\ \tan\eta &= \tan 2\alpha\, \csc 2\beta. \end{aligned} \tag{6.4}$$

The parameters $\alpha$ and $\beta$ can be expressed in terms of $\gamma$ and $\eta$ as follows

$$\begin{aligned} \tan 2\beta &= \tan 2\gamma\, \cos\eta, \\ \sin 2\alpha &= \sin 2\gamma\, \sin\eta. \end{aligned} \tag{6.5}$$

The ranges of $\alpha$, $\beta$, $\gamma$ and $\eta$ are defined as $-\pi/4 \leq \alpha \leq \pi/4$, $0 \leq \beta < \pi$, $0 \leq \gamma \leq \pi/2$ and $-\pi \leq \eta < \pi$. The polarization parameters are conveniently displayed on the Poincare sphere [14] as in Fig. 6.2.

Using (6.3) the electric field vector of the wave can be expressed in rectangular coordinates as

$$\mathbf{e} = -E\ \cos\gamma\, \sin\phi\ \mathbf{e}_x + E\ \cos\gamma\, \cos\phi\ \mathbf{e}_y - E\ \sin\gamma\, e^{j\eta}\ \mathbf{e}_z. \tag{6.6}$$

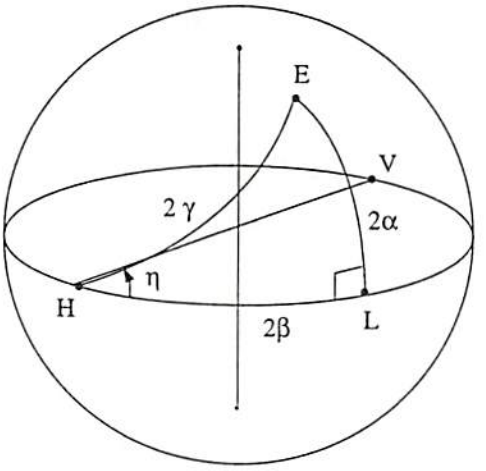


Figure 6.2: Poincare sphere. Any polarization $(\alpha, \beta)$ is represented by a point on the Poincare sphere with coordinates $(\alpha, \beta)$, The relationship between $(\gamma, \eta)$ and $(\alpha, \beta)$ is easily seen on the sphere. The points L, H, V and E correspond to linear, horizontal, vertical and elliptical polarizations, respectively.

Consequently, a plane wave impinging on the array is characterized uniquely by the four parameters $\{\phi,\ E,\ \gamma,\ \eta\}$ or $\{\phi,\ E,\ \alpha,\ \beta\}$. Parameters of the $p$th wave will be denoted by $\{\phi_p,\ E_p,\ \alpha_p,\ \beta_p\}$ where $1 \leq p \leq P$.

The problem of interest is to estimate the parameters $\{\phi_p, \alpha_p, \beta_p\}_{p=1}^{P}$ given $N$ snapshots received by the array. The parameters $\{E_p\}_{p=1}^{P}$ are not needed because they are not useful for discriminating the sources. In our formulation we focus on first determining $\{\phi_p,\ \gamma_p,\ \eta_p\}$ after which $\alpha_p$ and $\beta_p$ can be determined using (6.5).

## 6.2 New Solution

Consider an $M$-element array consisting of three short dipole antennas and an $M-3$ element arbitrary subarray. Assume that two of the dipoles are crossed, and that the third dipole is placed in parallel to either of the other two at a known distance, as shown in Fig. 6.3. The other $M-3$ elements may have *arbitrary* and *unknown* responses and locations.

Since the dipoles are assumed to be short, the measurement from each dipole is proportional to the electric field component along the dipole [40]; therefore,

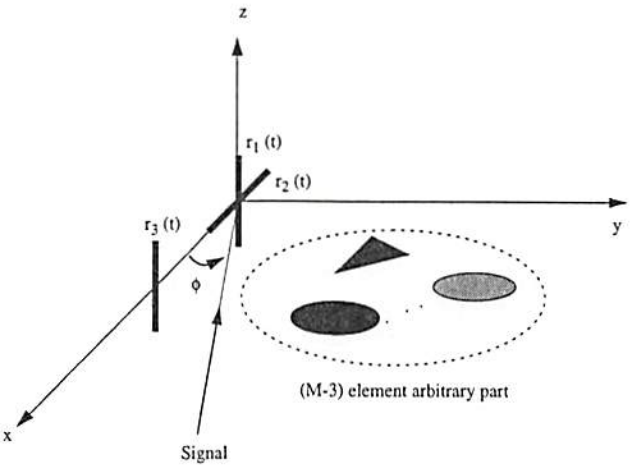


Figure 6.3: The array structure.

the measurement from the first and third dipoles will be proportional to the $z$-component of the electric field, whereas the measurement from the second dipole will be proportional to the $x$-component of the electric field. Hence, from (6.6), and by considering the separation between the first and third sensors, the received signals at the first three sensors are given [49] by

$$r_1(t) = -\sum_{p=1}^{P} \sin\gamma_p \, e^{j\eta_p} \, s_p(t) \tag{6.7}$$

$$r_2(t) = -\sum_{p=1}^{P} \cos\gamma_p \, \sin\phi_p \, s_p(t) \tag{6.8}$$

$$r_3(t) = -\sum_{p=1}^{P} \sin\gamma_p \, e^{j\eta_p} \, e^{-j\frac{2\pi d}{\lambda}\cos\phi_p} \, s_p(t) \tag{6.9}$$

where $s_p(t) = E_p a_p(t) e^{j(w_c t + \theta_p)}$ in which $a_p(t)$ is the modulating signal and $\theta_p$ is the carrier phase. The modulating signal $a_p(t)$ is assumed to be non-Gaussian, which is a valid assumption for communication signals.

The geometry of the assumed regular subarray leads to three cumulant-based invariance properties that may be exploited by the ESPRIT algorithm to jointly estimate the arrival angles and polarizations. We use fourth-order cumulants as they are typically the least-order non-zero cumulants of communication signals. Odd-order cumulants of communication signals are generally zero; because, these type of signals are symmetrically distributed. First, we shall show what the above

mentioned invariance properties are and how they can be obtained through the use of cumulants. Then, we shall consider the estimation of the appropriate cumulant matrices and provide a step-by-step summary of the proposed solution.

Consider first the $M \times M$ fourth-order cumulant matrix of the signals $r_1(t)$ and $\mathbf{r}(t)$ formed as follows:

$$\begin{aligned}
\mathbf{C}_0 &\triangleq \operatorname{cum}(r_1(t), r_1^*(t), \mathbf{r}(t), \mathbf{r}^H(t)) \\
&= \operatorname{cum}\left(-\sum_{i=1}^{P} \sin\gamma_i\, e^{j\eta_i}\, s_i(t), -\sum_{j=1}^{P} \sin\gamma_j\, e^{-j\eta_j}\, s_j^*(t), \sum_{k=1}^{P} \mathbf{a}_k s_k(t), \sum_{l=1}^{P} \mathbf{a}_l^H s_l^*(t)\right) \\
&\quad + \operatorname{cum}(n_1(t), n_1^*(t), \mathbf{n}(t), \mathbf{n}^H(t)) \\
&= \sum_{i=1}^{P}\sum_{j=1}^{P}\sum_{k=1}^{P}\sum_{l=1}^{P} \operatorname{cum}(\sin\gamma_i\, e^{j\eta_i}\, s_i(t), \sin\gamma_j\, e^{-j\eta_j}\, s_j^*(t), \mathbf{a}_k s_k(t), \mathbf{a}_l^H s_l^*(t)) \\
&= \sum_{i=1}^{P} \operatorname{cum}(\sin\gamma_i\, e^{j\eta_i}\, s_i(t), \sin\gamma_i\, e^{-j\eta_i}\, s_i^*(t), \mathbf{a}_i s_i(t), \mathbf{a}_i^H s_i^*(t)) \\
&= \sum_{i=1}^{P} \sin^2\gamma_i\, \mathbf{a}_i\, \mathbf{a}_i^H\, \mu_{4,i} \\
&= \mathbf{A}\boldsymbol{\Lambda}\mathbf{A}^H
\end{aligned} \tag{6.10}$$

where $\{\mu_{4,i}\}_{i=1}^{P}$ are the fourth-order cumulants of the source signals which are assumed to be non-zero, and

$$\boldsymbol{\Lambda} \triangleq \operatorname{diag}\{\sin^2\gamma_1\, \mu_{4,1}, \cdots, \sin^2\gamma_P\, \mu_{4,P}\} \tag{6.11}$$

which is nonsingular provided $\gamma_i \neq 0$, $i = 1, \cdots, P$. In deriving (6.10), we used the cumulant properties [**CP1**], [**CP3**], [**CP5**] and [**CP6**] in [47], the facts that cumulants of Gaussian processes are zero, and that cumulants of independent processes are delta functions.

Consider next the following $M \times M$ cumulant matrix of the signals $r_1(t)$, $r_2(t)$ and $\mathbf{r}(t)$:

$$\begin{aligned}
\mathbf{C}_1 &\triangleq \operatorname{cum}(r_1(t), r_2^*(t), \mathbf{r}(t), \mathbf{r}^H(t)) \\
&= \sum_{i=1}^{P} \sin\gamma_i\, \cos\gamma_i\, \sin\phi_i\, e^{j\eta_i} \mathbf{a}_i\, \mathbf{a}_i^H\, \mu_{4,i}
\end{aligned}$$

$$= \mathbf{A}\boldsymbol{\Phi}_1\boldsymbol{\Lambda}\mathbf{A}^H \tag{6.12}$$

where

$$\boldsymbol{\Phi}_1 \triangleq \text{diag}\{\frac{\sin\phi_1}{\tan\gamma_1}e^{j\eta_1}, \cdots, \frac{\sin\phi_P}{\tan\gamma_P}e^{j\eta_P}\} \tag{6.13}$$

Equation (6.12) was derived in a similar way to the derivation of $\mathbf{C}_0$.

Consider, finally, the following $M \times M$ cumulant matrix of the signals $r_1(t)$, $r_3(t)$ and $\mathbf{r}(t)$:

$$\begin{aligned}\mathbf{C}_2 &\triangleq \text{cum}(r_1(t), r_3^*(t), \mathbf{r}(t), \mathbf{r}^H(t)) \\ &= \sum_{i=1}^{P} \sin^2\gamma_i \, e^{j\frac{2\pi d}{\lambda}\cos\phi_i}\mathbf{a}_i\,\mathbf{a}_i^H\,\mu_{4,i} \\ &= \mathbf{A}\boldsymbol{\Phi}_2\boldsymbol{\Lambda}\mathbf{A}^H \end{aligned} \tag{6.14}$$

where

$$\boldsymbol{\Phi}_2 \triangleq \text{diag}\{e^{j\frac{2\pi d}{\lambda}\cos\phi_1}, \cdots, e^{j\frac{2\pi d}{\lambda}\cos\phi_P}\} \tag{6.15}$$

Equation (6.14) was also derived in a similar way to the derivation of $\mathbf{C}_0$.

The matrices $\mathbf{C}_0$, $\mathbf{C}_1$ and $\mathbf{C}_2$ essentially give correlations between the main array and its two hypothetical copies in terms of a new set of signals which are power-scaled versions of the original signals. Since scaling of signal powers does not affect estimation of the parameters of interest, our solution is similar to the one proposed by Li [40]; however, we use only three regular elements to achieve the same result instead of requiring two copies of the main array, or restricting it to be linear.

The cumulant matrices $\mathbf{C}_0$, $\mathbf{C}_1$ and $\mathbf{C}_2$ possess two invariance structures characterized by $\boldsymbol{\Phi}_1$ and $\boldsymbol{\Phi}_2$ which allows us to jointly estimate the polarization parameters and arrival angles of the incident waves. The diagonal matrix $\boldsymbol{\Phi}_2$ contains the arrival angles, whereas $\boldsymbol{\Phi}_1$ contains both the arrival angles and polarization parameters; hence, these parameters can be extracted from estimates of $\boldsymbol{\Phi}_1$ and $\boldsymbol{\Phi}_2$. We show next how $\boldsymbol{\Phi}_1$ and $\boldsymbol{\Phi}_2$ are estimated using the cumulant matrices $\mathbf{C}_0$, $\mathbf{C}_1$ and $\mathbf{C}_2$ in (6.10), (6.12) and (6.14), respectively.

The solution is based on the idea of rotational invariance of the underlying signal subspace which is the basis of the ESPRIT algorithm [66]. In ESPRIT,

the rotational invariance of the signal subspace is induced by the translational invariance of the array, i.e., an identical copy of the array which is displaced in the space is needed. On the other hand, in our cumulant-based algorithm, the same invariance is obtained without any need for an identical copy. In ESPRIT, the signal subspace is extracted from the eigendecomposition of the covariance matrix of the concatenated measurements from the main array and its copy. Here, the signal subspace is extracted from the singular value decomposition of the concatenated matrix of $\mathbf{C}_0$, $\mathbf{C}_1$ and $\mathbf{C}_2$ in (6.10), (6.12) and (6.14), respectively which, in turn, gives estimates of $\mathbf{\Phi}_1$ and $\mathbf{\Phi}_2$.

Let us define a new $3M \times M$ matrix $\mathbf{C}$ by concatenating $\mathbf{C}_0$, $\mathbf{C}_1$ and $\mathbf{C}_2$ as follows

$$\mathbf{C} \triangleq \begin{bmatrix} \mathbf{C}_0 \\ \mathbf{C}_1 \\ \mathbf{C}_2 \end{bmatrix} = \underbrace{\begin{bmatrix} \mathbf{A} \\ \mathbf{A}\mathbf{\Phi}_1 \\ \mathbf{A}\mathbf{\Phi}_2 \end{bmatrix}}_{\triangleq \mathbf{B}} \mathbf{\Lambda}\mathbf{A}^H. \tag{6.16}$$

Due to the nonambiguity assumption, for different arrival angles and polarization parameters, columns of $\mathbf{A}$ are linearly independent; therefore, if $\mathbf{\Lambda}$ is nonsingular, then rank($\mathbf{C}$)=$P$. Consequently, the singular value decomposition of $\mathbf{C}$ yields

$$\mathbf{C} = [\mathbf{U}_1 \mathbf{U}_2] \begin{bmatrix} \mathbf{\Sigma} & \mathbf{0} \\ \mathbf{0} & \mathbf{0} \end{bmatrix} \mathbf{V}^H \tag{6.17}$$

where $\mathbf{\Sigma} \triangleq \text{diag}(\sigma_1, \cdots, \sigma_P)$; $\mathbf{U}_1 \triangleq [\mathbf{u}_1, \cdots, \mathbf{u}_P]$ and $\mathbf{U}_2 \triangleq [\mathbf{u}_{P+1}, \cdots, \mathbf{u}_{3M}]$. It follows therefore that

$$\mathbf{C}^H \mathbf{U}_2 = \mathbf{0}, \tag{6.18}$$

or, equivalently

$$\mathbf{A}\mathbf{\Lambda}^* \mathbf{B}^H \mathbf{U}_2 = \mathbf{0}. \tag{6.19}$$

Since $\mathbf{A}\mathbf{\Lambda}^*$ is full-rank, (6.19) implies $\mathbf{B}^H \mathbf{U}_2 = \mathbf{0}$. Using also the fact that $\mathbf{U}_1$ is orthogonal to $\mathbf{U}_2$, it follows that

$$\text{span}(\mathbf{B}) = \text{span}(\mathbf{U}_1). \tag{6.20}$$

Therefore, there exists [1] a nonsingular $P \times P$ matrix $\mathbf{T}$ such that

$$\mathbf{U}_1 = \mathbf{BT} \tag{6.21}$$

which means that

$$\begin{bmatrix} \mathbf{U}_{11} \\ \mathbf{U}_{12} \\ \mathbf{U}_{13} \end{bmatrix} = \begin{bmatrix} \mathbf{A} \\ \mathbf{A}\boldsymbol{\Phi}_1 \\ \mathbf{A}\boldsymbol{\Phi}_2 \end{bmatrix} \mathbf{T} \tag{6.22}$$

where we partitioned $\mathbf{U}_1$ exactly the same way as $\mathbf{B}$, i.e., into three $M \times P$ matrices $\mathbf{U}_{11}$, $\mathbf{U}_{12}$ and $\mathbf{U}_{13}$. Equation (6.22) establishes the signal subspace and two of its rotationally invariant counterparts.

Note that these rotational invariances are obtained without requiring translational invariances of the array, as in ESPRIT. Having obtained these invariances, we apply the idea of ESPRIT twice as will be explained shortly. Equation (6.22) shows that $\mathbf{U}_{11}$, $\mathbf{U}_{12}$ and $\mathbf{U}_{13}$ share a common columnspace of dimension $P$; therefore, only $P$ columns of $[\mathbf{U}_{11}, \mathbf{U}_{12}]$ and $[\mathbf{U}_{11}, \mathbf{U}_{13}]$ are linearly independent. Consequently $\text{rank}([\mathbf{U}_{11}, \mathbf{U}_{12}]) = \text{rank}([\mathbf{U}_{11}, \mathbf{U}_{13}]) = P$ which means that $[\mathbf{U}_{11}, \mathbf{U}_{12}]$ and $[\mathbf{U}_{11}, \mathbf{U}_{13}]$ have nullspaces of dimension $P$. This last result implies there exists two $2P \times P$ matrices $\mathbf{F} \triangleq [\mathbf{F}_x; \mathbf{F}_y]$ and $\mathbf{G} \triangleq [\mathbf{G}_x; \mathbf{G}_y]$ which are rank-$P$ such that

$$\begin{aligned} \mathbf{0} &= [\mathbf{U}_{11}, \mathbf{U}_{12}]\mathbf{F} \\ &= \mathbf{U}_{11}\mathbf{F}_x + \mathbf{U}_{12}\mathbf{F}_y \\ &= \mathbf{ATF}_x + \mathbf{A}\boldsymbol{\Phi}_1\mathbf{TF}_y, \end{aligned} \tag{6.23}$$

and,

$$\begin{aligned} \mathbf{0} &= [\mathbf{U}_{11}, \mathbf{U}_{13}]\mathbf{G} \\ &= \mathbf{U}_{11}\mathbf{G}_x + \mathbf{U}_{13}\mathbf{G}_y \\ &= \mathbf{ATG}_x + \mathbf{A}\boldsymbol{\Phi}_2\mathbf{TG}_y, \end{aligned} \tag{6.24}$$

[1] *Theorem:* Let $\mathbf{A}$ and $\mathbf{B}$ be $n \times m$ matrices. There exists a nonsingular matrix $\mathbf{C}$ such that $\mathbf{AC} = \mathbf{B}$ if and only if $\mathbf{A}$ and $\mathbf{B}$ have the same column space [31].

Since $\mathbf{A}$ is full-rank, (3.23) and (3.24) result in

$$0 = \mathbf{T}\mathbf{F}_x + \mathbf{\Phi}_1\mathbf{T}\mathbf{F}_y, \tag{6.25}$$

and

$$0 = \mathbf{T}\mathbf{G}_x + \mathbf{\Phi}_2\mathbf{T}\mathbf{G}_y, \tag{6.26}$$

respectively, which are equivalent to

$$-\mathbf{F}_x\mathbf{F}_y^{-1} = \mathbf{T}^{-1}\mathbf{\Phi}_1\mathbf{T}, \tag{6.27}$$

and

$$-\mathbf{G}_x\mathbf{G}_y^{-1} = \mathbf{T}^{-1}\mathbf{\Phi}_2\mathbf{T}. \tag{6.28}$$

Equations (6.27) and (6.28) imply that the eigenvalues of $-\mathbf{F}_x\mathbf{F}_y^{-1}$ and $-\mathbf{G}_x\mathbf{G}_y^{-1}$ must be equal to the diagonal elements of $\mathbf{\Phi}_1$ and $\mathbf{\Phi}_2$, respectively. The reason is that (6.27) and (6.28) are similarity transformations and they preserve eigenvalues. To estimate the diagonal elements of $\mathbf{\Phi}_1$ and $\mathbf{\Phi}_2$, we, therefore, need two matrices $\mathbf{F}$ and $\mathbf{G}$ which satisfy (6.23) and (6.24). Two such matrices can be obtained by performing singular value decomposition on the two $M \times 2P$ matrices $[\mathbf{U}_{11}, \mathbf{U}_{12}]$ and $[\mathbf{U}_{11}, \mathbf{U}_{13}]$. Since $[\mathbf{U}_{11}, \mathbf{U}_{12}]$ and $[\mathbf{U}_{11}, \mathbf{U}_{13}]$ are both rank $P$, the last $P$ right singular vectors of $[\mathbf{U}_{11}, \mathbf{U}_{12}]$ and $[\mathbf{U}_{11}, \mathbf{U}_{13}]$ can be selected as $\mathbf{F}$ and $\mathbf{G}$, respectively.

Once $\mathbf{\Phi}_1$ and $\mathbf{\Phi}_2$ are obtained, the next step is to extract the polarization parameters and arrival angles from diagonal elements of $\mathbf{\Phi}_1$ and $\mathbf{\Phi}_2$.

The polarization parameters can be determined using $\mathbf{\Phi}_1$ and $\mathbf{\Phi}_2$; however to do so, we must first find the correct pairing of the diagonal elements of $\mathbf{\Phi}_1$ and $\mathbf{\Phi}_2$ so that the $i$-th diagonal elements of $\mathbf{\Phi}_1$ and $\mathbf{\Phi}_2$ contain parameters that belong only to the $i$-th source ($i = 1, \cdots, P$). The reason is that, the diagonal elements of $\mathbf{\Phi}_1$ and $\mathbf{\Phi}_2$ (which are the eigenvalues of $-\mathbf{F}_x\mathbf{F}_y^{-1}$ and $-\mathbf{G}_x\mathbf{G}_y^{-1}$, respectively) are ordered without regard to which sources they belong to during the eigendecompositions of $-\mathbf{F}_x\mathbf{F}_y^{-1}$ and $-\mathbf{G}_x\mathbf{G}_y^{-1}$, i.e., the $i$-th diagonal element of $\mathbf{\Phi}_1$ may contain parameters which belong to the $i$-th source whereas $i$-th diagonal element of $\mathbf{\Phi}_2$ may contain parameters which belong to the $j$-th source. This makes the

solution for polarization parameters impossible from just $\mathbf{\Phi}_1$ and $\mathbf{\Phi}_2$, which are coupled in terms of polarization parameters, unless the diagonal elements of $\mathbf{\Phi}_1$ and $\mathbf{\Phi}_2$ are correctly paired.

The pairing can be done as follows, the idea of which was first used in [40]. Let $\mathbf{P}$ be the product of $-\mathbf{F}_x\mathbf{F}_y^{-1}$ and $-\left(\mathbf{G}_x\mathbf{G}_y^{-1}\right)^{-1}$. From (6.27) and (6.28) it follows that

$$\mathbf{P} = \mathbf{T}^{-1}\mathbf{\Phi}_1\mathbf{\Phi}_2{}^{-1}\mathbf{T} \tag{6.29}$$

which implies that the eigenvalues of $\mathbf{P}$ must be the ratios of the diagonal elements of $\mathbf{\Phi}_1$ to those of $\mathbf{\Phi}_2$. Let the eigenvalues of $\mathbf{P}$ be $\{\lambda_p\}_{p=1}^{P}$. Focus on the $j$th diagonal element of $\mathbf{\Phi}_2$, $\Phi_2(j,j)$ $(j = 1, \cdots, P)$. Then the diagonal element of $\mathbf{\Phi}_1$ that is correctly associated with $\Phi_2(j,j)$ is found by minimizing

$$\left|\frac{\Phi_1(i,i)}{\Phi_2(j,j)} - \lambda_p\right|, \; i, p = 1, \cdots, P. \tag{6.30}$$

Reordering the elements of $\mathbf{\Phi}_1$ and $\mathbf{\Phi}_2$ so that they are paired correctly, we obtain two diagonal matrices $\bar{\mathbf{\Phi}}_1$ and $\bar{\mathbf{\Phi}}_2$. The arrival angles and polarization parameters can then be extracted from these matrices easily, as explained next.

The arrival angles $\phi_i$, $i = 1, \cdots, P$ can be determined from $\bar{\mathbf{\Phi}}_2$ as [see (6.15)]

$$\phi_i = \arccos\left(\frac{\lambda}{2\pi d}\,\text{angle}(\bar{\mathbf{\Phi}}_2\,(i,i))\right) \tag{6.31}$$

where $\bar{\mathbf{\Phi}}_2\,(i,i)$ is the $i$-th diagonal element of $\bar{\mathbf{\Phi}}_2$.

The polarization parameters $\eta_i$ and $\gamma_i$ $i = 1, \cdots, P$, can then be determined, as [see (6.13)]:

$$\eta_i = \text{angle}\left(\bar{\mathbf{\Phi}}_1\,(i,i)\right) \tag{6.32}$$

$$\gamma_i = \arctan\left(\sin\phi_i \,/\, |\,\bar{\mathbf{\Phi}}_1\,(i,i)|\right) \tag{6.33}$$

Finally, the polarization parameters $\alpha_i$ and $\beta_i$ are obtained from $\eta_i$ and $\gamma_i$ using the inverse relationships in (6.5).

## 6.3 Overall Computational Procedure

We provide a complete 12 steps computational procedure in this section, that is based on Section 1.3.

**Step 1:** From the $M \times 1$ array data, estimate the following $M \times M$ cumulant matrices:

$$\begin{aligned} \mathbf{C}_0 &\triangleq \text{cum}(r_1(t), r_1^*(t), \mathbf{r}(t), \mathbf{r}^H(t)) \\ \mathbf{C}_1 &\triangleq \text{cum}(r_1(t), r_2^*(t), \mathbf{r}(t), \mathbf{r}^H(t)) \\ \mathbf{C}_2 &\triangleq \text{cum}(r_1(t), r_3^*(t), \mathbf{r}(t), \mathbf{r}^H(t)), \end{aligned} \tag{6.34}$$

and, stack these matrices into a $3M \times M$ matrix $\mathbf{C}$ as follows:

$$\mathbf{C} \triangleq \begin{bmatrix} \mathbf{C}_0 \\ \mathbf{C}_1 \\ \mathbf{C}_2 \end{bmatrix} \tag{6.35}$$

**Step 2:** Perform SVD decomposition of $\mathbf{C}$; keep the first $3M \times P$ submatrix of the left singular vectors of $\mathbf{C}$, where $P$ is the number of the sources. Let this submatrix be $\mathbf{U}_1$.

**Step 3:** Partition $\mathbf{U}_1$ into three $M \times P$ matrices $\mathbf{U}_{11}$, $\mathbf{U}_{12}$ and $\mathbf{U}_{13}$ as follows:

$$\begin{bmatrix} \mathbf{U}_{11} \\ \mathbf{U}_{12} \\ \mathbf{U}_{13} \end{bmatrix} = \begin{bmatrix} \mathbf{A} \\ \mathbf{A}\boldsymbol{\Phi}_1 \\ \mathbf{A}\boldsymbol{\Phi}_2 \end{bmatrix} \mathbf{T}. \tag{6.36}$$

**Step 4:** Perform singular value decompositions of $[\mathbf{U}_{11}, \mathbf{U}_{12}]$ and $[\mathbf{U}_{11}, \mathbf{U}_{13}]$. Stack the last $P$ right singular vectors of $[\mathbf{U}_{11}, \mathbf{U}_{12}]$ and $[\mathbf{U}_{11}, \mathbf{U}_{13}]$ into the $2P \times P$ matrices denoted $\mathbf{F}$ and $\mathbf{G}$, respectively.

**Step 5:** Partition $\mathbf{F}$ and $\mathbf{G}$ as $\mathbf{F} \triangleq \begin{bmatrix} \mathbf{F}_x \\ \mathbf{F}_y \end{bmatrix}$ and $\mathbf{G} \triangleq \begin{bmatrix} \mathbf{G}_x \\ \mathbf{G}_y \end{bmatrix}$ respectively, where $\mathbf{F}_x, \mathbf{F}_y, \mathbf{G}_x, \mathbf{G}_y$ are $P \times P$ .

**Step 6:** Perform eigendecomposition of $-\mathbf{F}_x\mathbf{F}_y^{-1}$ and $-\mathbf{G}_x\mathbf{G}_y^{-1}$; keep the eigenvalues. Let the eigenvalue matrix of $-\mathbf{F}_x\mathbf{F}_y^{-1}$ and $-\mathbf{G}_x\mathbf{G}_y^{-1}$ be $\mathbf{\Phi}_1$ and $\mathbf{\Phi}_2$, respectively.

**Step 7:** Multiply $-\mathbf{F}_x\mathbf{F}_y^{-1}$ by $-\left(\mathbf{G}_x\mathbf{G}_y^{-1}\right)^{-1}$ from the right; let the product be $\mathbf{\Pi}$. (Note that $\mathbf{\Pi} = \mathbf{T}^{-1}\mathbf{\Phi}_1{\mathbf{\Phi}_2}^{-1}\mathbf{T}$).

**Step 8:** Perform an eigendecomposition of $\mathbf{\Pi}$. Let the eigenvalues of $\mathbf{\Pi}$ be $\{\lambda_p\}_{p=1}^{P}$.

**Step 9:** For $j = 1, \cdots, P$, minimize the following function with respect to $i$ and $p$.

$$\left|\frac{\mathbf{\Phi}_1(i,i)}{\mathbf{\Phi}_2(j,j)} - \lambda_p\right|, \; i, p = 1, \cdots, P. \tag{6.37}$$

Record the values of $i$ corresponding to each $j$. Reorder the elements of $\mathbf{\Phi}_1$ and $\mathbf{\Phi}_2$ such that the $i$th element of $\mathbf{\Phi}_1$ corresponds to the $j$th element of $\mathbf{\Phi}_2$. Let the reordered matrices be $\bar{\mathbf{\Phi}}_1$ and $\bar{\mathbf{\Phi}}_2$.

**Step 10:** Determine the arrival angles $\phi_i$, $i = 1, \cdots, P$, from $\bar{\mathbf{\Phi}}_2$ as

$$\phi_i = \arccos\left(\frac{\lambda}{2\pi d}\,\text{angle}(\bar{\mathbf{\Phi}}_2\,(i,i))\right) \tag{6.38}$$

where $\bar{\mathbf{\Phi}}_2\,(i,i)$ is the $i$-th diagonal element of $\bar{\mathbf{\Phi}}_2$.

**Step 11:** Determine the polarization parameters $\eta_i$ and $\gamma_i$, $i = 1, \cdots, P$, as:

$$\eta_i = \text{angle}\left(\bar{\mathbf{\Phi}}_1\,(i,i)\right) \tag{6.39}$$

$$\gamma_i = \arctan\left(\sin\phi_i \,/\, |\,\bar{\mathbf{\Phi}}_1\,(i,i)|\right) \tag{6.40}$$

**Step 12:** Determine the polarization parameters $\alpha_i$ and $\beta_i$ from $\eta_i$ and $\gamma_i$, $i = 1, \cdots, P$, using:

$$\begin{aligned} \tan 2\beta_i &= \tan 2\gamma_i \cos\eta_i, \\ \sin 2\alpha_i &= \sin 2\gamma_i \sin\eta_i. \end{aligned} \tag{6.41}$$

where $\alpha_i$, $\beta_i$, $\gamma_i$ and $\eta_i$ are restricted as $-\pi/4 \le \alpha_i \le \pi/4$, $0 \le \beta_i < \pi$, $0 \le \gamma_i \le \pi/2$ and $-\pi \le \eta_i < \pi$.

## 6.4 Simulation Experiments

### 6.4.1 Experiment 1

This experiment demonstrates our new joint polarization and bearing estimation algorithm. We assume four statistically independent sources having diverse polarizations. The array has five elements with the configuration in Fig. 6.4. The first three elements are short dipole antennas; the other two are assumed omnidirectional sensors. The arrival angles and polarization parameters of the sources are as in Table 6.1 The measurements are contaminated by circularly symmetric white Gaussian noise that is independent of the signals. The signals have equal signal-to-noise ratios. We considered two SNR values (20dB and 10dB) in this experiment. The Section 6.2 procedure was used to estimate the direction of arrival ($\phi$) and polarization parameters ($\alpha$, $\beta$) of the signals. 2000 snapshots were used. We performed a 100 run Monte Carlo experiment for each SNR value. The estimates are plotted as a function of realizations in Figs. 6.5 and 6.6 for $SNR = 20$dB and 10dB, respectively. We also present the sample mean and standard deviations of these estimates in Tables 6.2 and 6.3, respectively. Observe from the figures and tables that the means of the estimated signal parameters are very close to their actual values (given in Table 6.1), and the standard deviations are low. This experiment supports our earlier claim that it is possible to estimate bearings and polarizations of as many as $M - 1$ signals with $M$ sensors, $M - 3$ of which are arbitrary.

Table 6.1: The arrival angles and polarization parameters (in degrees) of the sources

| Source No | $DOA$ | $\alpha$ | $\beta$ |
|---|---|---|---|
| 1 | -60 | 40 | 70 |
| 2 | -20 | 10 | 50 |
| 3 | 50 | -10 | 30 |
| 4 | 70 | -30 | 10 |

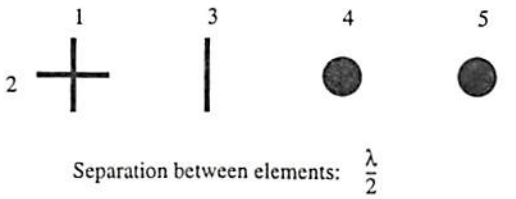


Figure 6.4: The array used in Experiments 1-3.

### 6.4.2 Experiment 2

In this experiment we examine the mean-squared error (MSE) performance of our joint DOA and polarization estimation method. We used the same array as in Experiment 1. One linearly polarized signal was assumed, i.e., $\alpha = 0^o$. The measurements are contaminated by circularly symmetric white Gaussian noise that is independent of the signals with $SNR = 10$dB. The arrival angle $\phi$ was variable in the range $(0^o, 90^o)$. For each value of $\phi$, the polarization parameter $\beta$ was increased by $10^o$ steps in the range $(10^o, 170^o)$. For each value of $\phi$ and $\beta$ we ran a 50-point Monte-Carlo experiment. For DOA estimates we used the usual measure for the mean-squared error. For polarization estimates, the estimation error is more conveniently defined as the spherical distance between the two points E and F on the Poincare sphere that represent the actual polarization $(\alpha, \beta)$ and the estimated polarization $(\hat{\alpha}, \hat{\beta})$ [see Fig. 6.7]. This measure of error was chosen, because it was shown [14] that the response of a receiving antenna of one polarization to a signal of different polarization depends only on the spherical distance between the two points. Let $\Delta$ be the angular distance between the two points. Then, $\Delta$ is given by

$$\cos\Delta = \cos 2\gamma \cos 2\hat{\gamma} + \sin 2\gamma \sin 2\hat{\gamma} \cos(\eta - \hat{\eta}). \tag{6.42}$$

The MSEs in dB in the DOA and polarization estimates obtained by averaging 50 Monte Carlo runs are shown in Figs. 6.8 and 6.9, respectively on a logarithmic scale. Note that the mean-squared error in the DOA and polarization estimates decreases as the actual value of the DOA is increased. The reason is that the signal power received by the second sensor is proportional to $\sin^2\phi$ which is maximum when $\phi = 90^o$. When $\phi = 0^o$ or $180^o$ the second sensor signal power is zero,

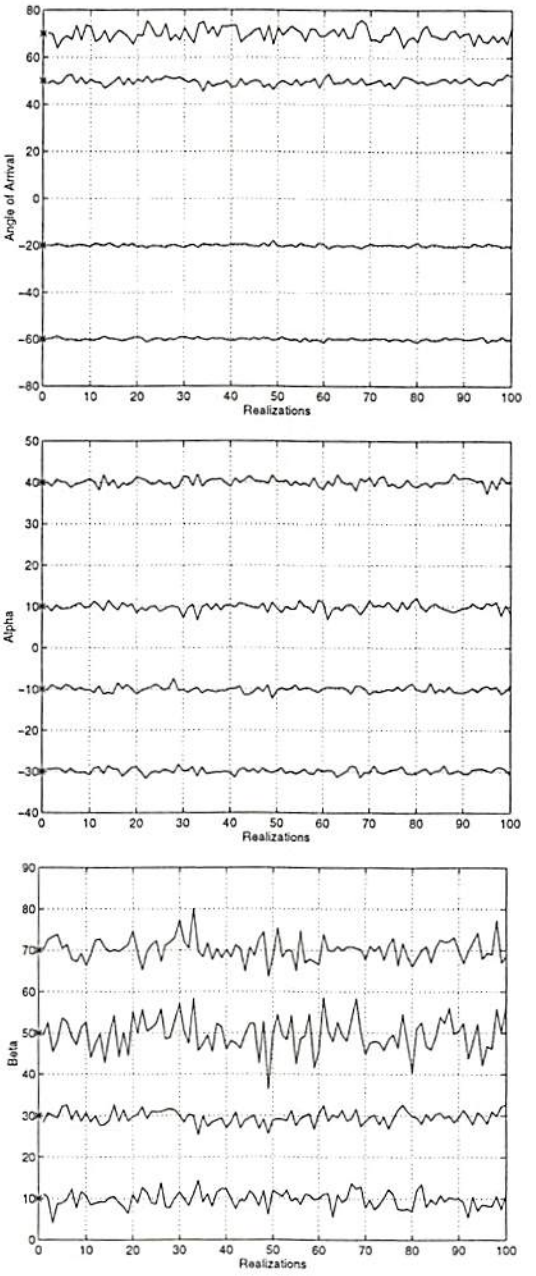


Figure 6.5: Bearing and polarization parameter estimates as a function of realizations for Experiment 1. $SNR = 20$dB. '*' denotes the actual value of the paramater.

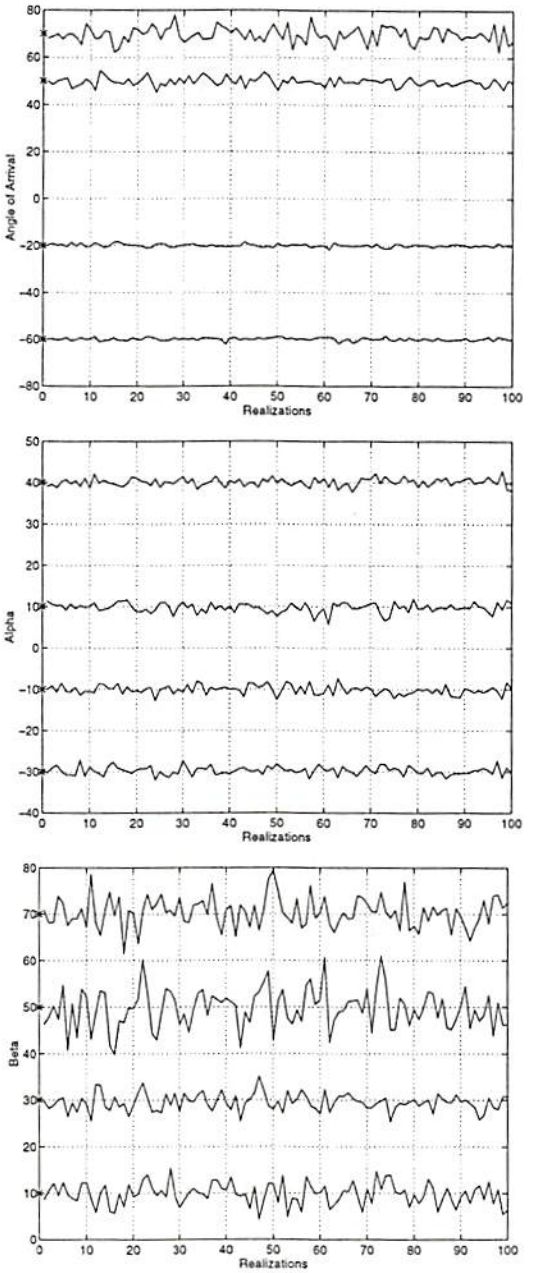


Figure 6.6: Bearing and polarization parameter estimates as a function of realizations for Experiment 1. $SNR = 10$dB. '*' denotes the actual value of the paramater.

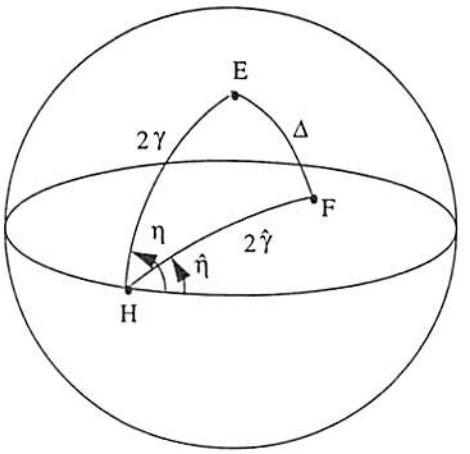


Figure 6.7: Polarization error on the Poincare sphere. E represents the actual value of polarization. F represents the estimate of E.

i.e., only noise is received; therefore, mean-squared error in the DOA estimates increases. Note, also, that as $\beta$ approaches $90^o$, MSE in the DOA estimates decreases, because, the total power received by the first three sensors is proportional to $1+\sin^2\beta$ [Note that $\gamma = \beta$ for $\alpha = 0^o$]. This power is maximum when $\beta = 90^o$.

### 6.4.3 Experiment 3

In this experiment we continue examining the mean-squared error (MSE) performance of our joint DOA and polarization estimation method. We used the same array as in Experiment 1. One elliptically polarized signal was assumed. The ellipticity angle $\alpha$ was variable in the range $-45^o, 45^o$, and the orientation angle $\beta = 90^o$. The measurements are contaminated by circularly symmetric white Gaussian noise that is independent of the signals with $SNR = 10$dB. The arrival angle $\phi$ was variable in the range $(0^o, 90^o)$. For each value of $\phi$, the ellipticity angle $\alpha$ was increased by $5^o$ steps in the range $(-45^o, 45^o)$. For each value of $\phi$ and $\alpha$, we ran a Monte-Carlo experiment using 1500 snapshots for 50 realizations. For DOA estimates we used the usual measure for the mean-squared error. For polarization estimates, the estimation error is defined as in Experiment 2.

The mean-squared errors in the DOA and polarization estimates obtained by averaging 50 Monte Carlo runs are shown in Figs. 6.10 and 6.11, respectively on a logarithmic scale. Note that for this case, $\eta = 90^o$; and, from the Poincare sphere

Table 6.2: Sample means and standard deviations of the bearing and polarization parameter estimates. $SNR = 20$dB.

| | DOA | | $\alpha$ | | $\beta$ | |
|---|---|---|---|---|---|---|
| Source No | *mean* | *std* | *mean* | *std* | *mean* | *std* |
| 1 | -59.9 | 0.57 | 40.1 | 0.96 | 70.2 | 2.76 |
| 2 | -19.9 | 0.61 | 9.8 | 0.99 | 49.5 | 4.16 |
| 3 | 49.7 | 1.49 | -10.0 | 0.76 | 29.6 | 1.55 |
| 4 | 69.8 | 2.70 | -29.8 | 0.71 | 9.7 | 1.90 |

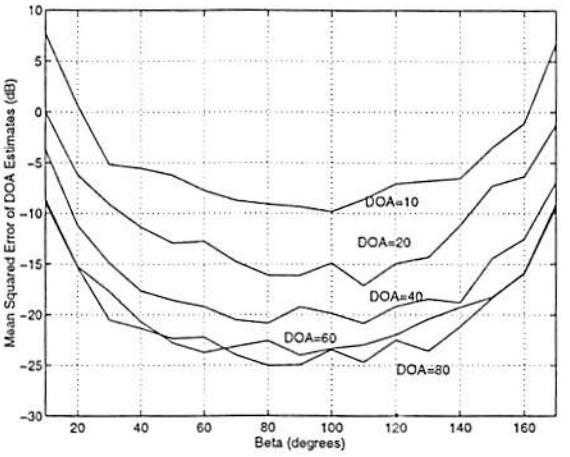


Figure 6.8: Mean-squared errors in the DOA estimates. DOAs are in degrees.

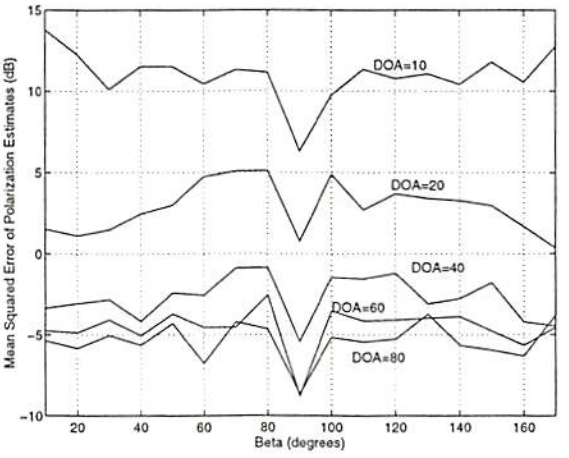


Figure 6.9: Mean-squared errors in the polarization estimates. DOAs are in degrees.

$45^o \leq \gamma \leq 90^o$ for $-45^o \leq \alpha \leq 0^o$; and, $90^o \geq \gamma \geq 45^o$ for $0^o \leq \alpha \leq 45^o$. The signal amplitudes at the first, second and third sensors are proportional to $sin(\gamma)$, $cos(\gamma)sin(\phi)$ and $sin(\gamma)$, respectively. Consequently, the signal power at the second sensor increases with increasing $\phi$; hence, the mean-squared errors in the DOA and polarization estimates decrease as $\phi$ increases. Observe from Fig. 6.11 that, for a fixed DOA, the mean-squared errors in the polarization estimates decrease as $\alpha$ gets near $0^o$. The reason is that the signal powers at the first and third sensors peak when $\gamma = 90^o$ (i.e., $\alpha = 0^o$).

### 6.4.4 Experiment 4

In this experiment we continue examining the mean-squared error (MSE) performance of our joint DOA and polarization estimation method. The 8-element Y-array in Fig. 6.12 which consists of 4 pairs of crossed short dipole antennas is used. Note that this array is a special case of the one in Fig. 6.3, in that all of its elements are short crossed dipoles. The response $\mathbf{a}(\theta)$ of the Y-array to a polarized signal received from $\theta$ with polarization parameters $\eta$ and $\gamma$ is given by

$$\begin{aligned}\mathbf{a}(\theta) \;=\; & [\sin\gamma\, e^{j\eta}, \sin\theta\cos\gamma, \\ & e^{-j\pi\cos\theta}\sin\gamma\, e^{j\eta}, e^{-j\pi\cos\theta}\sin\theta\cos\gamma, \\ & e^{-j\pi(2\cos\theta+\sin\theta)}\sin\gamma\, e^{j\eta}, e^{-j\pi(2\cos\theta+\sin\theta)}\sin\theta\cos\gamma, \\ & e^{-j\pi(2\cos\theta-\sin\theta)}\sin\gamma\, e^{j\eta}, e^{-j\pi(2\cos\theta-\sin\theta)}\sin\theta\cos\gamma] \qquad (6.43)\end{aligned}$$

We assume two polarized signals arrive at the array from the closely spaced directions $\phi_1 = 42^o$ and $\phi_2 = 40^o$. The polarization parameters of the signals are as follows: the orientation angles are $\beta_1 = \beta_2 = 45^o$; the signal from $42^o$ has ellipticity angle $\alpha_1 = 45^o$ whereas the other signal has $\alpha_2 = 45^o - \Delta\alpha$ where $\Delta\alpha$ is varied in the range $[0^o - 90^o]$ by $5^o$ increments. Note that the arrival angles are close to each other, and that the only difference between the polarizations of the two signals is their ellipticity angles. The measurements are contaminated by circularly symmetric white additive Gaussian noise with $SNR = 10dB$. For each value of $\Delta\alpha$, we ran a Monte-Carlo experiment using 2000 snapshots for 25 realizations. For DOA estimation we used the usual mean-squared error. For

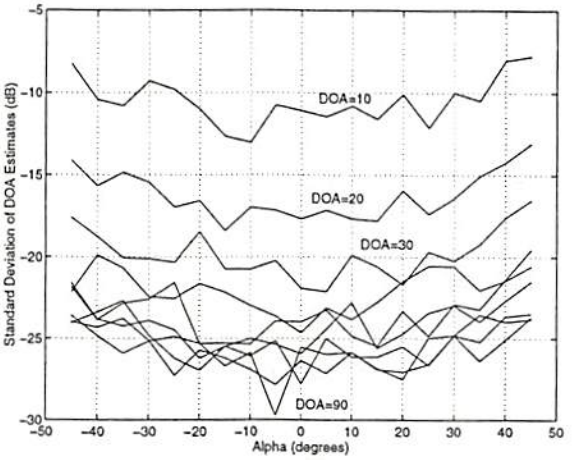


Figure 6.10: Mean-squared errors in the DOA estimates. DOAs are in degrees.

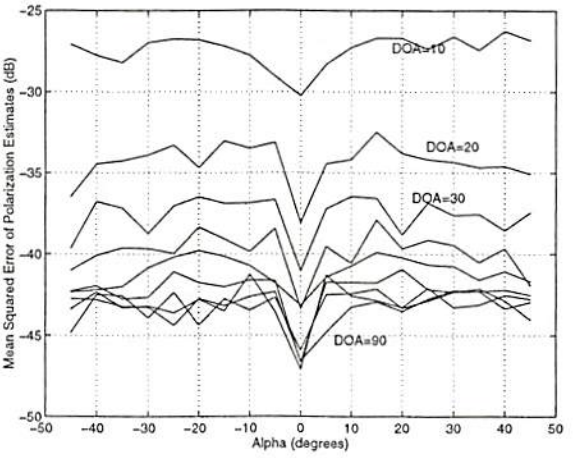


Figure 6.11: Mean-squared errors in the polarization estimates. DOAs are in degrees.

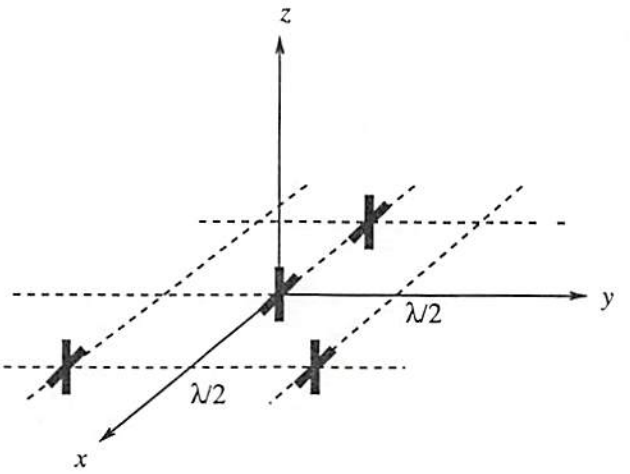


Figure 6.12: The Y-array used in Experiment 4.

polarization estimates, the estimation error is defined as in Experiment 2.

The mean-squared errors in dB in the DOA and polarization estimates, obtained by averaging 25 Monte Carlo runs, are shown in Figs. 6.13 and 6.14, respectively on a logarithmic scale. Observe from Figs. 6.13 and 6.14 that the mean-squared errors decrease as the polarization difference $\Delta\alpha$ of the two signals increase even though the arrival angles are very close to each other. This can be explained as follows. When the arrival angle and polarization parameters of the signals are close to each other, the columns of the steering matrix become nearly identical which means that the rank of the steering matrix is less than the number of the signals. In this case it is impossible to correctly identify the DOA and polarization parameters using the subspace-based DF methods including VESPA. However, the arrival angles may be close but the polarizations different, which is the case considered in this experiment. In this case, as demonstrated by the experimental results, the parameter estimates improve as the difference between the polarizations increases. Consequently, this experiment demonstrates that polarizations of the signals can be utilized into VESPA to incorporate diversity into the DOA estimation problem.

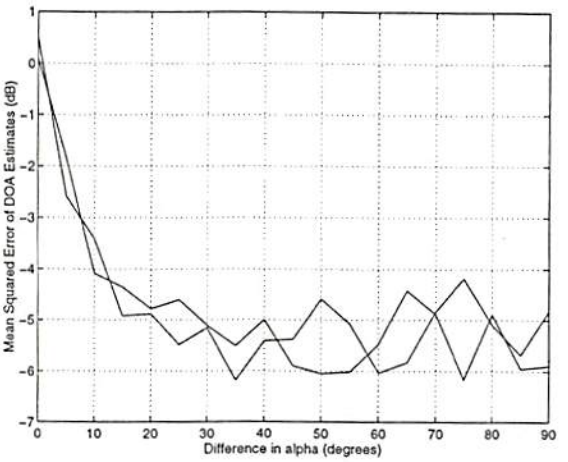


Figure 6.13: Mean-squared errors in the DOA estimates. DOAs are in degrees.

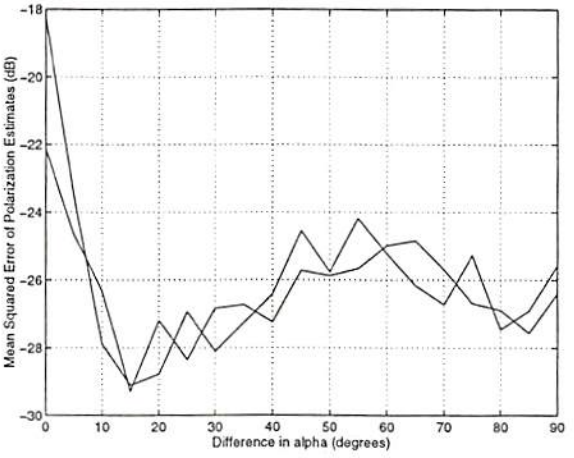


Figure 6.14: Mean-squared errors in the polarization estimates. DOAs are in degrees.

Table 6.3: Sample means and standard deviations of the bearing and polarization parameter estimates. $SNR = 10$dB.

| | DOA | | $\alpha$ | | $\beta$ | |
|---|---|---|---|---|---|---|
| Source No | *mean* | *std* | *mean* | *std* | *mean* | *std* |
| 1 | -59.9 | 0.66 | 40.1 | 0.98 | 70.4 | 3.26 |
| 2 | -19.9 | 0.66 | 9.7 | 1.17 | 49.65 | 4.25 |
| 3 | 49.7 | 1.74 | -10.12 | 1.10 | 29.16 | 1.83 |
| 4 | 69.60 | 3.20 | -29.75 | 1.0 | 9.89 | 2.34 |

## 6.5 Conclusions

We have presented a new method to estimate both arrival angles and polarization parameters of narrowband cochannel signals that is applicable to any arbitrary array of unknown geometry and response provided there exists a subarray consisting of three dipoles arranged in a fashion described in Section 6.2 and depicted in Fig. 6.3. With our method, parameters of $M-1$ signals can be estimated using an $M$-element array. This represents a 50% savings in hardware over the recently published method in [40]. Our solution requires estimation of three cumulant matrices followed by steps that are much like those of the ESPRIT algorithm.

# Chapter 7

# Conclusions

In this thesis, we have addressed the problems of parameter estimation and separation of multiple cochannel signals using antenna arrays. The conventional approach to solving these problems is to use the first- and second-order statistics of the measurements. In this thesis, the emphasis is on the advantages of using higher-order statistics (cumulants) in addition to first- and second order statistics of the signals for array signal processing. The key idea in this thesis is realizing that the extra arguments cumulants have can be utilized to obtain algorithms that are less-constrained in application than second-order statistics-based methods.

In Chapter 3, a cumulant-based subspace direction-finding method, *extended VESPA*, is developed for coherent signal environments. The coherent signals case often arises in practice when multipath propagation and/or smart jammers are present. In this case, most of the subspace-based approaches, including MUSIC, ESPRIT and VESPA which are the most favorable ones, fail. Cures have been proposed in the literature to the coherency problem; however, they are limited to very restrictive array configurations or impose unreasonable assumptions. Moreover, these solutions reduce the effective aperture of the array. We have shown that, using cumulants, direction-finding is possible in the coherent signals case, with arrays that have *arbitrary configuration* and *unknown response*, provided the array contains a linear subarray. We have also shown that both aperture extension and non-Gaussian noise suppression are possible for the coherent signals case. In other words, it is possible to detect more targets than sensors, which

is impossible to accomplish using covariance-based methods for arbitrary arrays, even in the case of *known* array response and *incoherent* signals. A uniform linear subarray is needed; the rest of the array may have arbitrary and unknown response, and does not require calibration. Unlike some of the proposed cures for handling coherence, we require no array calibration or search procedure. Our method, *extended VESPA*, can replace existing covariance-based processing in a given array without requiring any modification in the associated hardware, provided there is a linear subarray. Extended VESPA is a three-step procedure. The first step is based on our earlier work, the virtual ESPRIT algorithm (VESPA), in which the generalized steering vectors are estimated. In the second step the generalized steering vector for each coherent group is interpreted as a single snapshot received from the actual signal. Then, a spatial smoothing technique is used to restore the rank of the pseudo-covariance matrix estimated from the part of the generalized steering vector corresponding to the linear subarray. The third and final step is to apply any subspace technique to the pseudo-covariance matrix whose rank was restored in the previous step in order to get the angle-of-arrivals. Since the second and third steps are repeated for each coherent group, and they depend only on the results of the first step, the computations after the first step can be parallelized for drastic reduction in the computational load. We have also shown ways to improve the accuracy of extended-VESPA and to use the available data more efficiently. Among the three beamforming-based improvement methods described in our work, BFBI3 yields the best MSE performance; therefore, it is recommended for low SNRs. The performance of our method and the proposed methods for improvement were demonstrated in various scenarios by means of extensive simulations.

In Chapter 4, a cumulant-based *blind* beamformer for coherent signal environments is developed. Existing covariance-based beamforming methods assume that the array manifold is either known or can be estimated. If array manifold is unknown it is necessary to calibrate the array; however, array calibration is a very costly procedure requiring measurement and storage of array response for all possible signal parameters. In the incoherent case, the array manifold can be determined blindly using ESPRIT; however, ESPRIT requires translationally

equivalent subarrays with known displacement vectors, which is usually an impractical constraint on the array configuration. Besides, as in any other subspace method, ESPRIT fails in the coherent sources case. As mentioned in the previous paragraph, the existing cures to handle the coherent signals case are limited to very specific array configurations. In addition, existing beamformers fail to perform optimally when there are interferences coherent with the signal. Moreover, they tend to cancel the desired signal in the beamformer output. We have developed a cumulant-based optimum *blind* beamformer for the coherent signals case which is applicable to any *arbitrary* array configuration, that does not need *any knowledge* about its response, and relies *solely* on the measurements. For a blind beamformer the presence of coherent multipaths does not make any difference. In other words, the case of coherent multipath signals is identical to that of statistically independent signals with no multipath. Therefore, the developed method is applicable to independent sources as well. Our approach is based on the observation that using cumulants of received signals, two matrices can be formed which conform to the ESPRIT architecture. Neither identical subarrays nor an identical sensor pair is needed as opposed to ESPRIT or VESPA. The two cumulant matrices permit us to estimate the generalized steering vectors for each source blindly. Then, a number of cumulant-based beamformers can be designed whose optimality have already been shown in the second-order statistics framework. Note that since the steering vectors are estimated from the data, in some sense, the beamformer is tuned to the data, thereby avoiding sensitivity problems associated with mismatch in the assumed steering vectors, which occurs in the case of covariance-based processing. The next step is constellation rotation correction which handles the phase ambiguity problem inherent in the estimation of generalized steering vector. In our approach, powers of multipaths are effectively combined instead of trying to decorrelate them. As in extended VESPA, both Gaussian and non-Gaussian noise with unknown statistics can be suppressed as long as they are uncorrelated with the signals of interest. A comparable result using second-order statistics is not possible. Simulation results indicate that even if the array is restricted to be uniform linear, our method performs better (by as much as 10dB for hard-to-resolve cases) than second-order statistics-based

beamformer using spatial smoothing.

In Chapter 5, the beamspace VESPA and the iterative VESPA algorithms are developed. In beamspace direction finding the array data is first projected into several beamspaces of lower or equal dimension; then, each beamspace data is processed to obtain DOAs and source signals in the same way as if it were received from a pseudoarray of lower or equal dimension. A beamspace transformation results in a reduced parameter space, which brings a cubic decrease in computational complexity. Besides, beamspace transformation has been shown to offer numerous benefits such as enhanced resolution, improved performance in colored noise, and reduced sensitivity to sensor perturbations. The ESPRIT algortihm, is difficult to implement in beamspace, because the shift invariance induced by the two identical subarrays is lost during a beamspace transformation. A beamspace version of ESPRIT was developed, however, by Xu *et al*, who showed that if the beamspace transformation has the same invariance as the array shift invariance, then the lost invariance can be restored. This requirement restricts the usefulness of desired beamformers, which is a limitation of covariance-based processing. Using the the fact that fourth-order cumulants have more than two arguments, we have developed a beamspace version of the VESPA that retains the unique property of VESPA, namely, that there is no need for an identical copy of the array; only an identical response sensor pair is required. The beamspace VESPA is applicable to arbitrary beamspace transformations as opposed to its covariance-based counterpart, beamspace-ESPRIT. Using the beamspace approach, we have also developed an an iterative VESPA which can handle a problem that exists with VESPA: when the source cumulants and powers are highly different it is impossible to localize some of the sources correctly with VESPA due to the undesirable cross terms present in the sample statistics of the weakest source due to the dominant sources for small number of samples. In practice, this case occurs when the source signals have different constellations and powers that are significantly separated. The iterative VESPA handles the cross terms by eliminating one source (which is the strongest one) at each step of the iteration. This is achieved at the expense of computational load. We demonstrated the iterative VESPA on real data.

In Chapter 6, a joint estimation algorithm is developed for bearing and polarization parameter estimation of multiple signals with arrays that are minimally-constrained in response and geometry. It is advantageous to use diversely polarized signals and antennas for improved localization and discrimination of signals. Conventional methods for this problem assume that the array manifold is either *known* or obtained through array calibration. Li and Compton used ESPRIT which avoids array calibration; however, in their method, to estimate parameters of at most $M-1$ signals, it is required that the array be a 2M element ULA consisting of $M$-pairs of crossed dipoles. Their method is not applicable to arbitrary arrays. using fourth-order cumulants, We have shown that both directions of arrival and polarization parameters of at most $M-1$ cochannel signals can be estimated using any $M$ element array by adding a subarray consisting of three short dipole antennas displaced in space and configured in a certain fashion. This way the constraint on the array configuration is minimized. Our solution requires estimation of three cumulant matrices followed by steps that are much like those of the ESPRIT algorithm. Simulation results support our claims.

In all of the above work, we have successfully addressed challenging array processing problems which are either impossible or impractical to solve using just second-order statistics.

Two fundamental issues remain unexplored:

- Performance analyses of the higher-order statistics based methods developed in this thesis.
- Development of adaptive implementations of these algorithms for moving targets and nonstationary environments.

# References


[1] C. A. Balanis, *Antenna Theory*, Harper & Row Publishers, New York, 1982.

[2] Y. Bresler, V. U. Reddy, and T. Kailath, "Optimum beamforming for coherent signal and interferences," *IEEE Trans. on Acoustics, Speech, and Signal Processing*, vol. ASSP-36, no. 6, pp. 833–843, June 1988.

[3] D. R. Brillinger and M. Rosenblatt, Asymptotic theory of estimates of $k$th-order spectra. In B. Harris (Ed.). *Spectral Analysis of Time Series.* New York: Wiley, 1967, 189–232.

[4] J. A. Cadzow, "A high-resolution direction of arrival algorithm for narrow-band coherent and incoherent sources," *IEEE Trans. on Acoustics, Speech and Signal Processing*, vol. 36, pp. 965–977, July 1988.

[5] J. Capon, "High-resolution frequency-wavenumber spectral anlysis," *Proceedings of IEEE*, vol. 57, no. 8, pp. 1408–1418, Aug. 1969.

[6] J.-F. Cardoso and E. Moulines, "Asymptotic performance analysis of direction-finding algorithms based on fourth-order cumulants," *IEEE Trans. on Signal Processing*, vol. 43, no. 1, pp. 214–224, Jan. 1995.

[7] J. -F Cardoso, A. Souloumiac, "Blind beamforming for non gaussian signals," *IEE Proc. -F*, vol. 140, no. 6, pp. 362–370, December 1993.

[8] P. Comon, "Independent component analysis," *Int. Workshop on Higher-Order Statistics*, pp. 111–120, Chamrousse, France, 1991.

[9] Y. H. Chen and Y. S. Lin, "A modified cumulant matrix for DOA estimation," *IEEE Trans. on Signal Processing*, vol. 42, pp. 3287–3291, Nov. 1994.

[10] Q. C. Cheng and Y. Hua, "Performance analysis of the MUSIC and Pencil-MUSIC algorithms for diversely polarized array," *IEEE Transactions on Signal Processing*, vol. 42, no. 11, pp. 3150–3165, November 1994.

[11] H. H. Chiang and C. L. Nikias, "The ESPRIT algorithm with higher-order statistics," *Proceedings of Workshop on Higher-Order Spectral Analysis*, Vail, CO, pp. 163–168, June 28-30, 1989.

[12] R. T. Compton, Jr., "On the performance of a polarization sensitive adaptive array," *IEEE Transactions on Antennas and Propagation*, vol. AP-29, no. 5, pp. 718–725, September 1981.

[13] R. T. Compton, Jr., "The tripole antenna: an adaptive array with full polarization flexibility," *IEEE Transactions on Antennas and Propagation*, vol. AP-29, no. 6, pp. 944– 952, November 1981.

[14] G. A. Deschamps, "Geometrical representation of the polarization of a plane electromagnetic wave," *Proc. IRE*, vol. 39, pp. 540-544, May 1951.

[15] A. Di, "Multiple source location-a matrix decomposition approach," *IEEE Trans. on Acoustics, Speech, and Signal Processing*, vol. ASSP-33, pp. 1086–1091, October, 1985.

[16] M. C. Doğan, *Cumulants and Array Processing.* Ph.D. Dissertation, Signal and Image Processing Institute Report #245, University of Southern California, Los Angeles, California, September, 1993.

[17] M. C. Dogan and J. M. Mendel, "Applications of cumulants to array processing, Part I: Aperture extension and array calibration," *IEEE Trans. on Signal Processing*, vol. 43, no. 5, pp. 1200–1216, May 1995.

[18] M. C. Dogan and J. M. Mendel, "Applications of cumulants to array processing, Part II: Non-Gaussian noise suppression," *IEEE Trans. on Signal Processing*, vol. 43, no. 7, pp. 1661–1676, Jul. 1995.

[19] M. C. Doğan and J. M. Mendel, "Cumulant-based blind optimum beamforming," *IEEE Transactions on Aerospace and Electronic Systems*, vol. 30, no.3, pp. 722–741, July 1994.

[20] M. C. Dogan and J. M. Mendel, Oct. 17, 1995, "Method and apparatus for signal analysis employing a virtual cross-correlation computer," U. S. Patent No. 5,459,668.

[21] T. Ephraim, N. Merhav and H. L. Van Trees, "Min-norm interpretations and consistency of MUSIC, MODE and ML," *IEEE Trans. on Signal Processing*, vol. 43, no. 12, pp. 2937–2941, Dec. 1995.

[22] J. E. Evans, J. R. Johnson, and D. F. Sun, "High resolution angular spectrum estimation techniques for terrain scattering analysis and angle of arrival estimation," in *Proc. First ASSP Workshop Spectral Estimation*, Communication Research Lab., McMaster University, Aug. 1981.

[23] E. Ferrara and T. Parks, "Direction finding with an array of antennas having diverse polarizations," *IEEE Transactions on Antennas and Propagation*, vol. 32, pp. 231-236, March 1983.

[24] B. Friedlander, "A sensitivity analysis of the MUSIC algorithm," *IEEE Trans. on Acoustics, Speech and Signal Processing*, vol. 38, pp. 1740–1751, Oct. 1990.

[25] B. Friedlander and A. J. Weiss, "Direction finding using spatial smoothing with interpolated arrays," *IEEE Transactions on Aerospace and Electronic Systems*, vol. 28, no. 2, pp. 574-587, April, 1992.

[26] E. Gönen, M. C. Doğan, J. M. Mendel, "Applications of cumulants to array processing: direction finding in coherent signal environment," *Proc. of 28th Asilomar Conference on Signals, Systems, and Computers*, Asilomar, CA, pp. 633–637,1994.

[27] E. Gönen and J. M. Mendel, "Applications of cumulants to array processing, part III: optimum blind signal recovery for coherent signals," submitted for publication.

[28] E. Gönen and J. M. Mendel, "Optimum cumulant-based blind beamforming for coherent signals and interferences," *Proceedings of ICASSP-95*, pp. 1908–1911, Detroit, Michigan, May 1995.

[29] E. Gonen and J. M. Mendel, "An iterative virtual-ESPRIT," *Proceedings of Eighth IEEE Signal Processing Workshop on Statistical Signal and Array Processing*, Corfu, GREECE, June 1996.

[30] E. Gönen and J. M. Mendel, "Applications of cumulants to array processing, part IV: direction finding in coherent signal environment," submitted for publication.

[31] F. A. Graybill, *Matrices with Applications in Statistics*, Wadsworth Publishing Company, Pacific Grove, California, 1983.

[32] F. Haber, and M. Zoltowski, "Spatial spectrum estimation in a coherent signal environment using an array in motion," *IEEE Trans. Antennas Propagation*, vol. AP-34, no. 3, pp. 301–310, March, 1986.

[33] S. S. Haykin, Adaptive Filter Theory, Prentice Hall, Englewood Cliffs, New Jersey, 1991.

[34] Y. Hua, "A Pencil-MUSIC algorithm for finding two-dimensional angles using crossed dipoles," *IEEE Transactions on Antennas and Propagation*, vol. 41, no. 3, pp. 370–376, March 1993.

[35] D. H. Johnson and D. E. Dudgeon, Array Signal Processing: Concepts and Techniques, Prentice Hall, Englewood Hills, New Jersey, 1993.

[36] M. Kaveh and A. J. Barabell, "The statistical performance of the MUSIC and the Minimum-Norm algorithms in resolving plane waves in noise," *IEEE Trans. on Acoustics, Speech and Signal Processing*, vol. 34, pp. 331–341, Apr. 1986.

[37] R. Kumaresan and D. W. Tufts, "Estimating the angles of arrival multiple plane waves," *IEEE Trans. on Aerosp. Electron. Syst.*, vol. AES-19, pp. 134-139, Jan. 1983.

[38] S. Y. Kung, C. K. Lo and R. Foka, "A Toeplitz approximation approach to cohernet source direction finding," in *Proceedings ICASSP*, 1986.

[39] H. Lee and M. Mengrovitz, "Resolution threshold of beamspace root-MUSIC for two closely-spaced emitters," *IEEE Trans. on Acoust. Speech and Signal Processing*, vol. 38, pp. 1545–1559, Sept. 1990.

[40] J. Li and R. T. Compton, Jr., "Angle and polarization estimation using ESPRIT with a polarization sensitive array," *IEEE Transactions on Antennas and Propagation*, vol. 39, no. 9, pp. 1376– 1383, September 1991.

[41] J. Li and R. T. Compton, Jr., "Angle estimation using a polarization sensitive array," *IEEE Transactions on Antennas and Propagation*, vol. 39, no. 10, pp. 1539–1543, October 1991.

[42] J. Li and R. T. Compton, Jr., "Two dimensional angle and polarization estimation using the ESPRIT algorithm," *IEEE Transactions on Antennas and Propagation*, vol. 40, no. 5, pp. 550–555, May 1992.

[43] J. Li and R. T. Compton, Jr., "Direction and polarization estimation using arrays with small loops and short dipoles," *IEEE Transactions on Antennas and Propagation*, vol. 41, no. 3, pp. 379–387, March 1993.

[44] J. Li and R. T. Compton, Jr., "Angle and polarization estimation in coherent signal environment," *IEEE Transactions on Aerospace and Electronic Systems*, vol. 29, no. 3, pp. 706–716, July 1993.

[45] F. Li and R. J. Vaccaro, "Unified anlysis for DOA estimation algorithms in array signal processing," *Signal Processing*, vol. 25, no. 2, pp. 147–169, Nov. 1991.

[46] S. L. Marple, Digital Spectral Analysis with Applications, Prentice Hall, Englewood Cliffs, New Jersey, 1987.

[47] J. M. Mendel, "Tutorial on higher-order statistics (spectra) in signal processing and system theory: theoretical results and some applications," *Proc. IEEE*, vol. 79, no. 3, pp. 278–305, March, 1991.

[48] R. A. Monzingo and T. W. Miller, *Introduction to Adaptive Arrays*, John-Wiley & Sons, Inc., New-York, 1980.

[49] E. Nicolau and D. Zaharia, *Adaptive Arrays*, Elsevier, 1989.

[50] C. L. Nikias and A. P. Petropulu, Higher-order spectra analysis: a nonlinear signal processing framework, Prentice Hall, Englewood Cliffs, New Jersey, 1993.

[51] C. L. Nikias and M. R. Raghuveer, "Bispectrum estimation: a digital signal processing framework," *Proc. IEEE*, vol. 75, no. 7, pp. 869–892, July 1987.

[52] B. Ottersten, M. Viberg, and T. Kailath, "Performance analysis of total least squares ESPRIT algorithm," *IEEE Trans. on Signal Processing*, vol. 39, no. 5, pp. 1122–1135, May 1991.

[53] B. Ottersten, M. Viberg and T. Kailath, "Analysis of subspace fitting and ML techniques for parameter estimation form sensor array data," *IEEE Trans. on Signal Processing*, vol. 40, no. 3, pp. 590–599, March 1992.

[54] R. Pan and C. L. Nikias, "Harmonic decomposition methods in cumulant domains," *Proceedings of ICASSP'88*, pp. 2356–2359, New York, 1988.

[55] A. Paulraj, R. Roy and T. Kailath, "Estimation of signal parameters via rotational invariance techniques-ESPRIT," Proceedings of 19th Asilomar Conference on Signals, Systems, and Computers, Asilomar, CA, Nov. 1985.

[56] S. U. Pillai, Array Signal Processing, Springer-Verlag, New York, 1989.

[57] B. Porat amd B. Friedlander, "Analysis of the asymptotic relatice efficiency of the MUSIC algorithm," *IEEE Trans. on Acoustics, Speech, Signal Processing*, vol. 36, pp. 532–543, Apr. 1988.

[58] B. Porat and B. Friedlander, "Direction finding algorithms based on high-order statistics," *IEEE Trans. on Signal Processing*, vol. 39, no. 9, pp. 2016–2023, Sep. 1991.

[59] B. M. Radich and K. Buckley, "The effect of source number underestimation on MUSIC location estimates," vol. 42, no. 1, pp. 233–235, Jan. 1994.

[60] D. V. B. Rao and K. V. S. Hari, "Weighted subspace methods and spatial smoothing," *IEEE Trans. on Signal Processing*, vol. 41, no. 2, pp. 788–803, Feb. 1993.

[61] D. V. B. Rao and K. V. S. Hari, "Performance analysis of Root-MUSIC," *IEEE Trans. on Acoustics, Speech, Signal Processing*, vol. ASSP-37, pp. 1939–1949, Dec. 1989.

[62] D. V. B. Rao and K. V. S. Hari, "Performance analysis of ESPRIT and TAM in determining the direction of arrival of plane waves in noise," *IEEE Trans. on Acoustics, Speech, Signal Processing*, vol. ASSP-37, pp. 1990–1995, Dec. 1989.

[63] V. U. Reddy, A. Paulraj, and T. Kailath, "Performance analysis of the optimum beamformer in the presence of correlated sources and its behavior under spatial smoothing," *IEEE Trans. on Acoustics, Speech, and Signal Processing*, vol. ASSP-35, no. 7, pp. 927–936, July 1987.

[64] M. Rosenblatt, *Stationary Sequences and Random Fields*, Birkhauser Boston Inc., Boston 1985.

[65] R. H. Roy, "ESPRIT-Estimation of signal paramaters via rotational invariance techniques," Ph.D. dissertation, Stanford University, Stanford, CA, 1987.

[66] R. Roy and T. Kailath, "ESPRIT—Estimation of signal parameters via rotational invariance techniques," *Optical Engineering*, vol. 29, no. 4, pp. 296–313, April, 1990

[67] R. O. Schmidt, "A signal subspace approach to multiple emitter location and spectral estimation," Ph.D. dissertation, Stanford Univ., Stanford, CA, Nov. 1981.

[68] O. Shalvi and E. Weinstein, "New criteria for blind deconvolution of nonminimum phase systems (channels)," *IEEE IT*, vol. 36, no. 2, pp. 312–321, 1990.

[69] S. Shamsunder and G. B. Giannakis, "Detection and parameter estimation of multiple nonGaussian sources via higher order statistics," *IEEE Trans. on Signal Processing*, vol. 42, pp. 1145–1155, May 1994.

[70] T. J. Shan and T. Kailath, "Adaptive beamforming for coherent signals and interference," *IEEE Trans. on Acoustics, Speech, and Signal Processing*, vol. ASSP-33, no. 3, pp. 527–536, June 1985.

[71] T. J. Shan, M. Wax, and T. Kailath, "On spatial smoothing for direction-of-arrival estimation of coherent signals," *IEEE Trans. on Acoustics, Speech, and Signal Processing*, vol. ASSP-33, no. 4, pp. 806–811, August 1985.

[72] J. J Shynk and R. P. Gooch, "The constant modulus array for cochannel signal copy and direction finding," *IEEE Trans. on Signal Processing*, vol. 44, no. 3, pp. 652–660, March 1996.

[73] P. Stoica and M. Viberg, "Weighted LS and TLS approaches yield asymptotically equivalent results," *Signal Processing*, vol. 45, pp. 255–259, 1995.

[74] P. Stoica and A. Nehorai, "Performance comparison of subspace rotation and MUSIC methods for direction estimation," *IEEE Trans. on Signal Processing*, vol. 39, no. 2, pp. 446–452, Feb. 1991.

[75] P. Stoica and A. Nehorai, "MUSIC, maximum likelihood and Cramer-Rao bound, " *IEEE Trans. on Signal Processing*, vol. 37, pp. 720–741, May 1989.

[76] P. Stoica and A. Nehorai, "MUSIC, maximum likelihood and Cramer-Rao bound: Further results and comparisons, " *IEEE Trans. on Signal Processing*, vol. 38, pp. 2140–2150, Dec. 1990.

[77] Y. L. Su, T. J. Shan, and B. Widrow, "Parallel spatial processing: a cure for signal cancellation in adaptive arrays,"*IEEE Trans. on Antennas and Propagation*, vol. AP-34, no. 3, pp. 945–947, March 1986.

[78] A. L. Swindlehurst and T. Kailath, "A performance analysis of subspace-based methods in the presence of model erros, Part1: the MUSIC algorithm," *IEEE Trans. on Signal Processing*, vol. 40, no. 7, pp. 1758–1774, July 1992.

[79] P. Tichavsky, "High-SNR asymptotics to signal-subspace methods in sinusoidal frequency estimation," *IEEE Trans. on Signal Processing*, vol. 41, no. 7, pp. 2448–2460, July 1993.

[80] L. Tong, Y. Inouye and R. Liu, "Waveform preserving blind estimation of multiple independent sources," *IEEE Trans. on Signal Processing*, vol. 41, pp. 2461–2470, July 1993.

[81] M. Viberg, B. Ottersten and T. Kailath, "Detection and estimation in sensor arrays using weighted subspace fitting," *IEEE Trans. on Signal Processing*, vol. 39, no. 11, pp. 2436–2448, Nov. 1991.

[82] M. Viberg and B. Ottersten, "Sensor array processing based on subspace fitting," *IEEE Trans. on Signal Processing*, vol. 39, no. 5, pp. 1110–1120, May 1991.

[83] M. Wax and T. Kailath, "Detection of signals by information theoretic criteria," *IEEE Trans. on Acoustics, Speech, Signal Processing*, vol. ASSP-33, no. 2, pp. 387–392, Apr. 1985.

[84] M. Wax, "Detection and estimation of superimposed signals," Ph.D. dissertation, Stanford Univ., Stanford, CA, Mar. 1985.

[85] R. T. Williams, S. Prasad, and A. K. Mahalanabis, "An improved spatial smoothing technique for bearing estimation in a multipath environment," *IEEE Trans. on Acoustics, Speech, and Signal Processing*, vol. ASSP-36, no. 4, pp. 425–432, April, 1988.

[86] X.-L. Xu and K. Buckley, "Bias and variance of direction-of-arrival estimates from MUSIC, MIN-NORM and FINE," *IEEE Trans. on Signal Processing*, vol. 42, no. 7, pp. 1812–1816, July 1994.

[87] X.-L. Xu and K. Buckley, "Bias analysis of the MUSIC location estimator," *IEEE Trans. on Signal Processing*, vol. 40, no. 10, pp. 2559–2569, Oct. 1992.

[88] X. L. Xu and K. Buckley, "Reduced-dimension beamspace broadband source localization: Preprocessor design and evaluation," in *Proc. IEEE ASSP 4th Workshop Spectrum Estimation Modeling*, Aug. 1988, pp. 22–27.

[89] G. Xu, S. D. Silverstein, R. H. Roy and Thomas Kailath, "Beamspace-ESPRIT," *IEEE Trans. on Signal Processing,* vol. 42, no. 2, pp 339–355, Feb 1994.

[90] N. Yuen and B. Friedlander, "DOA estimation in multipath based on fourth-order cumulants," in *Proc. IEEE Signal Processing ATHOS Workshop on Higher-Order Statistics*, pp. 71–75, June 1995.

[91] I. Ziskind and M. Wax, "Maximum likelihood localization of diversely polarized sources by simulated annealing," *IEEE Transactions on Antennas and Propagation*, vol. 38, pp. 1111–1114, July 1990.

[92] M. Zoltowski, and F. Haber, "A vector space approach to direction finding in a coherent multipath environment,"*IEEE Trans. Antennas Propagation*, vol. AP-34, no. 9, pp. 1069–1079, September, 1986.

[93] M. D. Zoltowski, "On the performance analysis of the MVDR beamformer in the presence of correlated interference,"*IEEE Trans. on Acoustics, Speech, and Signal Processing*, vol. ASSP-36, no. 6, pp. 945–947, June 1988.

[94] M. D. Zoltowski, G. M. Kautz and S. D. Silverstein, "Beamspace Root-MUSIC," *IEEE Trans. Signal Processing*, vol. 41, no. 1, pp 344–364, Jan. 1993.